A Rational Approach to the Design of Propulsors behind Axisymmetric Bodies

by

Mesut GÜNER

A Thesis submitted for the degree of
Doctor of Philosophy

Marine Technology

The University of Newcastle upon Tyne
1994

Abstract

In the context of "Lifting Line Methodology", this thesis presents a rational approach to Marine Screw Propeller design and its applications in combination with a "Stator" device for further performance improvement.

The rational nature of the approach is relative to the Classical Lifting Line procedure and this is claimed by more realistic representation of the propeller slipstream tube which contracts in radial direction along the tube at downstream. Therefore, in accordance with the Lifting Line Methodology, the design procedure presented in this thesis involves the representation of the slipstream shape by a trailing vortex system. The deformation of this system is considered by means of the so-called "Free Slipstream Analysis Method" in which the slipstream tube is allowed to deform and to align with the direction of local velocity which is the sum of the inflow velocity and induced velocities due to the trailing vortices. This deformation is neglected in the Classical Lifting Line approach.

The necessary flow field data or the wake for the design is predicted by using a three-dimensional "Panel Method" for the outer potential flow, whilst a "Thin Shear Layer Method" is used for the inner boundary layer flow. The theoretical procedures in both methods neglect the effect of the free surface and therefore the implemented software for the flow prediction caters only for deeply submerged

bodies. However, the overall design software is general and applicable to surface ships with an external feedback on the wake.

Since the realistic information on the slipstream shape is one of the key parameter in the design of performance improvement devices, the proposed design methodology has been combined with a stator device behind the propeller and the hydrodynamic performance of the combined system has been analysed. The design analysis involved the torque balancing characteristics of the system and the effects of systematic variations of the key design parameters on the performance of torpedo shape bodies and surface ships at varying loading conditions.

The overall conclusions from the thesis indicate that a more realistic representation of the slipstream shape presents a higher efficiency in comparison to the regular slipstream shape assumption, in particular for heavily loaded propellers. Moreover, this representation is essential for sound design of the stator devices as it will determine the radius of the stator. From the investigation on the stator it was found that the undesirable effect of the unbalanced propeller torque can be avoided by the stator. The efficiency of the system will increase with the increase in the number of stator blades and the distance between the stator and the propeller over a practical range of the design parameters.

It is believed that the procedure and software tool provided in this thesis could provide the designer with capability for more sound propeller and the stator design for, partly, surface ships and for submerged ships in particular torpedos, Autonomous Underwater Vehicles (AUV) and submarines.

Although the improvement gained by the present procedure will be accompa-

nied by an increase in computer time, this is not expected to be a major problem considering the enormous power of existing computers. In fact, this has been the major source of encouragement for the recommendation in this thesis to improve the present procedure by using the "Lifting Surface Methodology" as the natural extension of the Lifting Line Methodology.

Acknowledgements

This work has been carried out under the supervision of Dr. E.J. Glover in the Department of Marine Technology, University of Newcastle upon Tyne. I would like to express my deep gratitude to Dr. E.J. Glover for his direction, continuous encouragement, very valuable stimulating discussions and guidance throughout this research.

My thanks are also extended to the staff of the Department of Marine Technology and in particular, Dr. Mehmet Atlar and Mr. G.H.G Mitchell for their help and advice in every respect.

The extra resources, which were necessary in the development and running of the programs, provided by the Computing Laboratory is greatly appreciated.

I also wish to thanks to my colleagues and in particular Dazheng Wang for his many helpful discussions.

Financial assistance from the Education Ministry of Turkey is also gratefully acknowledged.

Finally, I would like to thank my parents and friends for their encouragement and support which they have given me over this period of my life.

Notations and Symbols

Most of the symbols are defined explicitly when they first appear in the text. The principal symbols used in the present work are as follows:

A: Area

C: Chord length

C_D: Drag coefficient

C_L: Lift coefficient

D: Propeller diameter, Drag force

D_s: Stator diameter

dD: Elementary drag of blade section

dL: Elementary lift of blade section

F: Rate of flow

G: Non-dimensional bound circulation

g: Non-dimensional vortex intensity

H: Shape parameter

I: Induction factor

J: Advance coefficient

K_T: Thrust coefficient

K_Q: Torque coefficient

L: Lift force

m: Strength of source

n: Propeller rate of rotation

P: Pressure

P_B: Engine brake power

P_D: Delivered power

P_i: Pitch at i^{th} section of propeller

Q: The rate of fluid mass, torque

R: Propeller radius

R_s: Stator radius

r: Distance between two points, radius of propeller section

T: Thrust

t: Maximum thickness of blade section

U: Inflow velocity

V_A: Advance speed

V_R: Resultant velocity

V_s: Ship speed

U_a: Non-dimensional axial inflow

u: Non-dimensional induced velocity

u_e: External velocity

u_{apm}: Axial mean induced velocity by propeller

u_{tpm}: Tangential mean induced velocity by propeller

W_Q: Torque identity wake fraction

x: Non-dimensional radius

Y: Axial distance downstream

Z: Number of propeller bades

Z_s: Number of stator blades

α: Slope of the vortex line

β: Angle of advance

β_i: Hydrodynamic pitch angle

Γ: Circulation

γ: Vortex intensity

δ: Boundary layer thickness

δ^*: Displacement thickness

ϵ: Vortex pitch angle in ultimate wake

η: Efficiency

θ: Momentum thickness, the rate of fluid flow

ρ: Density

σ: Source of strength

ϕ: Velocity potential, angular coordinate

w: Angular velocity of the propeller

Subscripts:

a, t, r: Axial, tangential and radial components of the inductions factors or velocities.

Contents

LIST OF FIGURES

LIST OF TABLES

Chapter I

Introduction

1.1 General

Screw propellers are the most common form of marine propulsion device. They are used to supply the thrust needed to overcome the resistance experienced by a moving marine vehicle. Such propellers produce thrust through the production of lift and drag on their rotating blades.

The design of marine propellers has traditionally been performed on the basis of open water experimental systematic series. Such procedures have served, and continue to serve, propeller designers well for the design of typical ship propellers, but do not readily allow for the analysis of less traditional propulsor alternatives, such as a rotor/stator combination. The use of series data also does not allow the designer to properly tailor the propulsor to the wake and physical arrangement of a particular ship.

Over the past decades analytical procedures for the design of marine propellers have become well established. These procedures are based on computer models of propellers varying from a simplified representation of the propeller hydrodynamics (e.g. lifting line method) to more complex representations (e.g. lifting surface method). In the historical development of these procedures, the hydrodynamic design of a propeller is accomplished on two levels. First, a lifting line model is used to determine the basic propeller geometry and operating conditions as well as

to determine a radial distribution of circulation over the blades that will provide the total thrust and, usually, maximum efficiency. In the second step the final shape of the blade is determined using a lifting surface analysis procedure.

The lifting line model of the propeller, where the blades of the propeller are considered to be sufficiently thin and narrow and substituted by a single bound vortex line, is used to estimate propeller forces and determine the radial distribution of bound circulation.

Since the lifting line theory alone cannot accurately represent the effect of the actual blade geometry, more elaborate representations of the propeller are required. For this purpose lifting surface methods, where the blades are modelled as sheet of singularities, are usually employed. More sophisticated lifting surface or surface panel representations of the propeller can then be used to analyse the performance of the resulting blade geometry. Consideration of the unsteady forces or cavitation predicted by these methods might then lead back to new design constraints at the lifting line level.

Within the context of the widely recognised design procedures the major steps for the design and analysis of propeller can be listed as

- Determination of diameter, blade surface area and thickness of a basic propeller to satisfy the given conditions.
- Using lifting line design procedure to achieve wake adaptation of the propeller.
- Generating blade sections using simple blade section design methods.
- Using lifting surface theory to predict the performance of the blade and to

investigate the effects of changes in blade geometry. (Glover, [47])

In developing propeller theories, hydrodynamic modelling of the trailing vortex lines behind the propeller is an essential part of accurate representation. In the past the vortex lines downstream of the propeller were assumed to have constant pitch and lie on cylinders of constant radius. In the actual propeller, the trailing vortices leave the trailing edge of the propeller blade and flow into the slipstream with the local velocity at that position. Therefore, the velocity distribution behind the propeller should be known in order to establish the realistic model of the trailing vortex lines. Within this context, the methods used to obtain the velocity distribution can be experimental or theoretical. The analysis of the velocities in the slipstream by model experiment is expensive, difficult and also time consuming. On the other hand the use of computer software, based on theoretical methods, provides a solution of complex analysis calculations in a short time and also many variations of the design can be done. But it still needs experimental work to validate and sometimes verify the calculation.

In order to achieve the goal of an improved propulsive efficiency some alternative propulsors have been proposed, the aim of which is to reduce the energy losses associated with the action of the propeller. These losses are due mainly to the transfer of energy to the water in the slipstream of the propeller, the axial energy loss arising from the acceleration of the water necessary to create thrust and the rotational energy loss from the transfer of torque from the propeller to the water. There is also a viscous drag loss due to the movement of the blades through the water.

Recovery of the rotational energy loss and significant gains in efficiency can

be achieved from the use of contrarotating propellers. At the moment there is renewed interest in the use of these propulsors on large ocean going ships but their widespread use is inhibited by the mechanical complexities of the transmission system and costs.

A cheaper and less complicated alternative to contrarotation is the use of fixed guide vanes placed upstream or downstream of the propeller, the penalty being a smaller gain in propulsor efficiency due to the drag of the fixed vanes. The combination of propeller and guide vanes is now referred to as a propeller/stator propulsor.

1.2 Objectives and Layout

The main objective of this thesis is the further improvement of the lifting line procedure with an emphasis on more realistic representation of the slipstream deformation. As this deformation is one of the key parameters in the design of performance improvement devices, the secondary objective of the thesis is to design a stator behind the propeller and analyse the performance characteristics of the combined propulsor system.

In achieving the above objectives, in the present chapter of the thesis an introductory section is given together with the objectives and the layout. The second chapter of the thesis includes a review of the three key issues involved in the propeller design as well as in the objectives of the thesis. These issues are the propeller design procedures, propeller/stator combination and flow around a torpedo body and propeller. The main reason of selecting the torpedo body is to reduce the complexity of the procedure, since it is a submerged body of revolution and there-

fore some effects such as free surface effect need not be taken into account. The selection of a torpedo body also has some practical significance. Glover, in unpublished work on the design of rotor/stator propulsors for torpedoes, demonstrated the difficulty of defining the true flow in the slipstream of the propulsor with the two components at different positions on a steep conical after body. This defined a requirement for a flow model of the combined body and propulsor.

In Chapter 3 the flow around a slender body is analysed. This effort provides a set of wake data which is important in designing a propeller. The interactions between the flow and propeller are also studied by introducing the idea of effective wake.

In Chapter 4, a review is given of traditional propeller design methods. Having explained these methods, a new propeller design procedure, which is based on lifting line theory, will be presented in Chapter 5. This is a more advanced lifting line method than others and it covers the realistic hydrodynamic model of propeller as much as possible.

In Chapter 6 a design procedure for the stator will be described. The theoretical formulations are derived to calculate the stator circulation and consequently the velocities induced by the stator. In Chapter 7, some numerical examples will be given. Finally general remarks and conclusion will be shown in Chapter 8.

Chapter II

Review of Literature

2.1 General

In this review the main emphasis is placed on propeller and propulsor design. In order to establish a realistic modelling of the propeller, the flow around and behind the propeller should also be investigated. As will be appreciated, modelling of the flow is a very wide and general subject and cannot be covered in such a short space. Therefore a very short summary of the review of this subject is presented.

2.2 Propeller

The development of the theory of propeller action stems from both the axial momentum theory and the blade element theory. The first theory of propeller action was introduced by Rankine [11] and was further developed by R.E. Froude [12]. Although the momentum theory leads to a number of important conclusions regarding the action of the propeller, it gives no indication of the propeller geometry necessary to produce the required forces. A different theory concerned with the blade geometry was developed by W. Froude [38] and it is called the blade element theory. The use of the blade element theory is based on the assumption that the elements act independently of each other and that the flow across the blade is entirely in the direction of the chords of the sections.

These two theories were well developed but they did not completely overcome

the lack of understanding of the effects of the blade number and of choice of appropriate lift and drag values for the blade elements. The problems encountered were not solved until the advent of the vortex theory of the wing which was initiated by Lanchester [13].

In 1919 Prandtl [14] showed that the effect of the free vortices shed at the ends of an aerofoil of finite span is to induce a downwash velocity on it and hence reduce its effective angle of incidence. Furthermore, the energy loss in the slipstream can be considered as an induced drag the magnitude of which is minimum when the spanwise circulation of the foil is elliptical.

The introduction of the vortex theory for the analysis and design of marine propeller requires some assumptions to be made in its application. The first is related to the representation of the blade. Based on the assumption that the blade section is sufficiently thin, it may be replaced by a distribution of vortices along its mean line. Hence the whole blade is represented by a thin bound vortex sheet, referred to as a lifting surface. Considerable simplification of the model, and in particular the numerical techniques for its solution, are achieved if the blades are assumed to be narrow enough for them to be represented by a lifting line. The second refers to the shape of the free vortices in the slipstream. The combined rotation and translation of the blades causes free vortices which trail downstream along helical paths.

A method, providing the performance analysis of marine propellers where the effect of the above assumptions is allowed, was developed by Burrill [8]. This method is based on the combination of the momentum theory and the blade element theory together with aspects of the vortex theory. In this method the

slipstream contraction and downstream increase in vortex line pitch are taken into consideration in an approximate manner. The effect of the finite number of blades on the magnitude of the induced velocities is considered by the use of correction factors. These are due to Goldstein and are derived on the basis of a theoretical examination of the flow past a number of helicoidal surfaces of infinite length. The finite width and thickness of the blades in Burrill's method are taken into account by a modification of the lift curve slope and no lift angle derived from Gutsche's cascade data. A similar correction derived from NACA data is applied for the effects of viscosity.

In 1955 a wake adapted design method was introduced by Burrill [9]. The Burrill wake adapted design method makes use of the expressions established in the analysis process together with a minimum energy loss condition.

Propeller design methods based on the lifting line theory can be divided into two groups: the approximate and rigorous or induction factor methods. The former has been used by Eckhart and Morgan [15]. In this the condition of normality is used and the axial and tangential induced velocities are expressed in terms of simple trigonometric relationships that contain the Goldstein factors. The effect of the radial induced velocities is ignored.

The use of induction factors gives more reliable and accurate results. This is due to the fact that a more accurate representation of the slipstream is considered. An analytical method, developed by Lerbs [16], determines the axial and tangential factors. Another method, based on the concept of the induction factor, was developed by Strscheletzky [7]. Unlike Lerbs' method this is based on the calculation of the incremental induction factor by the Biot-Savart Law. This method provides

the equations for the determination of the induction factors. These induction factors are used to calculate velocities induced by the propeller in axial, tangential and radial directions. Consequently by calculating the induced velocities in the slipstream the slipstream deformation can be determined.

In 1973 Glover [2] proposed a new lifting line theory for heavily loaded propellers based on Burrill's minimum energy loss condition applying induction factors for the calculation of induced velocities. This method allows the extension of the lifting line model of the propeller to take into account slipstream deformation. The downstream contraction of the cylinder radius and increase in vortex pitch downstream are calculated using the obtained induced velocities and the results provide the new shape of the slipstream for the next input data.

In 1976, the lifting line theory was used for calculating the characteristics of a supercavitating propeller by Anderson [49]. Some correction factors were developed for the improvement of the numerical results by comparison with model tests.

Van Gent and Van Oossanen [24] introduced their lifting line design method for the wake adapted propeller based on the precalculated hydrodynamic pitch using the Van Manen [25] criterion and induced velocities calculated using Lerbs' induction factors.

Koumbis [6] extended Glover's approach to obtain the final balanced slipstream shape using a successive iteration process. The bound circulation distribution and the slipstream geometry are continuously changed and interact freely in order to form a new shape during the iteration process while satisfying Burrill's minimum energy loss condition. He also introduced a concentrated tip vortex of finite core

radius in order to improve the results. He suggested that the tip vortex core extends from $x = 0.96$ to 1.00 and that the resulting induced velocity at the tip is equal to that induced at $x = 0.95$ multiplied by a coefficient H_{Tip}. He further suggested that the induced axial velocity is zero outside of the tip vortex.

A different representation of the propeller wake [48], is based on the assumption that, after a short distance downstream, the free vortices shed at the center of the lifting line move outwards to wrap around the strong tip and boss vortices. This, commonly referred to as roll-up vortex wake model, basically consists of two concentrated helical vortices which carry the whole of the lifting line bound circulation downstream.

Cummings [26] showed that the ultimate tip vortex radius is approximately 85% of the propeller radius for various types of propellers and loading conditions, and insists that Glover's procedure will result in a rolled up geometry providing that successive computation is made, but this claim turns out to be untrue as a consequence of Koumbis' work.

Greeley and Kerwin [27] revised the former slipstream model by including the slipstream alignment procedure in which the trailing vortex lines in the transition slipstream region are located corresponding to the local flow. This revised slipstream model recognises partly the importance of vortex pitch and partly takes account of experimental results showing that the tip vortex was not completely rolled up. Again this procedure requires slipstream shape defining parameters.

Recently Hoshino [28] took an important step towards a better understanding of the trailing vortex problem by combining theoretical and experimental methods.

Using experimental results he defined polynomal expressions for the variation of slipstream contraction and pitch of the tip vortex. He then used these expressions in his propeller method and obtained results which are in good agreement with experimental data.

2.3 Propeller/Stator Combination

The propeller/stator combination is now gaining recognition as a propulsive device for the reduction of energy losses. Recently there has been considerable interest in this subject and a summary of the published works is given below.

In 1988 Kerwin et al. [22] presented a theoretical method for determining optimum circulation distributions for propeller/stator propulsor. This work included cavitation tunnel measurements for a given propeller running behind an axisymmetric and non-axisymmetric stator. In this study a 6% gain was predicted theoretically and confirmed experimentally. In the same year Mautner et al. [29] introduced a new design method for a stator upstream of the propeller by taking zero r.p.m for the forward propeller of the contrarotating propeller system. They demonstrated that the increase in efficiency is greater than 50% of that achieved by the contrarotating propeller. A propulsor designed using this method has been manufactured and tested on an axisymmetric, underwater vehicle. The test results showed a good agreement with the design predictions.

A theoretical method was developed to model a ducted propeller with stator by Hughes et al. [30]. Using this method a duct and a range of stators were designed to operate efficiently with an existing propeller. Experiments were carried out on the ducted propeller and stator combination and a good agreement between the

theoretical and experimental results was obtained.

Iketaha [33] developed a method for theoretical calculation of propulsive performance of the propeller/stator combination. In this combination a stator was located behind the propeller and covered with a ring. It was theoretically shown that a 5%-7% percent gain was performed by the application of the method.

In a recent paper Patience [23] presents a very useful current state of the art in Marine Propellers with emphasis upon developments over the last 20 years and moving market direction. In this review work, he categorised the stator as a reaction device and indicates its greater advantages compared to other propeller and flow devices. He draws attention to the flow controlling capability of an upstream stator and conjectures that in a properly designed system, the stator device could evolve into the basic propulsor to be expected for the future possibility with the added component of a duct.

In 1992, Gaafary and Mosaad [31] predicted the gain in propulsor efficiency due to the presence of an upstream stator using linearised lifting surface theory. They found that a 6% increase in propeller efficiency and the results showed a good agreement with those obtained by theoretical and experimental work at MIT [22].

Coney [32] has extended the work described in [22] and developed a new design method for determining the optimum circulation distribution for both single and multiple stage propulsors. The lifting line model was used for the design. A good result was obtained from the application of the method. An attempt was also made in the same year by Chen [34] to develop a design method for postswirl propulsors.

A description of the lifting line procedure for the design of upstream and downstream stator was given by Glover [3]. In his work, the influence of the number of stator blades, variations in stator load factor and axial separation of the propeller and stator were investigated. This work showed that the combination of the propeller and a downstream stator was more efficient than the combination of the propeller and an upstream stator for the same number of stator blades. The gain was about 3.5%-4.5% for the propeller/upstream propulsors and 4.5%-6% for the propeller/downstream propulsors.

2.4 Potential Flow and Boundary Layer

As is well known the flow around a body, moving with a constant velocity on the otherwise undisturbed free surface of a fluid, can only be computed by adopting certain assumptions. Although the basic assumptions allow us to formulate the problem within the framework of the classical potential theory, the existence of a free surface and the representation of the body surface create additional problems, which necessitate some further simplifications.

Generally a solution for the potential flow about a body leads to a solution of the Laplace equation subject to the boundary condition that the velocity normal to the body surface be zero. The potential due to a surface distribution of singularities, may be written in form of a Fredholm integral equation of the second kind which is a solution to the Neumann problem. Smith and Pierce [18] at the Douglas Aircraft company used a set of linear algebraic equations to solve this integration. Hess and Smith [17, 19] extended the Douglas-Neumann program to include non-lifting three dimensional flows and the methods of surface source distribution have been applied to various problems.

The original approach by Hess and Smith does not include the free surface effect and hence gives the solution of the Neumann problem for a given form and its image, (i.e. Double model in a infinite fluid). In order to improve the accuracy of the result obtained from the Neumann problem, Brard [35], and many others studied the Neumann-Kelvin problem which again takes the exact body surface in its linearised form.

In most of the source distribution methods, the body surface is replaced by quadrilateral elements or facets. One of the major drawbacks of this approximation is that the planes formed by all four corners of each element do not necessarily match the real body surface hence, either a discontinuity will occur on the source surface or the centroids of each element will form a different body shape than the original one. This statement becomes particularly significant at highly curved regions. In order to avoid such errors it is possible to

- increase the number of elements and hence reduce the element sizes,
- employ curved surface elements with variable source density as is investigated by Hess [21],
- use triangular surface elements, Webster [36].

As is expected any increase in the number of surface elements will increase the computer time. The second alternative, the use of higher-order surface elements, has also its own drawbacks. Having considered these alternatives it was decided that the body surface should be discretised by using quadrilateral flat elements and that more elements should be introduced in regions of high body surface curvature. Therefore the Hess-Smith method is chosen to define the velocities around the body.

The potential flow solution gives the velocity and pressure distribution around the body, together with the characteristics related to body geometry, i.e. coordinates of the control points, areas, components of the unit normal vectors etc. The results from the potential flow solution can be used for the boundary layer calculation.

Available methods for calculating boundary layer equations may be divided into two groups; integral methods and differential methods. In the integral methods the main interest lies in the determination of the global properties of the shear layer and hence the momentum transport equations are integrated in the normal direction thus reducing the number of unknowns by one. Distribution of the properties across the shear layer are determined by means of empirical expressions derived from the experimental data. Differential methods on the other hand deal with the spatial variation of the properties by solving the momentum transport equations for a thin shear layer (TSL) together with some additional equations. These additional equations are introduced to model the transport of Reynolds stress and to achieve the closure, that is to make the number of variables equal to the number of equations. In the present work thin shear equations have been used to predict the flow around the body. The method, given by Cebeci [39], is chosen to obtain the solution of these equations. A description of the method will be given in the next chapter.

Chapter III

Flow around and in the Wake of a Body

3.1 Introduction

Knowledge of the flowfield into, around and behind a marine propeller is essential and important from the point view of propeller design and analysis. The flow into the propeller and in its slipstream depends on the form of the body behind which the propeller operates. Accurate determination of the flow around and behind the body is therefore of prime importance. An efficient way of computing the flow around a body is to divide the flow into different regions, applying in each region the most efficient method available. Interactions between the regions, including the influence of the operating propeller, have to be considered.

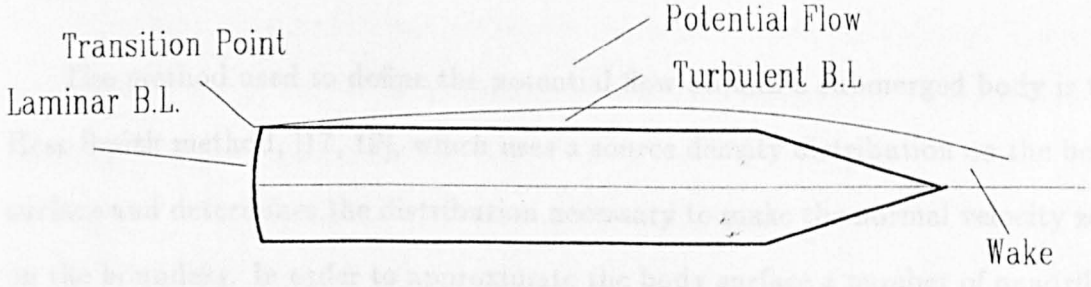

Figure 3.1 — The Flow around a Submerged Body

A fundamental picture of the flow around a deeply submerged body is shown in Figure 3.1. Two main regions may be distinguished: One adjacent to the body surface, extending backwards, and one outside this region. The former is usually referred to as the boundary layer, while the latter is called the potential flow. There is one major difference between the two: viscosity may be neglected in the potential flow, while it has a strong effect on the boundary layer.

For the evaluation of the flow characteristics, it is necessary to start with the potential flow solution so that the velocity distribution on the body can be calculated. These results are then used as a basis of determining the viscous flow around the body, which is in general, much different from the potential flow. Although the interest is confined to the flow into the propeller plane and slipstream of a body of revolution, the methods used are general enough to be utilised for other aims.

3.2 Potential Flow

3.2.1 Introduction

The method used to define the potential flow around a submerged body is the Hess-Smith method, [17, 19], which uses a source density distribution on the body surface and determines the distribution necessary to make the normal velocity zero on the boundary. In order to approximate the body surface a number of quadrilateral source panels are used. Having solved for the unknown source densities, the flow velocities at the points on and off the body surface can be calculated. In the following section the procedure will be described briefly, the detailed procedure of the formulation can be found in [17].

3.2.2 Fundamental Concepts

A fluid is generally defined as a substance which continues to deform in the presence of any shearing stress. The laws of fluid motion are applicable to flows of any medium so long as the same properties are involved. Fluids possess a sub-microscopic molecular structure in which elementary particles are in continuous motion through relatively large expanses of empty space. The details of such motion are often of primary importance, particularly if the scale of the motion is very small or the pressure very low. In most studies of fluid flows, however, neither the molecular structure nor molecular movement as such is of specific interest, and a greatly simplified yet highly useful picture can then be obtained by assuming that the fluid under study is continuous even to the infinitesimal limit. Under the assumed conditions, not only the fluid properties but such characteristics as velocity and pressure can be regarded as continuously variable throughout the region of flow, and can be defined mathematically at any particular point. This approach is taken not only for the resultant simplicity of analysis, but also because the behaviour of the individual molecules whose properties are varying. Therefore the average properties of the molecules in a small parcel of fluid are used as the properties of the continuous material.

In the potential flow problem, it is assumed that there exists a scalar function that satisfies Laplace's equation in the fluid domain. The fluid characteristics, such as the velocity and pressure, at any point in the fluid can be explicitly described in terms of this function. In order for such a scalar function to exist the following assumptions should be made

- The fluid is incompressible

$$\nabla.V = 0 \tag{3.1}$$

where V is the flow velocity

- The fluid is irrotational

$$\nabla \times V = 0 \tag{3.2}$$

- The fluid is inviscid and homogeneous.

3.2.3 Flow Governing Equation

From the law of mass and momentum conservation, the velocity V and the pressure P must be obtained simultaneously. However, the pressure P is taken to be the required independent variable. Thus the problem is obtaining the velocity V under the given pressure field.

The law of conservation of mass forms the basis of what is called the principle of continuity. This principle states that the rate of increase of the fluid mass contained within a given space must be equal to the difference between the rates of influx into and efflux out of the space. The assumption of a continuous fluid medium then permits this principle to be expressed in differential form.

If the velocity of flow of a fluid in three dimensions is denoted by V, and the mass density of the fluid at a point by $\rho(x, y, z)$, then the vector $Q = \rho V$ has the same direction as the flow and has a magnitude Q numerically equal to the rate of the flow of the fluid mass through the unit area perpendicular to the direction of the flow. The differential rate of the flow through a directed element of surface area $dA = ndA$ is then given by $A.dA = Q.ndA$, this quantity being positive if the

projection of Q on the vector n is positive. In particular, if dA is an element of a closed surface then $Q.dA$ is positive if the flow is outward from the surface. The components of Q are

$$Q = Q_x i + Q_y j + Q_z k \tag{3.3}$$

Taking a small closed differential element of volume which consists of rectangles with one vertex at $[x, y, x]$ and with edges dx, dy, dz parallel to the coordinate axes, the left-hand face is then represented by the differential surface vector, $jdxdz$, and the differential rate of the flow through this face is given by

$$Q.(-jdxdz) = -Q_y dxdz \tag{3.4}$$

the negative sign indicating that if Q_y is positive, the direction of flow through this face is into the volume element. Similarly, the differential rate of the flow through the right-hand face is given by

$$Q_{y+dy}.(jdxdz) = (Q_y + \frac{\partial Q_y}{\partial y} dy)dxdz \tag{3.4}$$

If the remaining four faces are treated in the same manner, the resulting differential rate of the flow outward from the volume element $dT = dxdydz$ is given by

$$dF = (\frac{\partial Q_x}{\partial x} + \frac{\partial Q_y}{\partial y}\frac{\partial Q_z}{\partial z})dxdydz \tag{3.5}$$

or

$$dF = (\nabla.Q)dT \tag{3.6}$$

Thus, the divergence of Q at point $[x, y, z]$ can be said to represent the rate of the fluid flow, per unit volume, outward from a differential volume associated with the point $[x, y, z]$, or to be the rate of decrease of the mass per unit volume in the neighbourhood of the point. If no mass is added to or subtracted from the element dT, the following relation is obtained,

$$\nabla.Q = -\frac{\partial \rho}{\partial t} \tag{3.7}$$

where ρ denotes the mass density of the fluid.

For an incompressible fluid $\rho = constant$, hence

$$\nabla.Q = \rho \nabla.V = 0 \tag{3.8}$$

It has been assumed here that no mass is introduced into, or taken from the system, that is, there are no points in the element dT where the fluid is added to or withdrawn from the system. If such points are assumed to be present, a vector V with non-zero divergence can be considered as a velocity vector of an incompressible fluid in a region. Points at which fluid is added to or taken from the system are referred to as source and sinks respectively.

If V is continuously differentiable in a simply connected region R and if $\nabla \times V = 0$ at all points in R, then a scalar function ϕ exists such that $d\phi = Vdr$. In other words, if $\nabla \times V = 0$ in a region, then V is the gradient of a scalar function ϕ in that region.

$$V = \nabla \phi \tag{3.9}$$

where, ϕ is called velocity potential. Flows derived from ϕ are referred to as potential flow. An important observation pertaining to Equation 3.9 is that a vector function V may be exchanged for a single scalar function ϕ, if the motion is irrotational. In general, a vector function contains three scalar functions which are the components of the vector, so substitution of $\nabla\phi$ for V should simplify the equations of motion. If the fluid is incompressible and there is no distribution of sources or sinks in the region, we have

$$\nabla.V = 0 \qquad 3.10$$

Combining Equations 3.9 and 3.10,

$$\nabla.V = \nabla.\nabla\phi = \nabla^2\phi = 0 \qquad (3.11)$$

That is, in the flow of an incompressible irrotational fluid without distributed sources and sinks, the velocity vector is the gradient of a potential ϕ which satisfies the Laplace equation,

$$\nabla^2\phi = 0 \qquad or \qquad \frac{\partial\phi}{\partial x^2} + \frac{\partial\phi}{\partial y^2} + \frac{\partial\phi}{\partial z^2} = 0 \qquad (3.11)$$

This equation will be solved with the appropriate boundary conditions for some particular problem.

If sources and sinks exist in an irrotational flow of incompressible ideal fluid one obtains Poisson's equation,

$$\nabla^2\phi = m \qquad (3.12)$$

where m the strength of the source or sink. The particular solution of this equation is

$$\phi(p) = -\frac{1}{r(p,q)}\frac{m(q)}{4\pi}dV(q) \tag{3.13}$$

where $\phi(p)$ is the potential at a point p generated by a source or sink.

If boundaries are represented with source or sinks, the disturbance in the flow field due to these singularities will be the sum of the contribution from each singularity. In the flow domain (outside the distributed singularities), however, the Laplace equation still holds as there are no singularities present in that regime.

3.2.4 Boundary Conditions

The behaviour of quantities on the existing boundaries is determined usually from physical reasoning such as the vanishing normal velocity condition on a solid boundary when there is a relative velocity between the body and the surrounding fluid. This is possible when the nature of the field and the boundary concerned are of simple character but if either or both of them are not simple, it may not be easy to decide by physical insight what conditions must be applied. The partial differential equation representing a field is frequently common in form in many physical situations and for a given field an identical form governs it regardless of some important physical parameters involved such as boundary shape or initial state. These physical parameters, the so called boundary conditions, make an individual problem unique and choose "the solution" out of arbitrary functions of some argument or an infinite number of possible solutions of the field equation.

The distribution of the field quantity inside the domain is constrained to some extent by that along the boundaries. In other words, it adjusts itself to be com-

patible with the given environment. It is therefore of great interest to expound the manner by which the field quantity adjusts itself at the boundary and its effect on the rest of the field in the expectation that the same principles would hold for any problem under the same circumstances. In this connection, the type of boundary conditions are:

- Cauchy boundary condition specifies both field value and normal gradients on the boundary.

- Dirichlet boundary condition specifies only the field value, if it were zero everywhere on the boundary the condition would be homogeneous, otherwise inhomogeneous.

- Neumann boundary condition specifies only the normal gradient, and again homogeneous and inhomogeneous Neumann conditions are defined in the same way as above.

- Mixed boundary condition specifies a linear combination of field value and normal gradient homogeneously or inhomogeneously.

The application of a particular type of boundary condition has a different effect on the solution depending on the type of the field equation.

When a flow field is governed by the Laplace equation of velocity potential the relevant boundary condition is usually the homogeneous Neumann condition stating that there is no flux of fluid across a solid boundary. That is, at each control point of the source panels, the normal component of the induced velocity potential satisfies the tangential velocity condition.

The boundary condition on the body surface is

$$\phi_n = 0 \tag{3.14}$$

This means that the streamlines are all tangential to the surface and the normal component of the velocity must be zero.

3.2.5 Method of Solution

The surface of the body is replaced by a number of quadrilateral source panels. The solution is constructed in terms of the source strengths on the surface. The integral equation for the source strengths is approximated by a matrix equation on the assumption of uniform strength on each panel. The strength of each source panel is chosen so that the normal component of the velocity is zero at the centroid of each quadrilateral.

When the whole flow domain is envisaged to be wrapped by sources and sinks, the singularities have the strengths adequate to produce the freestream condition. This original undisturbed free stream is characterised by the unique velocity which is constant everywhere in the domain. When the body is put into the flow, the freestream will be disturbed by the existence of the sources. The potential due to the sources is called the disturbance potential, ϕ_d.

Consider a unit point source located at a point q whose cartesian coordinates are $[x', y', z']$ then at a point p, whose coordinates are $[x, y, z]$, the potential due to this source is

$$\phi_d = \frac{1}{r(p,q)} \tag{3.15}$$

where r(p,q) is the distance between p and q,

$$r(p,q) = [(x-x')^2 + (y-y')^2 + (z-z')^2]^{\frac{1}{2}}$$

If the local intensity of the distribution is denoted by $\sigma(q)$, where the source point q now denotes a general point of the surface A, then the potential of the distribution is

$$\phi_d = \int_A \frac{\sigma(q)}{r(p,q)} dA(q) \tag{3.16}$$

The flow can be described then as sum of a freestream flow at infinity plus a flow induced by source surface.

$$\phi = \phi_\infty + \phi_d \tag{3.17}$$

where ϕ_∞ is freestream potential.

Then the velocity must satisfy the normal velocity boundary condition on the surface A.

$$\left.\begin{aligned} V_n &= -n(p)[\nabla\phi_n(p)] \\ &= n(p).U_\infty + \int_A n(p)\frac{p-q}{r^3(p,q)}\sigma(q)dA(q) \\ &= 0 \end{aligned}\right\} \tag{3.18}$$

where the $n(p)$ is the unit outward normal vector at point p due to the unit source at the point q.

When q approaches p along the local normal direction, the principal part $2\pi\sigma(p)$ must be extracted in this case,

$$n(p).U_\infty + 2\pi\sigma(p) + \int_A n(p)\frac{p-q}{r^3(p,q)}\sigma(q)dA(q) = 0 \tag{3.19}$$

3.2.6 Discretization

The rather arbitrary shape of the boundary surfaces prevents the construction of a simple functional expression to represent them, which in turn, makes it impractical to express the source strengths in an explicit functional form. Therefore, an attempt is made to express the continuous variation of source strengths on the surfaces by a set of numerical values at a finite number of points representing the surface.

The body surface is replaced by a number of plane elements, the dimensions of which are small in comparison with the body. The value of the source density over each of the panels is assumed to be constant. The total disturbance potential can be found from the equation below,

$$\phi(p) = \sum_{j=1}^{N} \sigma_j \int_{A_j} \frac{1}{r(p,q)} dA(q) \tag{3.20}$$

Where N is the number of panels on the body surface, A_j is the area of j^{th} panel and σ_j is the source strength of j^{th} panel.

A set of simultaneous equation can be constructed in terms of N unknown source strengths. The N simultaneous equations can be set up by applying the boundary conditions on each of the panels, more specifically at each control point of the panels.

Because of the singular behaviour, the induced velocity at a control point on the source panel itself is $2\pi\sigma$. Thus the disturbance velocity will be

$$v_d(p_i) = (2\pi\sigma_i)n_i + \sum_{j=1_{j\neq i}}^{N} \sigma_j \int_{A_j} \frac{p-q}{r^3(p,q)} dA(q) \tag{3.21}$$

Let us define matrices $u(i,j)$, $v(i,j)$ and $w(i,j)$ as follow

When $j \neq i$

$$\left.\begin{aligned} u(i,j) &= \int_{A_j} \frac{x_i - x'}{r^3(p,q)} dA(q) \\ v(i,j) &= \int_{A_j} \frac{y_i - y'}{r^3(p,q)} dA(q) \\ w(i,j) &= \int_{A_j} \frac{z_i - z'}{r^3(p,q)} dA(q) \end{aligned}\right\} \tag{3.22}$$

when $j = i$

$$\left.\begin{aligned} u(i,j) &= 2\pi n_{xi} \\ v(i,j) &= 2\pi n_{yi} \\ w(i,j) &= 2\pi n_{zi} \end{aligned}\right\} \tag{3.23}$$

where n_{xi}, n_{yi} and n_{zi} are the components of n along the x, y and z directions respectively. These matrices U, V and W are the components of the induced velocity at the i^{th} control points by the j^{th} source panel of unit strength and will be called the induced velocity matrices. Equation 3.21 can be written in terms of the induced velocity matrices.

$$v_i = \sum_{j=1}^{N} [u(i,j)i + v(i,j)j + w(i,j)k]\sigma_j \tag{3.23}$$

When the body surface boundary condition is applied on the i^{th} panel for

instance, the following equation is obtained.

$$\left.\begin{aligned} n_i.V_i &= (n_{xi}i + n_{yi}j + n_{zi}k) \\ &.[(U_\infty i + u_i)i + (V_\infty i + v_i)j + (W_\infty i + w_i)k] \\ &= n_{xi}U_\infty + n_{yi}V_\infty + n_{zi}W_\infty \\ &+ \sum_{j=1}^{N}[n_{xi}u(i,j) + n_{yi}v(i,j) + n_{zi}w(i,j)]\sigma_j \\ &= 0 \end{aligned}\right\} \quad (3.24)$$

If the induced normal velocity matrix, $A(i,j)$, is defined as

$$A(i,j) = n_{xi}u(i,j) + n_{yi}v(i,j) + n_{zi}w(i,j) \quad (3.25)$$

the following equation is obtained.

$$\sum_{j=1}^{N} A(i,j)\sigma_j = -(n_{xi}U_\infty + n_{yi}V_\infty + n_{zi}W_\infty) \quad (3.25)$$

When applied to all of the N panels this equation will yield N simultaneous equation for N unknown values of σ's. In the matrix form this system of simultaneous equation is

$$\begin{pmatrix} A(1,1) & A(1,2) & \dots & A(1,N) \\ A(2,1) & A(2,2) & \dots & A(2,N) \\ \vdots & \vdots & \ddots & \vdots \\ A(N,1) & A(N,2) & \dots & A(N,N) \end{pmatrix} \begin{pmatrix} \sigma_1 \\ \sigma_2 \\ \vdots \\ \sigma_N \end{pmatrix} = \begin{pmatrix} n_{x1}U_\infty + n_{y1}V_\infty + n_{z1}W_\infty \\ n_{x2}U_\infty + n_{y2}V_\infty + n_{z2}W_\infty \\ \vdots \\ n_{xN}U_\infty + n_{yN}V_\infty + n_{zN}W_\infty \end{pmatrix} \quad (3.26)$$

If the geometry of the body were known, the equations could be solved without difficulty as the column vector on the left hand side is the only unknown. Having calculated the value of σ_j, the flow velocity at any point P can be calculated as follows;

$$V_p = V_\infty + \sum_{j=1}^{N} \sigma_j \nabla \phi_d \tag{3.27}$$

3.3 Boundary Layer

3.3.1 General

By the boundary layer (B.L.) is meant the region of fluid close to a solid body where, owing to viscosity, the transverse gradients of velocity are large as compared with the longitudinal variations, and the shear stress is significant. The boundary layer may be laminar, turbulent, or transitional, and sometimes called the frictional belt.

When there is a homogeneous flow along a flat plate, the velocity of the fluid just at the surface of the plate will be zero owing to frictional forces, which retard the motion of the fluid in a thin layer near to plate. In the boundary layer the velocity of the fluid U increases from zero at the plate to its maximum value, which corresponds to the velocity in the external frictionless flow U_∞, Figure 3.2

If the shape of the outer surface of the boundary layer is known, analysis of the flow outside the boundary layer as potential flow is possible. We can predict accurately its characteristics and these will be relevant to the real flow. When the boundary layer is very thin, as it is when the streamlines outside it converge, the solid surface itself may be used as an approximation for the outer edge, and

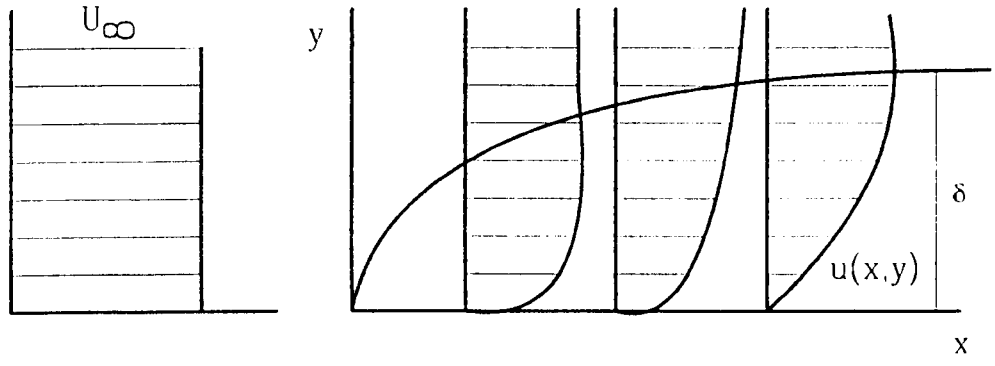

Figure 3.2 — Boundary Layer along a Plane Surface

the potential flow analysed before the thickness of the boundary layer is known. Boundary layer theory also provide qualitative explanations for the aspects of the flow, such as separation and form drag, which are not entirely amenable to calculation. The crux of the matter is that the boundary layer is thin. Only then is it valid to divide the whole region of the flow into two parts: the boundary layer and the potential flow outside it.

3.3.2 Laminar and Turbulent Flow

In a laminar flow a fluid moves in laminas or layers. The layers do not mix transversely but slide over one another at relative speeds, which varies across the flow.

In turbulent flow the fluid's velocity components have random fluctuations. The flow is broken down and the fluid is mixed transversely in eddying motion.

The flow is broken down and the fluid is mixed transversely in eddying motion. The velocity of the flow has to be considered as the mean value of velocities of the particles.

Factors that determine whether a flow is laminar or turbulent are the fluid, the velocity, the form and the size of the body placed in the flow, the depth of water and if the flow is in a channel, the channel configuration and size. Both laminar and turbulent flows occur in nature, but turbulent form is the more common. As the velocity increases, the flow will change from laminar to turbulent, passing through a transition regime. The transition takes place at a Reynolds number $R_n = 10^5 - 10^6$. Thus in model experiments the flow over an unknown area of the model can be laminar, which means that the experiment's accuracy is often not as good as is wanted. The effects of viscosity are present in turbulent flow, but they are usually masked by the dominant turbulent shear stresses.

3.3.3 Boundary Layer Characteristics

The main effect of a boundary layer on the external flow is to displace the streamlines away from the surface in the direction of the surface normal. This occurs because the fluid near the surface is slowed down by viscous effects. In a two dimensional flow, the rate at which fluid mass passes the plane x=constant between $y = 0$ and $y = h$, where h is slightly larger than the boundary thickness, δ, is

$$\int_0^h \rho u dy \qquad 3.28$$

per unit distance in the z (spanwise) direction, where ρ is the density of and u is an internal stream of velocity. In the absence of a boundary layer, u will be equal

to the external stream velocity, u_e and $\rho = \rho_e$. Therefore, the reduction in mass flow rate per unit span between $y = 0$ and $y = h$ caused by the presence of the boundary layer is

$$\int_0^h (\rho_e u_e - \rho u) dy \tag{3.29}$$

The thickness in the y direction of a layer of external stream fluid carrying this mass flow per unit span in constant density flow is

$$\delta^* = \int_0^h (1 - \frac{u}{u_e}) dy \tag{3.30}$$

This is the distance by which the external-flow streamlines are displaced in the y direction by the presence of the boundary layer and is called the displacement thickness.

The thickness of a layer of external stream fluid carrying a momentum flow rate equal to the reduction in momentum flow rate is defined as the momentum thickness, θ and can be expressed as follows:

$$\theta = \int_0^h \frac{u}{u_e}(1 - \frac{u}{u_e}) dy \tag{3.31}$$

The velocity inside of the boundary layer is calculated by the power-law assumption:

$$\left.\begin{aligned} n &= \frac{2}{(H-1)} \\ \frac{\delta^*}{\delta} &= \frac{1}{(n+1)} \\ \frac{u(\delta)}{u_e} &= (\frac{y(\delta)}{\delta})^{1/7} \end{aligned}\right\} \tag{3.32}$$

where H is the shape parameter.

3.3.4 Determination of the B.L. Characteristics

Solving shear layer equations or simply using empirical formulas provides the characteristics of the boundary layer, e.g. displacement thickness, momentum thickness and skin friction.

In this work the thin-shear-layer (TSL) approximation for two dimensional flow is used since it is a simplified form of the Navier-Stokes equations. TSL equations are valid when the ratio of the shear layer thickness, δ, to the streamwise length of the flow, l, is very small. These equations are written for two dimensional incompressible flows with eddy viscosity concept:

$$\left.\begin{aligned} u\frac{\partial u}{\partial x} + v\frac{\partial u}{\partial y} &= -\frac{1}{\rho}\frac{\partial p}{\partial x} + \frac{1}{\rho}\frac{\partial}{\partial y}[\mu\frac{\partial u}{\partial y} - \rho u'v'] \\ \frac{\partial u}{\partial x} + \frac{\partial v}{\partial y} &= 0 \\ \frac{\partial p}{\partial y} &= 0 \end{aligned}\right\} \tag{3.33}$$

where μ is the viscosity, and p is pressure.

A numerical procedure for the solution of the TSL equations and its source program are given in [39]. This program has been modified for the present use. The laminar and turbulent boundary layer are calculated by starting the calculations at the forward stagnation point of the body with a given external velocity distribution and a given transition point where the turbulent flow starts. Having run the program, δ^*, θ and H are obtained. Using Equation 3.32 the boundary layer thickness and velocities inside of the boundary layer are calculated.

3.4 Interactions

Interaction Between the Boundary Layer and Potential Flow

The boundary layer moves the streamlines away from the body surface and a new body geometry is generated by adding the local displacement thickness to the original body geometry. This body will be called the displacement body, Figure 3.3.

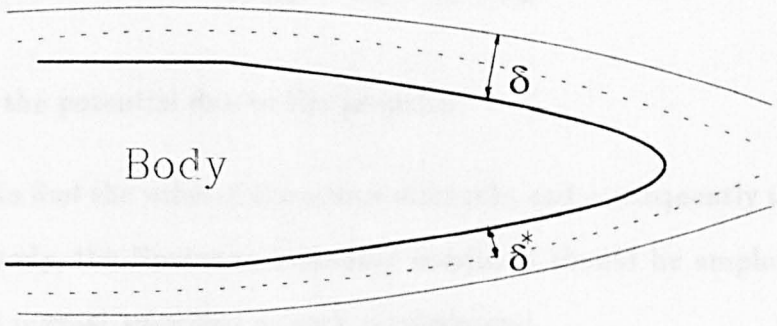

Figure 3.3 — Displacement Body Outline

The outline of the displacement body can be found by an iteration as follows:

1. Calculate the inviscid flow around the body by potential flow theory.

2.Using the external velocity obtained from step 1 , calculate the displacement thickness by TSL method.

3. Add δ^* , obtained from step 2, to the body shape to form a new displacement surface and recalculate the potential flow. Repeat steps 2 and 3 until the results converge.

Interaction Between the Propeller and Body

The flow for a body with an operating propeller can be described as the sum of the freestream flow plus the flow induced by propeller and panels. The total potential velocity can be written by

$$\phi_{Total} = \phi_\infty + \phi_d + \phi_{pr} \tag{3.34}$$

where ϕ_{pr} is the potential due to the propeller.

In order to find the value of the source strengths and consequently the velocities around the body, the Neumann boundary condition should be employed in order to cancel the normal velocities at each quadrilateral.

$$\frac{\partial \phi_{Total}}{\partial n} = V_n = 0$$

or

$$V_n = u_\infty \cdot n + [\sum_{j=1}^{N} \sigma_j \nabla \phi_d] \cdot n + u_{n_{pr}} \tag{3.35}$$

where $u_{n_{pr}}$ is normal velocity induced by the propeller on each panel.

The solution of the above equation gives the new value of the source strengths. The total velocity then becomes

$$V = V_\infty + V_{pr} + \sum_{j=1}^{N} \sigma_j \nabla \phi_d \tag{3.36}$$

The achievement of the above procedures can be arranged as follows: Initially the potential flow and boundary layer is calculated and nominal velocity distribution is found. Using this nominal wake for the propeller design procedure, the velocity induced by the propeller is obtained for appropriate points on the panels. The effect of the propeller is assumed to be potential and hence the source strengths on the surface of the body are modified to account for the propeller induced normal velocities. This modified potential flow is then used for the estimation of boundary layer and displacement thickness and a original body is replaced by the displacement body. Using this newly created body the potential flow and boundary layer theories are applied taking account of the propeller induction effect. This process is repeated until the newly obtained wake is equal the previous one, Figure 3.4.

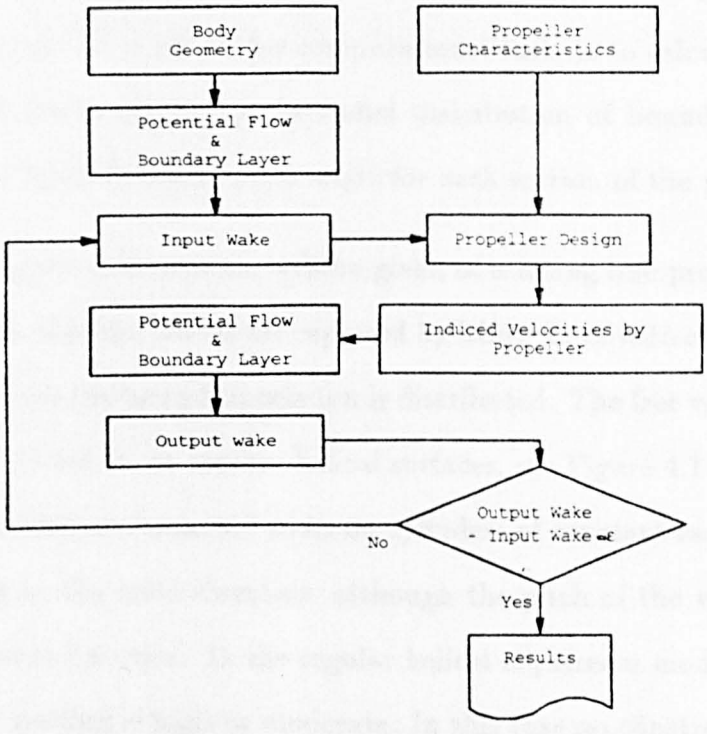

Figure 3.4 — Flow Chart for Interaction between the Flows

Chapter IV

The Conventional Lifting Line Model of Propeller Action

4.1 Introduction

The design of the marine propeller is a subject that has received the attention of many researchers during the last century as evidenced from the large numbers of papers and reports in the technical literature. One of these methods called lifting line theory is widely used in propeller design [1, 2, 5, 6, 23, 37, 40, 44, 45].

In the theory one of the major computational tasks is to calculate the induced velocities and hence determine the radial distribution of bound circulation, lift coefficient and hydrodynamic pitch angle for each section of the propeller blade.

In this chapter a description will be given of a lifting line procedure based on the assumption that the blades are replaced by lifting lines with zero thickness and width along which the bound circulation is distributed. The free vortex sheets shed from the lifting lines lie on regular helical surfaces, see Figure 4.1. In other words, the trailing vortices are assumed to lie on cylinders of constant radius and to be of constant pitch in the axial direction, although the pitch of the vortex sheets can vary in the radial direction. In the regular helical slipstream model, it is assumed that propeller loading is light or moderate. In this case no slipstream deformation is taken into account. In the next chapter a new design method will be introduced to take account of the local flow and induced velocities along the slipstream and the resultant slipstream deformation. Before explaining the lifting line

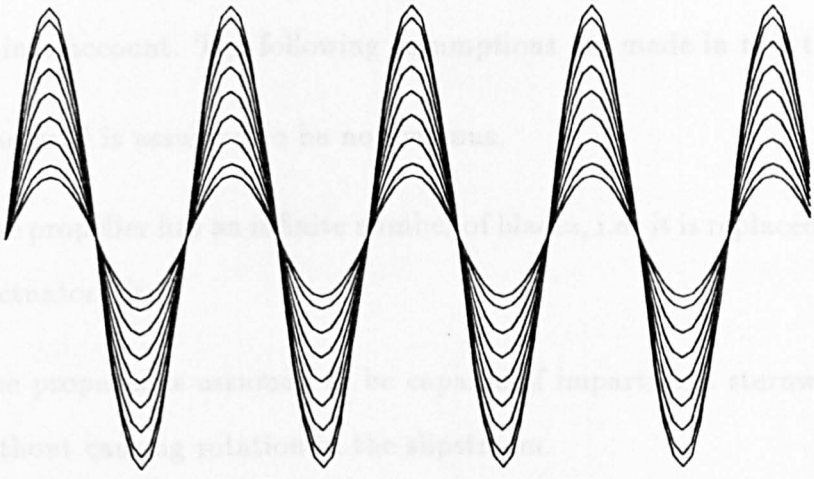

Figure 4.1 — Regular Helical Slipstream

procedure, it is better to give some explanation of the basic theories such as momentum theory, blade element theory and circulation theory which have been building bricks in the later development of the advanced propeller theories.

4.2 Momentum Theory

The first rational theory of propeller action was developed by Rankine and R.E Froude [11, 12]. The theory is based on the concept that the hydrodynamic forces on the propeller blades are due to momentum changes which occur in the region of the fluid acted upon by the propeller. This region of fluid forms a circular column which is acted upon by a disc representing the propeller and which forms what is termed the "slipstream" of the propeller. The slipstream has both an axial and angular motion; in the simple momentum theory only the axial motion

is considered, while in the extended momentum theory the angular motion also is taken into account. The following assumptions are made in this theory:

- The fluid is assumed to be non-viscous,
- The propeller has an infinite number of blades, i.e. it is replaced by the so-called "actuator disc".
- The propeller is assumed to be capable of imparting a sternward axial thrust without causing rotation in the slipstream.
- The thrust is assumed to be uniformly distributed over the disk area.

The important result derived from this theory is that the axial induced velocity at the propeller plane is one half of its value at infinity downstream. This can be proven from the simple Bernoulli equation as re-stated in Equation 4.1 through Equation 4.4 with the aid of Figure 4.2.

Behind the propeller the equation can be written as;

$$\frac{1}{2}\rho V_2^2 + P_0 = \frac{1}{2}\rho V_1^2 + P_A \tag{4.1}$$

where $V_2 = V_0 + u_a$

Forward of the propeller the equation can be written as;

$$\frac{1}{2}\rho V_0^2 + P_0 = \frac{1}{2}\rho V_1^2 + P_F \tag{4.2}$$

Therefore the increase in pressure at the disc is given by

$$P_A - P_F = \Delta P = \rho V_1 u_a \tag{4.3}$$

Having combined above equations, the following statement can be obtained

$$V_1 = V_0 + \frac{u_a}{2} \tag{4.4}$$

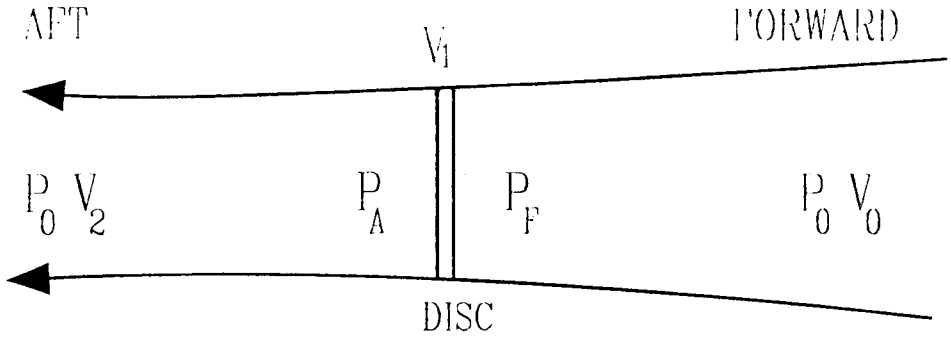

Figure 4.2 — Momentum Theory

4.3 Blade Element Theory

In the blade element theory, which is based on the early work by W. Froude [38] and others, each blade of the propeller is divided into a number of chordwise elements each of which is assumed to operate as if it were part of a hydrofoil, Figure 4.3.

As seen in Figure 4.4 the velocity of fluid relative to each blade element is the resultant of the axial and angular velocities. A torque Q is applied to the propeller by the driving shaft, and the propeller and shaft rotate at the rotational speed

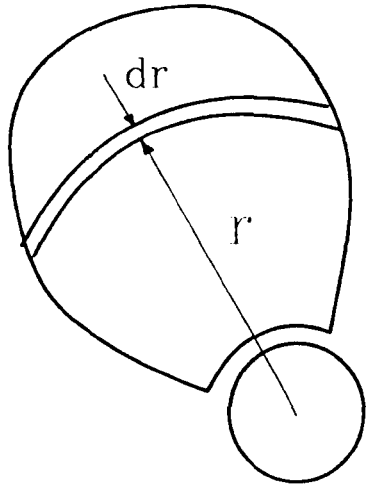

Figure 4.3 — Propeller Blade Definition

n. Consequently the blade section has a speed, $2\pi nr$, in the tangential direction and a speed of advance, V_a, in the axial direction. The hydrodynamic forces on each blade element are a lift force dL acting perpendicular to the direction of the resultant velocity, and a drag force dD opposing the movement of element and acting along the line of the resultant velocity, V_r

The blade section element forces at radius r are resolved in the axial and tangential directions, giving a blade element thrust dT and a blade element torque force dQ_F and hence a blade element torque dQ. The blade element thrust and torque values are integrated for all the blade elements to determine the overall thrust and torque of the propeller.

The blade element theory described above takes no account of the influence of

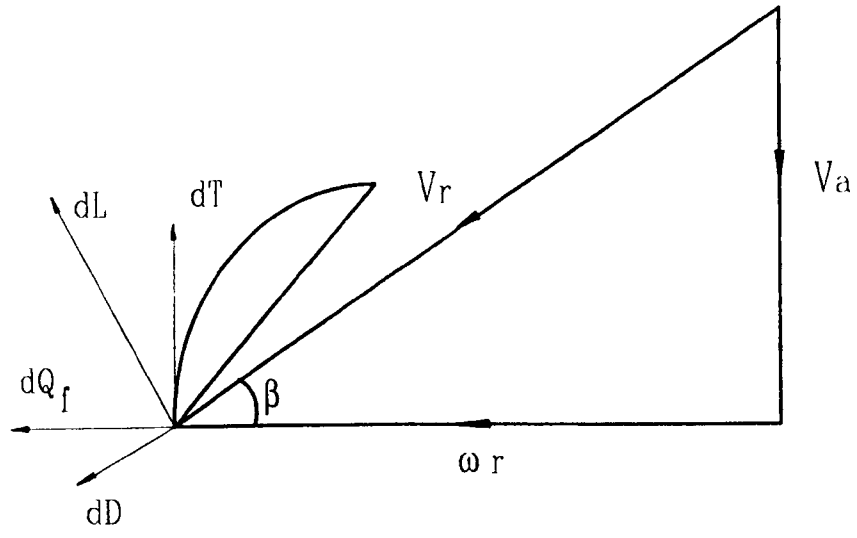

Figure 4.4 — Blade Element Theory

the propeller on the flow. This can be accounted for by introducing the axial and rotational induced velocity components, the existence of which is explained by the momentum theory, Figure 4.5. The direction of the resultant flow is modified by the presence of the induced velocities and now lies on a helical line defined by the hydrodynamic pitch angle, β_i.

However, the expressions for the induced velocities derived from the momentum theory relate to the actuator disc which is virtually an infinitely bladed propeller. The problem of accounting for the fact that the propeller has a finite number of blades is overcome by the introduction of the circulation or vortex theory of propeller action.

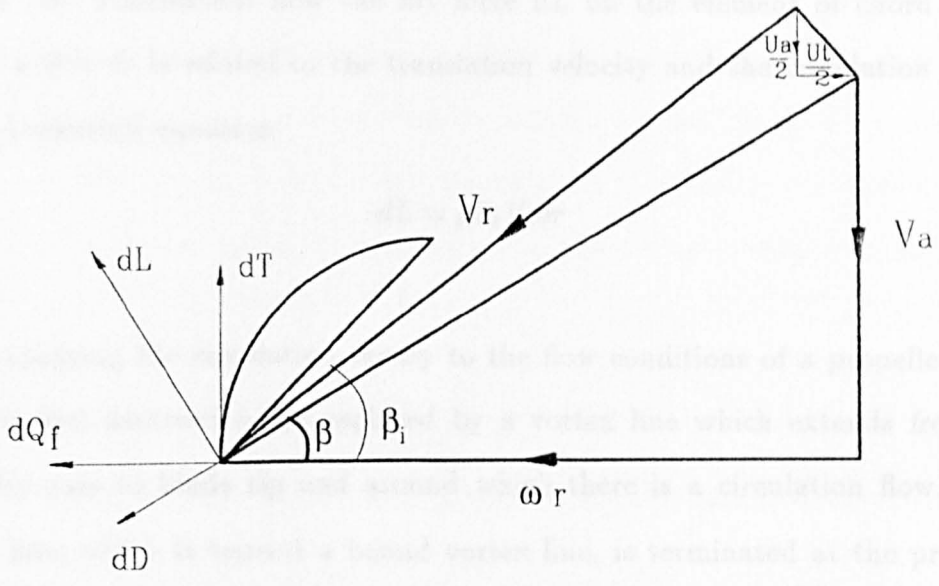

Figure 4.5 — Combined Momentum and Blade Element Theories

4.4 Circulation Theory

The circulation theory is based on a concept due to Lanchester [13] which states that the lift developed by the propeller blades is caused by the circulatory flow which is set up around the blades. This causes an increased local velocity across the back of the blade, and a reduced local velocity across the face of the blade. The fluid velocities relative to a blade element around which there is a circulatory flow in a non-viscous fluid can be specified by a translation velocity V_r together with a circulation velocity v_c. The circulation, Γ_r, around the element is defined as the line integral of the circulation velocity, v_c, around any path which encloses the element. Thus, for a given circulation, the circulation velocity diminishes with distance from the element.

For two dimensional flow the lift force dL on the element of chord length C and width dr is related to the translation velocity and the circulation by the Kutta-Joukowski equation

$$dL = \rho \Gamma_r V_r dr \tag{4.5}$$

In applying the circulation theory to the flow conditions of a propeller, each blade is first assumed to be replaced by a vortex line which extends from the propeller axis to blade tip and around which there is a circulation flow. This vortex line, which is termed a bound vortex line, is terminated at the propeller axis and blade tip by two trailing vortex lines. The axial vortex line follows a path along the propeller axis and the tip vortex line follows a helical path which traces out the boundary of the slipstream. If the circulation is constant from the propeller axis to the tip then the circulation of each trailing vortex line will be equal to that of the bound vortex line. If the circulation varies radially, as in the propeller case, then a system of trailing vortex lines of similar form to the tip vortex line is shed along the radial length of the blade, and the single bound vortex line is replaced by a series of bound vortex lines all extending from the propeller axis but each terminating at, and of circulation equal to, one of trailing vortex lines. This system of trailing vortex lines forms a helicoidal sheet associated with which is an induced velocity. If the slipstream contraction is neglected and if it is assumed that pitch of the vortex sheets is radially uniform it can be shown that the direction of the induced velocity is normal to the vortex sheet. However, in the more general case of non-uniform vortex sheet pitch, this "condition of normality" is not fulfilled. These induced velocities can be resolved into components in the axial, tangential and radial directions.

The first major problem to be overcome in deriving a vortex theory of propeller action is to build a model of the vortex distribution over the blade surface. The level of complexity of the problem can be reduced by the lifting line method in which a propeller section having a bound circulation Γ_r at radius r is replaced by a single point vortex and hence the entire blade can be represented by a single bound vortex line on the basis of zero blade width and thickness, as shown in Figure 4.6.

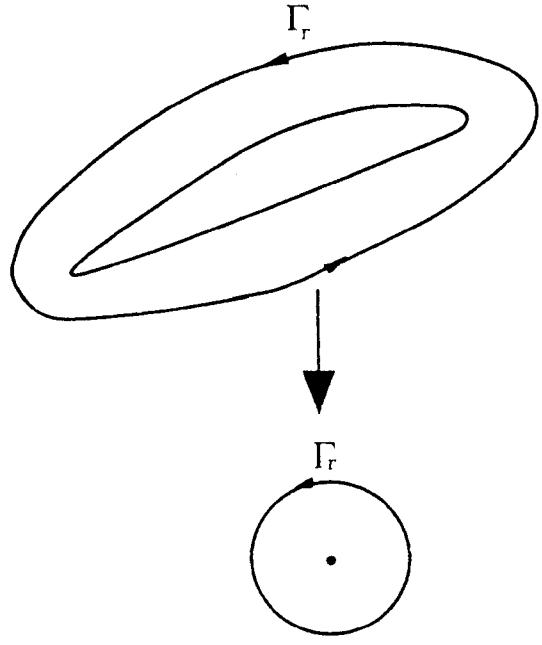

Figure 4.6 — The Replacement of the Blade Section by a Single Vortex

4.5 Lifting Line Design Method with Regular Helical Slipstream

4.5.1 Design Variables

Apart from some special cases propellers are normally designed to absorb the rated power of the machinery at the required rate of rotation. This implies that

two of the input design parameters are associated with the engine, while the other parameters are listed as follows:

- Engine brake power, P_B kw
- Shaft efficiency, η_s
- Delivered power, $P_D = P_B \times \eta_s$
- Propeller rate of rotation, N
- Ship speed, V_S
- Torque identity wake fraction, w_Q
- Number of blades, Z

Using these data and an appropriate $B_p - \delta$ diagram the optimum diameter, D, and the mean face pitch ratio of a "basic" propeller to satisfy the design condition can be determined.

The blade surface area required to minimise the risk of cavitation can be determined using a cavitation diagram, such as that due to Burrill [8]. The distribution of this area on an appropriate blade outline gives the blade chord widths at the design radii.

A simple stressing calculation can be used to calculate the blade section thickness and drag coefficients determined as function of the section thickness ratios.

The wake-adaptation of the design, i.e. optimisation with respect to the radial wake distribution in which the propeller is assumed to work, is then carried out

using the lifting line procedure.

In this procedure the above design conditions are represented by the requirement that the propeller should achieve a torque coefficient, K_Q, given by

$$K_Q = \frac{33.55 P_D}{[\frac{ND}{10}]^3 D^2} \tag{4.6}$$

Optimisation of the design, i.e. the determination of the radial loading distribution corresponding to maximum efficiency, is achieved by introducing a minimum energy loss condition into the solution of the lifting line model. In this work the condition derived by Burrill [9] is used, in which the vortex sheets on the ultimate wake are assumed to have uniform pitch radially, i.e. :

$$x_i \pi \tan \varepsilon_i = constant \tag{4.7}$$

where $x_i = r_i/R$ is the non-dimensional form of the i^{th} section radius, R is the propeller radius and ε_i is the pitch angle of helical vortex sheets at infinity.

4.5.2 Mathematical Model

In the development of the mathematical model of the propeller, a satisfactory formulation of the induced velocities is essential. In general there are two ways of obtaining the velocities induced on the lifting line by a regular helical vortex line. The first involves the solution of Laplace's differential equation whilst the second method is based on the use of the Biot-Savart Law to calculate the incremental velocity induced by a vortex element at any point. Then the total induced velocity at the point is calculated by numerically integrating the individual effects of the

elements constituting the vortex line.

The induced velocities calculated by either method are finite except for the case where the reference point lies on the vortex and especially, the leading end where the velocity components become infinite. The induction factors are introduced to overcome this difficulty. An induction factor is defined as the ratio of the velocity induced at a point by a semi-infinite helical vortex line to that induced by a semi-infinite straight vortex line of the same strength. They can be evaluated either by the solution of a partial differential equation subject to boundary conditions [16] or by the Biot-Savart method.

Based on the assumption that the circulation of the lifting line, or bound circulation, is assumed to go continuously to zero at both the tip and the boss, the associated expression for the circulation can be defined by a Fourier sine series and written in non-dimensional form as follows

$$G_i = \frac{\Gamma_i}{\pi D V_s} = \sum_{n=1}^{\infty} A_n \cdot \sin n\phi_i \tag{4.8}$$

Where Γ_i is the bound circulation at x_i and A_n is the bound circulation coefficient whose value is to be determined.

The angular coordinate, ϕ_i, is defined in terms the radial coordinate, x_i, as follows,

$$x_i = x_h + (\frac{1 - x_h}{2})(1 - \cos\phi_i) \tag{4.9}$$

Where x_h is the non-dimensional hub radius and ϕ_i varies from 0 at the hub to π at the tip.

The problem is now the determination of the unknown A_n's. Once these values

are calculated, the axial, tangential and radial induced velocities at any point of the lifting line can be estimated and finally the hydrodynamic pitch angle, lift coefficient and torque, thrust coefficient can be calculated.

At the ${x_i}^{th}$ radial lifting line location, a free vortex will be shed of strength

$$(\frac{dG}{dx}dx)_i \tag{4.10}$$

and circulation at the ${x_{i+dx}}^{th}$ radial location is

$$G_{x_{i+dx}} = G_{x_i} + (\frac{dG}{dx}dx)_i \tag{4.11}$$

The total velocity induced at a point at radius x_i by helical lines starting at points x_k can be given in terms of the induction factors as follows

$$u_{a,t,r} = \int_{x_h}^{1} I_{a,t,r}(\frac{dG}{dx})_k \frac{dx_k}{2(x_i - x_k)} \tag{4.12}$$

where I represents induction factors which depend only on the geometry of slipstream and can be calculated by the two methods mentioned earlier. The subscript a, t and r denote axial, tangential and radial components respectively.

For the induction factors Lerbs, [16], expressed analytical formulations as follows:

For the internal field ($x_i > x_k$)

$$\left.\begin{aligned} I_a &= -Z\frac{x_i}{x_k \tan\beta_k}\left(\frac{x_k}{x_i}-1\right)B_1 \\ I_t &= -Z\left(\frac{x_k}{x_i}-1\right)(1+B_1) \end{aligned}\right\} \tag{4.13}$$

For the external field ($x_i < x_k$)

$$\left.\begin{aligned} I_a &= Z\frac{x_i}{x_k \tan\beta_k}\left(\frac{x_k}{x_i}-1\right)(1+B_2) \\ I_t &= Z\left(\frac{x_k}{x_i}-1\right)B_2 \end{aligned}\right\} \tag{4.14}$$

where the following are defined:

$$\left.\begin{aligned} B_{1,2} &= \left(\frac{1+{\lambda_0}^2}{1+\lambda^2}\right)^{0.25}\left[\frac{1}{e^{ZA_{2,1}}-1} \pm \frac{1}{2Z}\frac{{\lambda_0}^2}{(1+{\lambda_0}^2)^{1.5}} ln\left(1+\frac{1}{e^{ZA_{2,1}}-1}\right]\right. \\ A_{1,2} &= \mp\left(\sqrt{1+\lambda^2}-\sqrt{1+{\lambda_0}^2}\right) \pm \frac{1}{2} ln \frac{\left(\sqrt{1+{\lambda_0}^2}-1\right)\left(\sqrt{1+\lambda^2}+1\right)}{\left(\sqrt{1+{\lambda_0}^2}+1\right)\left(\sqrt{1+\lambda^2}-1\right)} \\ \lambda_0 &= \frac{1}{tan\beta_k} \\ \lambda &= \frac{x_i}{x_k tan\beta_k} \end{aligned}\right\} \tag{4.15}$$

Although the above equations yield a very fast computation in terms of the Central Processor Unit (CPU) time, the use of these induction factors has disadvantages defined as follows:

- The expressions are applicable only to a regular helical slipstream,
- They do not provide the radial component of induced velocity,
- They can only be used to calculate induction factors and hence velocities on the lifting line.

However, by the use of the Biot-Savart Law, [2], the induced velocities and the induction factors for a regular helical vortex have been calculated as re-stated in the following for the three components.

In Figure 4.7 a regular helical vortex line is defined as one of constant pitch lying on the surface of a cylinder of constant radius. The non-dimensional velocities induced at $N(0, x_i, 0)$ by a short element of the vortex line length ds situated at $M(\eta + y, x_k, \phi + \theta)$ is given by

In the axial direction

$$\frac{u_a}{V_s} = \frac{G}{2} \int_0^\infty \frac{x_k}{a^3} \Big[x_i - x_k \cos(\theta + \phi) \Big] d\theta \tag{4.16}$$

In the tangential direction

$$\frac{u_t}{V_s} = \frac{G \tan \beta_i}{2} \int_0^\infty \frac{x_k}{a^3} \Big[x_i - x_k \cos(\theta + \phi) - (x_k \theta \tan \beta_k + \eta) \cot \beta_k \sin(\theta + \phi) \Big] d\theta \tag{4.17}$$

In the radial direction

$$\frac{u_r}{V_s} = \frac{G \tan \beta_i}{2} \int_0^\infty \frac{x_k}{a^3} \Big[-(x_k \theta \tan \beta_k + \eta) \cot \beta_k + x_k \sin(\theta + \phi) \Big] d\theta \tag{4.18}$$

where a is defined as

$$a = \sqrt{[(x_k \theta \tan \beta_k + \eta)^2 + x_k^2 - 2 x_i x_k \cos(\theta + \phi)]} \tag{4.19}$$

When these equation are used to determine the velocities induced on the lifting line they can be further simplified by putting $\eta = 0$ and $\phi = 0$ giving:

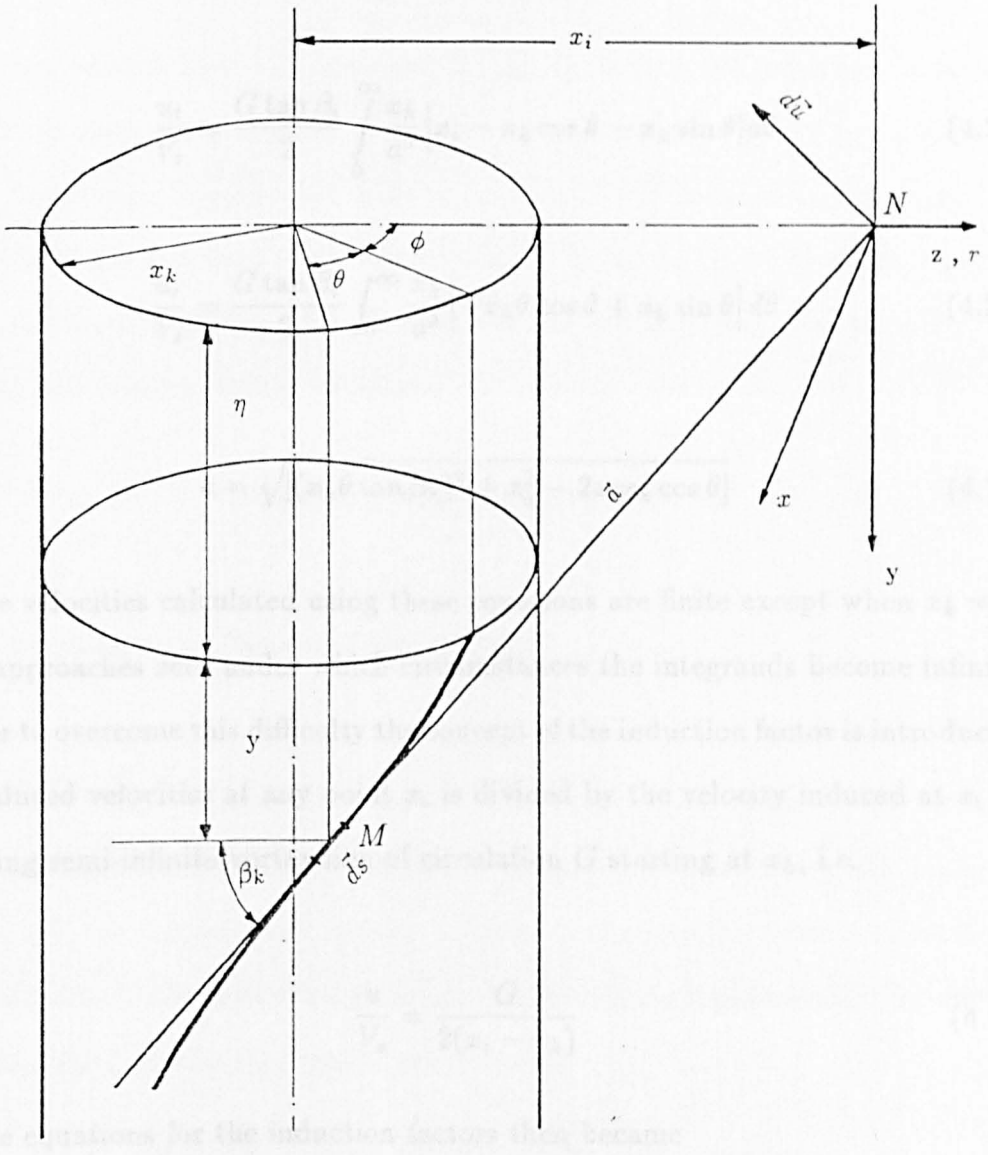

Figure 4.7 — Regular Helical Slipstream

$$\frac{u_a}{V_s} = \frac{G}{2}\int_0^\infty \frac{x_k}{a^3}\Big[x_i - x_k\cos\theta\Big]d\theta \tag{4.20}$$

$$\frac{u_t}{V_s} = \frac{G\tan\beta_i}{2}\int_0^\infty \frac{x_k}{a^3}\Big[x_i - x_k\cos\theta - x_k\sin\theta\Big]d\theta \tag{4.21}$$

$$\frac{u_r}{V_s} = \frac{G\tan\beta_i}{2}\int_0^\infty \frac{x_k}{a^3}\Big[-x_k\theta\cos\theta + x_k\sin\theta\Big]d\theta \tag{4.22}$$

$$a = \sqrt{[(x_k\theta\tan\beta_k)^2 + x_k^2 - 2x_i x_k\cos\theta]} \tag{4.23}$$

The velocities calculated using these equations are finite except when $x_k = x_i$ and θ approaches zero under which circumstances the integrands become infinite. In order to overcome this difficulty the concept of the induction factor is introduced. The induced velocities at any point x_i is divided by the velocity induced at x_i by a starting semi-infinite vortex line of circulation G starting at x_k, i.e.

$$\frac{u}{V_s} = \frac{G}{2(x_i - x_k)} \tag{4.24}$$

The equations for the induction factors then became

$$I_a = (x_i - x_k)\int_0^\infty \frac{x_k}{a^3}\Big[x_k - x_i\cos\theta)\Big]d\theta \tag{4.25}$$

$$I_t = (x_i - x_k)\tan\beta_k\int_0^\infty \frac{x_k}{a^3}\Big[x_i - x_k\cos\theta - x_k\theta\sin\theta\Big]d\theta \tag{4.26}$$

$$I_r = (x_i - x_k)\tan\beta_k \int_0^\infty \frac{x_k}{a^3}\left[-x_k\theta\cos\theta + x_k\sin\theta\right]d\theta \qquad (4.27)$$

It can be seen from the equations for I_a, I_t, I_r that the induction factors are completely independent of the circulation. They depend entirely upon the pitch of the free vortex line and the relative position of the point of inception and the point where the velocities are being calculated. It can be shown that the induction factor factors remain finite for all values of the variables and that when $x_k = x_i$ they assume limiting values as below:

$$I_t = \sin\beta_k, \quad I_a = -\cos\beta_k, \quad I_r = 0 \qquad (4.28)$$

4.5.3 Determination of Bound Circulation

The solution of the lifting line design problem involves determination of the value of the unknown bound circulation coefficient, A_n, in Equation 4.8. In order to obtain a tractable solution, the infinite series is truncated to a small number of terms. It is convenient if the number of terms is equal to the number of blade section considered. Generally the blade can be adequately represented by 11 sections including the hub and tip, typical values being

x_h , 0.25 , 030 , 0.40 , 0.50 , 0.60 , 0.70 , 080 , 0.90 , 0.95 , 1.0

However, since the circulation is zero at the hub and at the tip, it is sufficient to consider a 9-term series to be solved in relation to reference points between the hub and tip.

In Equation 4.12, x_k is replaced by the angular coordinate, ϕ, and x_i by a

similar angular coordinate, ψ, then the equation for the induced velocities becomes

$$u_{i_{a,t,r}} = \int_0^{\pi} \frac{I_{a,t,r}[A_1 \cos\phi + 2A_2 \cos 2\phi + ... + 9A_9 \cos 9\phi]}{2L(\cos\phi - \cos\psi)} d\phi \qquad (4.29)$$

where

$$L = \frac{1 - x_h}{2}$$

In the above integral expression, the integration is carried out numerically such that for each of nine values of x_i, the nine term of equations for the induced velocity components are set up in terms of the unknown A_n's.

In order to optimise the radial loading distribution of the wake-adapted propeller Burrill's minimum energy loss condition is used as given by Equation 4.7. For the 9 reference points, the tangential and axial induced velocities in terms of the 9 unknown Fourier coefficients are substituted into Equation 4.7. Finally a system of nine simultaneous equations is formed as follows:

$$u_{ai} - u_{ti} \tan\varepsilon_i = \frac{1}{2}[\frac{x_i \pi \tan\varepsilon_i}{J_s} - (1 - w_i)] \quad i = 1, 2, ..., 9 \qquad (4.30)$$

Where $J_s = \frac{V_s}{nD}$ is advance coefficient and w_i is the local wake fraction at the blade section radius x_i.

These equations can be solved by commonly used matrix methods to give the circulation coefficients. Having established the circulation, the final parameters associated with the propeller may be investigated by the equations given in Appendix A.

4.5.4 Calculation of the Mean Induced Velocities

In the solution of the lifting line model, it is only necessary to calculate the velocities induced on the line itself by the helical free vortex lines in the slipstream. Since the free vortex system rotates with the propeller, the induced velocities on the lifting line do not vary with time.

In the case of a compound propulsor with a fixed component, such as a duct or stator, the velocities induced by the propeller on the component will vary with time at blade frequency. Normally these fluctuations in induced velocities can not be accounted for in designing the fixed component and it is necessary to have the means of calculating the mean velocities induced by the propeller at a fixed point in the fluid, i.e. a field point.

The mean velocities can be calculated by applying the Biot-Savart method to a number of points over the blade phase angle and integrating the induced velocities at these points to find the time. This approach is very expensive in terms of CPU time. In the case of the regular helical slipstream the mean induced velocities can be calculated more economically by assuming that the helical vortex lines can be replaced by a vortex cylinder comprising a semi-infinite tube of ring vortices and an infinite number of horse-shoe vortices, consisting of bound vortices and straight vortices , Figure 4.8.

When considering a system of Z helical vortex lines of constant pitch P_i, radius r_i and strength $(\frac{d\Gamma}{dr}dr)_i$, the circulation due to this helical vortex can be written $-Z(\frac{d\Gamma}{dr}dr)_i$, [41]. Also the circulation due to a continuous distribution of ring vortices of constant strength is $(\gamma_{ri}P_i dr)$, where γ_{ri} the vortex intensity of the ring

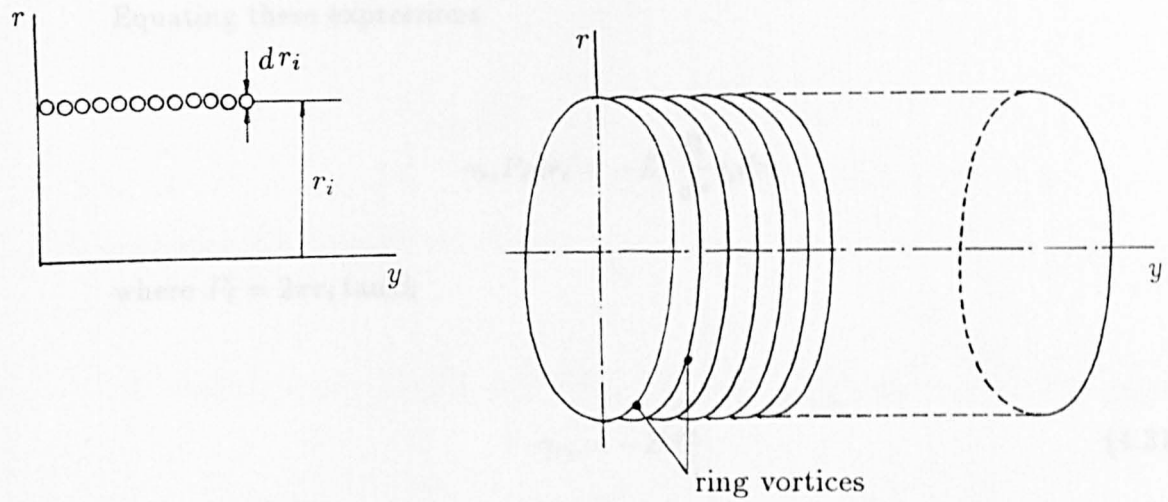

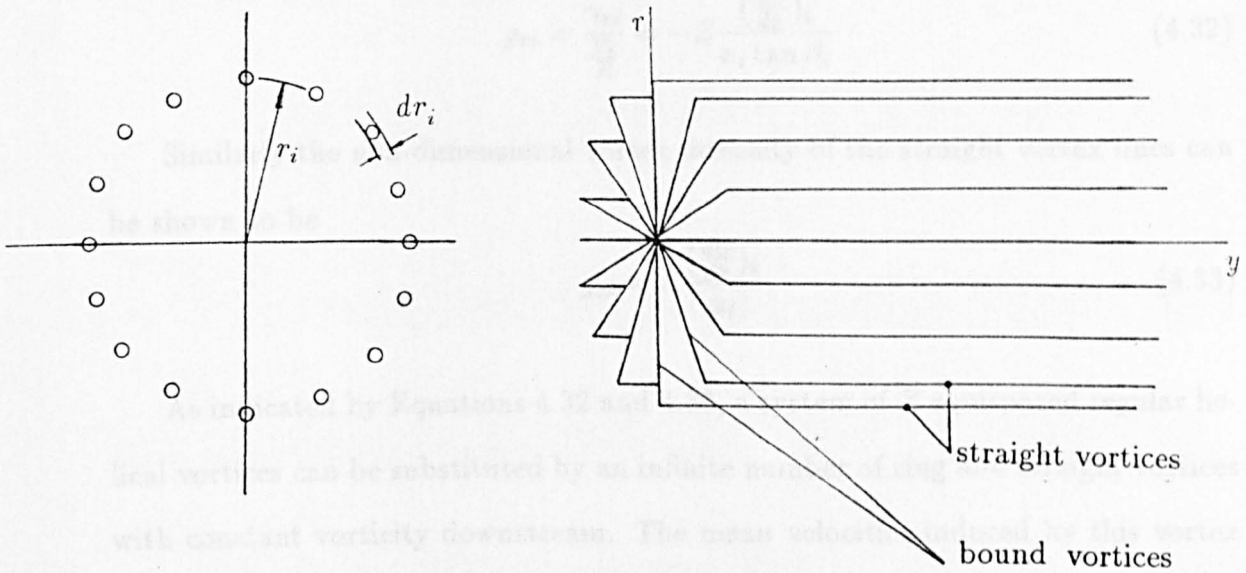

Figure 4.8 — Elementary Vortex System

vortices.

Equating these expressions

$$\gamma_{ri} P_i dr_i = -Z(\frac{d\Gamma}{dr})_i dr_i$$

where $P_i = 2\pi r_i \tan\beta_i$

$$\gamma_{ri} = -Z\frac{\frac{d\Gamma}{dr}}{P_i} \tag{4.31}$$

This can be expressed in its non-dimensional form as follows:

$$g_{ri} = \frac{\gamma_{ri}}{\frac{V_i}{R}} = -Z\frac{(\frac{dG}{dx})_i}{x_i \tan\beta_i} \tag{4.32}$$

Similarly the non-dimensional vortex intensity of the straight vortex lines can be shown to be

$$g_{si} = Z\frac{(\frac{dG}{dx})_i}{x_i} \tag{4.33}$$

As indicated by Equations 4.32 and 4.33, a system of Z equispaced regular helical vortices can be substituted by an infinite number of ring and straight vortices with constant vorticity downstream. The mean velocities induced by this vortex cylinder at any field point can be calculated by a piecewise integration along its length. However, it has been shown in [46] that the velocity induced by a semi-infinite vortex cylinder of unit strength can be expressed in terms of complete elliptic integrals of the first, second and third kind.

The total induced velocity can be found by the integration of the effect of the free vortices from the boss to the tip as follows:

$$u_{a,t,r} = -\int_{x_h}^{x_t} \delta u_{a,t,r} \frac{Z(\frac{dG}{dx})_i}{x_i \tan\beta_i} dx \tag{4.34}$$

or in terms of the angular coordinate

$$u_{a,t,r} = -Z \int_0^{\pi} \frac{\delta u_{a,t,r}}{x_i \tan\beta_i} \sum_{n=1}^{\infty} A_n n \cos n\phi_i d\phi \tag{4.35}$$

where $\delta u_{a,t,r}$ are the incremental axial, tangential and radial induced velocities due to each cylinder which can be calculated using following equations:

Mean axial induced velocity component

$$\delta u_a = \frac{1}{2\pi}[A + \frac{y}{\sqrt{y^2 + (r+1)^2}}[K(k) - \frac{(r-1)}{(r+1)}\Pi(\alpha^2, k)]] \tag{4.36}$$

Where

$$A = \pi \quad \text{if} \quad r^2 < 1, \quad A = 0 \quad \text{if} \quad r^2 > 1$$

Mean tangential induced velocity component

$$\delta u_t = \frac{1}{2\pi}[B + \frac{\frac{y}{r}}{\sqrt{y^2 + (r+1)^2}}[K(k) + \frac{(r-1)}{(r+1)}\Pi(\alpha^2, k)]] \tag{4.37}$$

Where

$$B = 0 \quad \text{if} \quad r^2 < 1, \quad B = \frac{\pi}{r} \quad \text{if} \quad r^2 > 1$$

Mean radial induced velocity component

$$\delta u_r = \frac{1}{\pi k^2} \frac{2}{\sqrt{y^2 + (r+1)^2}} [E(k) - (1 - \frac{k^2}{2}) K(k)] \tag{4.38}$$

where

$$y = \frac{y_j}{x_i}, \qquad r = \frac{x_0}{x_i}, \qquad k = \frac{4r}{y^2 + (x^2+1)^2}, \qquad \alpha = \frac{4r}{(r+1)^2}$$

x_i : Radius of the vortex cylinder

x_0 : Radius of field point

y_j : Axial distance of the field point from the propeller axis

The symbols $K(k)$, $E(k)$ and $\Pi(\alpha^2, k)$ denote complete elliptical integrals of the first, second and third kind respectively.

4.5.5 Effect of the Bound Vortices

The equations for the calculation of the induced velocities due to bound vortices can be derived from the use of the Biot-Savart's Law. In terms of cylindrical polar coordinates the velocities induced at $P(y, r_o, \theta)$ by a vortex element δr located at $(0, r, \phi)$, Figure 4.9, will, when reduced to non-dimensional terms, be given by

$$du_a = \frac{G}{2} \frac{x_0 \sin(\theta - \phi)}{a^3} dx \tag{4.39}$$

$$du_t = -\frac{G}{2} \frac{y \cos(\theta - \phi)}{a^3} dx \tag{4.40}$$

$$du_r = -\frac{G}{2} \frac{y \sin(\theta - \phi)}{a^3} dx \tag{4.41}$$

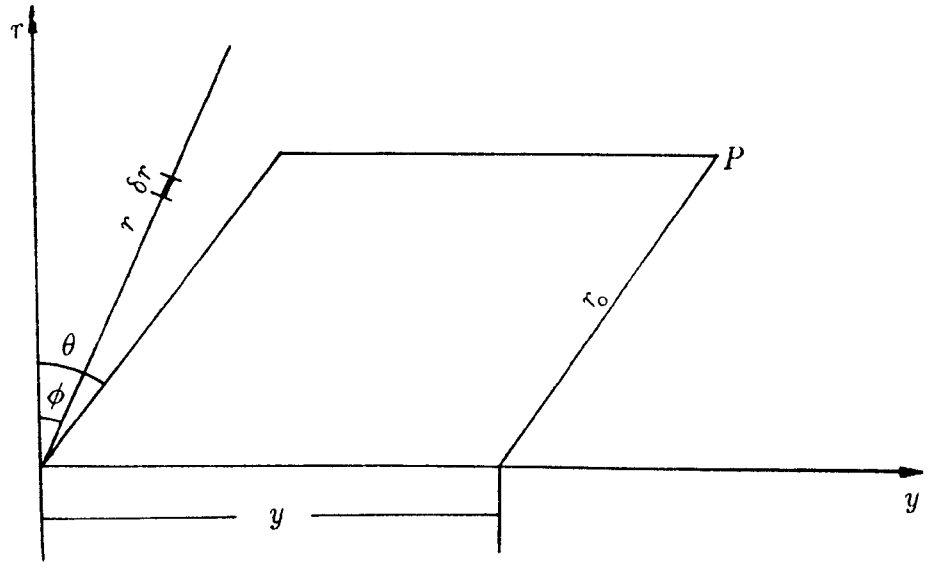

Figure 4.9 — Bound Vortex Line

where

$$a = \sqrt{x_o^2 + x^2 - 2x_o x \cos(\theta - \phi) + y^2} \tag{4.42}$$

The total velocities induced at P a system Z equally spaced lifting lines are therefore given by

$$du_a = \sum_1^Z \int_{x_h}^{x_t} \frac{G}{2} \frac{x_0 \sin(\theta - \phi)}{a^3} dx \tag{4.43}$$

$$du_t = \sum_1^Z \int_{x_h}^{x_t} -\frac{G}{2} \frac{y \cos(\theta - \phi)}{a^3} dx \tag{4.44}$$

$$du_r = \sum_1^Z \int_{x_h}^{x_t} -\frac{G}{2} \frac{y \sin(\theta - \phi)}{a^3} dx \tag{4.45}$$

Chapter V

Advanced Lifting Line Model

5.1 Introduction

In this Chapter a description is given of the development of a lifting line design procedure in which the body wake flow velocities are taken into account in addition to the velocities induced by the propeller. The major characteristic of the procedure compared to that described in Chapter 4 is that account is taken of the true shape of the slipstream. The slipstream is assumed to comprise deformed helical vortex sheets, the shape of which is a function of the velocities induced in the slipstream by the propeller and the body wake velocities.

5.2 Design Considerations

The aim of the design is the solution of the vortex model of the propeller and in particular the determination of the distribution of the bound circulation on the lifting line such that it absorbs a given power at a specified rate of rotation. The design input parameters, derived from the standard series diagrams, are the same as those for the regular helical slipstream design, only the local wake velocities in the slipstream are extra input parameters.

As before, the solution of the lifting line model requires the introduction of a condition for minimum energy loss and hence the specification of the optimum radial distribution of the bound circulation. In previous Chapter the condition

proposed by Burrill was used. For the case of the irregular slipstream, this condition was defined as "$\pi x_\infty \tan\varepsilon = constant$", [1]. In this expression x_∞ refers to the contracted radius of a slipstream line starting at radius x_0 on the lifting line and the ultimate pitch angle, ε, is given by

$$\varepsilon = \tan^{-1}\left[\frac{(1 - Wn_\infty) + 2u_{ai}}{\frac{\pi x_\infty}{J_{vs}} - 2u_{ti}}\right] \tag{5.1}$$

where Wn_∞ is the wake at infinity downstream, u_{a_i} and u_{t_i} axial and tangential induced velocity at i^{th} section of the lifting line.

In the present method Wn_∞ approaches to zero and x_∞ becomes much smaller than x_0. Therefore the solution for the bound circulation by using Equation 5.1 presents unrealistic values. Therefore it was decided to use the wake values (Wn) and radius (x_0) on the lifting line rather than Wn_∞ and x_∞. For the initial value of $x\pi\tan\varepsilon$ is assumed and entered to the design program.

5.3 Mathematical Formulation of the Model

The major numerical calculations mainly involve the determination of the induction factors. In order to obtain the induction factors for an irregular helix Glover [1] suggests that the helix should be split up into a number of finite regular helical elements. The length of these elements should be small in areas where the pitch and diameter of the irregular helix change most. Furthermore, their pitch and diameter should be equal to the arithmetic mean of the irregular element they represent.

In this present work, however, a different procedure will be used. Initially the Biot-Savart Law is introduced to find the equation for the calculation of the induc-

tion factors and induced velocities. Having obtained the equations, the induction factors and induced velocities are calculated by a direct numerical integration.

The incremental velocity induced by a vortex element length ds at the point N, Figure 5.1, according to the Biot-Savart Law is

$$d\vec{u} = \frac{\Gamma}{4\pi} \frac{d\vec{s} \times \vec{a}}{a^3} \tag{5.2}$$

or

$$d\vec{u} = \frac{\Gamma}{4\pi a^3} \Gamma dy \begin{pmatrix} \vec{i} & \vec{j} & \vec{k} \\ \cot\beta_{kj} \cos(\theta_{kj} + \phi_z) & 1 & -\cot\beta_{kj} \sin(\theta_{kj} + \phi_z) \\ r_{kj} \sin(\theta_{kj} + \phi_z) & -y_{kj} & -r_i - r_{kj} \sin(\theta_{kj} + \phi_z) \end{pmatrix} \tag{5.3}$$

where

$$a = \sqrt{y_{kj} + r_i^2 + r_{kj}^2 - 2r_i r_{kj} \cos(\theta_{kj} + \phi_z)} \tag{5.4}$$

Γ = Strength of vortex line

$d\vec{s}$ = Length of vortex element

$\vec{a}$ = Distance from $d\vec{s}$ to the point where the velocity induced by the vortex line.

r_i = radius of the reference point

r_{kj} = radius of the vortex element

θ_{kj} = rotational distance of the vortex element from the lifting line

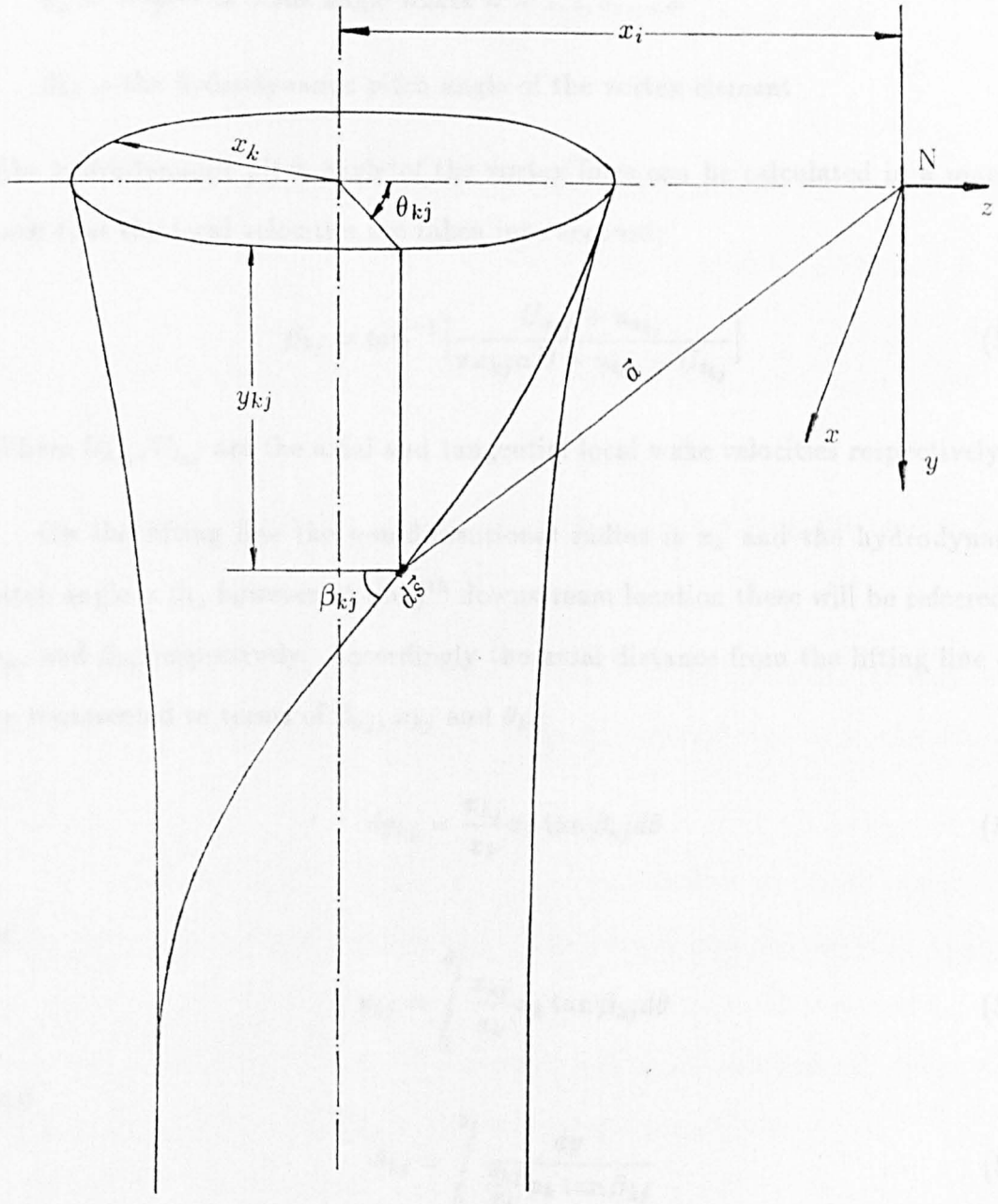

Figure 5.1 — Irregular Helical Slipstream

y_{kj} = axial distance from the axes of the reference point

$\phi_z = \frac{2\pi(n-1)}{Z}$ is blade angle where $n = 1, 2, 3, ..., Z$

β_{kj} = the hydrodynamic pitch angle of the vortex element

The hydrodynamic pitch angle of the vortex lines can be calculated in a manner such that the local velocities are taken into account;

$$\beta_{kj} = tan^{-1}\Big[\frac{U_{a_{kj}} + u_{a_{kj}}}{\pi x_{kj} nD - u_{t_{kj}} - U_{t_{kj}}}\Big] \tag{5.5}$$

Where $U_{a_{kj}}, U_{t_{kj}}$ are the axial and tangential local wake velocities respectively.

On the lifting line the non-dimensional radius is x_k and the hydrodynamic pitch angle is β_k, however at the j^{th} downstream location these will be referred as x_{kj} and β_{kj} respectively. Accordingly the axial distance from the lifting line can be represented in terms of β_{kj}, x_{kj} and θ_{kj}.

$$dy_{kj} = \frac{x_{kj}}{x_k} x_k \tan\beta_{kj} d\theta \tag{5.6}$$

or

$$y_{kj} = \int_0^{\theta_j} \frac{x_{kj}}{x_k} x_k \tan\beta_{kj} d\theta \tag{5.7}$$

and

$$\theta_{kj} = \int_0^{y_j} \frac{dy}{\frac{x_{kj}}{x_k} x_k \tan\beta_{kj}} \tag{5.8}$$

The induction factors in the axial, tangential and radial directions can be obtained from the Equation 5.3 and summing up the effect of all blades they are written in non-dimensional quantities as follows:

The induction factor in axial direction

$$I_a = \sum_{1}^{Z}(x_i - x_k) \int_{0}^{\infty} \tan\beta_{kj} \frac{x_{kj}}{a^3} \left[x_{kj} - x_i \cos(\theta_{kj} + \phi_z)\right] d\theta_j \tag{5.9}$$

The induction factor in tangential direction

$$I_t = \sum_{1}^{Z}(x_i - x_k) \int_{0}^{\infty} \tan\beta_{kj} \frac{x_{kj}}{a^3} \left[x_i - x_{kj}\cos(\theta_{kj} + \phi_z) - y_{kj}\cot\beta_{kj}\sin(\theta_{kj} + \phi_z)\right] d\theta_j \tag{5.10}$$

The induction factor in radial direction

$$I_r = \sum_{1}^{Z}(x_i - x_k) \int_{0}^{\infty} \tan\beta_{kj} \frac{x_{kj}}{a^3} \left[-y_{kj}\cot\beta_{kj}\cos(\theta_{kj} + \phi_z) + x_{kj}\sin(\theta_{kj} + \phi_z)\right] d\theta_j \tag{5.11}$$

These equations form the major part of the numerical calculation leading to the determination of the velocity induced by the Z vortex lines at x_i on the reference blade.

The induction factors calculated using these equation are finite except when $x_i = x_{kj}$ and $\theta_{kj} \to 0$ at the point $y_{kj} = 0$ in which case the integrals approach infinity. By examining the behaviour of the equation for small values of θ_{kj} it has been shown in [1] that the integrals can be analytically determined. When θ_{kj} is small and lies within the range 0 to ψ it can be assumed that

$$\cos\theta = 1 - \frac{\theta^2}{2} \quad and \quad \sin\theta = \theta \tag{5.12}$$

The deformed vortex in this location can be replaced by one of constant pitch and diameter as follows:

The hydrodynamic pitch angle

$$\beta_m = \frac{\beta_k + \beta_{kj}}{2} \tag{5.13}$$

The radius of the vortex line

$$x_m = \frac{x_k + x_{kj}}{2} \quad and \quad \delta_m = \frac{x_m}{x_i} \tag{5.14}$$

The integration between 0 and ψ gives

$$\left.\begin{aligned}\Delta I_a \approx (1-\delta_k)\Big[&\frac{\psi}{(1-\delta_m)\sqrt{\psi^2(\delta^2\tan^2\beta_m+\delta_m)+(1-\delta_m)^2}} - \frac{\delta_m}{2(\delta^2\tan^2\beta_m+\delta_m)^{1.5}}\\ &(ln\frac{\sqrt{\psi^2(\delta_m^2 tan^2\beta_m+\delta_m)(1-\delta_m)^2}+\psi\sqrt{\delta^2\tan^2\beta_m+\delta_m}}{|1-\delta_m|}\\ &-\frac{\sqrt{\psi^2(\delta^2\tan^2\beta_m+\delta_m)}}{\sqrt{\psi^2(\delta^2\tan^2\beta_m+\delta_m)+(1-\delta_m)^2}})\Big]\delta_m\end{aligned}\right\} \tag{5.15}$$

As $x_{kj} \rightarrow x_i$ the above equation approach the indefinite value, according to the rule of de L'Hospital the result has been found, as in [1], to be

$$\Delta I_a = -\cos\beta_i \tag{5.16}$$

Similarly for the tangential induction factor

$$\left.\begin{aligned}\Delta I_t \approx (1-\delta_k)\Big[&\frac{\psi}{(1-\delta_m)\sqrt{\psi^2(\delta^2\tan^2\beta_m+\delta_m)+(1-\delta_m)^2}} - \frac{\delta_m}{2(\delta^2\tan^2\beta_m+\delta_m)^{1.5}}\\ &(ln\frac{\sqrt{\psi^2(\delta_m^2 tan^2\beta_m+\delta_m)(1-\delta_m)^2}+\psi\sqrt{\delta^2\tan^2\beta_m+\delta_m}}{|1-\delta_m|}\\ &-\frac{\sqrt{\psi^2(\delta^2\tan^2\beta_m+\delta_m)}}{\sqrt{\psi^2(\delta^2\tan^2\beta_m+\delta_m)+(1-\delta_m)^2}})\Big]\delta_m\tan\beta_m\end{aligned}\right\} \tag{5.17}$$

At the limit $\delta_m \rightarrow 1$

$$\Delta I_t = \sin\beta_i \tag{5.18}$$

For the radial induction factor

$$\left.\begin{aligned}\Delta I_r \approx \frac{2}{3}\frac{(1-\delta_k)\delta^2\tan\beta_m}{(\delta^2\tan^2\beta_m+\delta_m)^2}\Big[\sqrt{(1-\delta_m)^2+\psi^2(\delta^2\tan^2\beta_m+\delta_m)}\\ +\frac{(1-\delta_m)^2}{\sqrt{(1-\delta_m)^2+\psi^2(\delta^2\tan^2\beta_m+\delta_m)}}-2(1-\delta_m)\Big]\end{aligned}\right\} \tag{5.19}$$

and at the limit $\delta_m \rightarrow 1$

$$\Delta I_r = 0 \tag{5.20}$$

These equations will be used for the first element of the first blade to calculate the induction factors. The rest of the induction factors can be easily determined from the Equations 5.9, 5.10 and 5.11.

If I is the axial, radial and tangential induction factor due to helical vortex shed at x_k, the the total velocity induced at x_i can be written as

$$u = \int_{x_h}^{x_t} I(\frac{dG}{dx})_k \frac{dx_k}{2(x_{ij}-x_{kj})} \tag{5.21}$$

5.4 Calculation of the Induced Velocities

The calculation of induced velocities due to the trailing vortex sheet at points on the lifting line and in the slipstream involves evaluation of the induction factors defined by Equation 5.9 to 5.11. The integration of these equation from $\theta = 0$ to $\theta = \infty$ is impracticable and it is therefore truncated to an upper limit (i.e 10π) with a compromise between accuracy and computational time.

The calculation of the induced velocities on the lifting line is carried out for a small number of reference points distributed between the hub and the tip. A helical free vortex line starts at each reference point and these vortex lines will be referred to as reference vortices. The induced velocities in the slipstream will be calculated at a number of control points distributed along the reference vortices.

The total induced velocities at any reference point or control point are derived by integrating Equation 5.21 numerically for a large number of field vortices distributed on either side of the reference point and reference vortex. The induction factors corresponding to the field vortices being calculated from Equation 5.9 to 5.11.

The induction factor at a slipstream control point representing the velocity induced by a field vortex will be that due to a finite length of the field vortex lying between the control point and the lifting line (i.e. the Left Hand Side Effect, L.H.S) and that due to the semi-infinite line lying downstream from the point (the Right Hand Side Effect, R.H.S), Figure 5.2. As far as the tangential and axial induction factors are concerned the effects of these two vortex system are additive but in the case of the radial component the opposite applies. The total induction factor at a point in the slipstream are then calculated as follows:

in the tangential and axial components

$$I = I_{R.H.S} + I_{L.H.S} \tag{5.22}$$

in the radial component

$$I = I_{R.H.S} - I_{L.H.S} \tag{5.23}$$

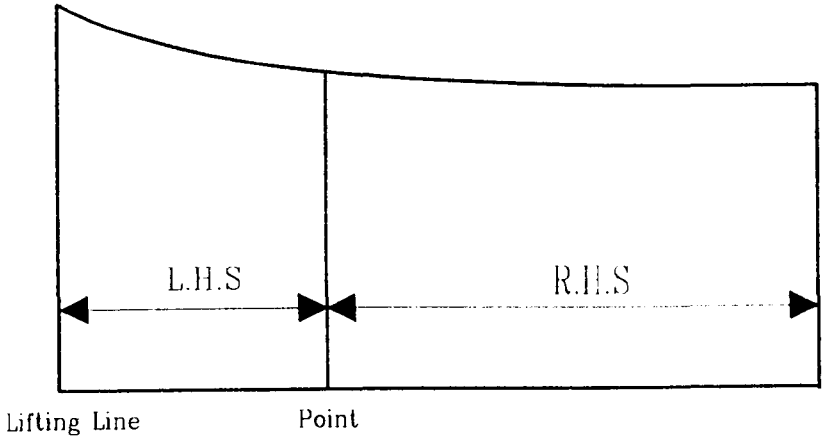

Figure 5.2 — Model of Slipstream shape

5.5 Location of Field and Reference Vortices

The number and location of the field and reference vortices have an important effect on the length of the calculation and the accuracy of the results. The reference points will be situated at the blade design sections and form part of the input data. According to these values, the field points can be spaced on either side of each reference point in a special manner that more points have to be taken where the maximum changes are expected. Therefore it is essential to concentrate the points at the end of lifting line within the general rule of discretisation.

A field vortex is assumed to be shed on both sides of each reference helix and the space between two field vortices is referred to as the mid-zone. If ε_0 is the width of the mid-zone and ε_f the approximate spacing of the field vortices, Figure 5.3, then the location of them relative to a reference point at ϕ_i can be set up as

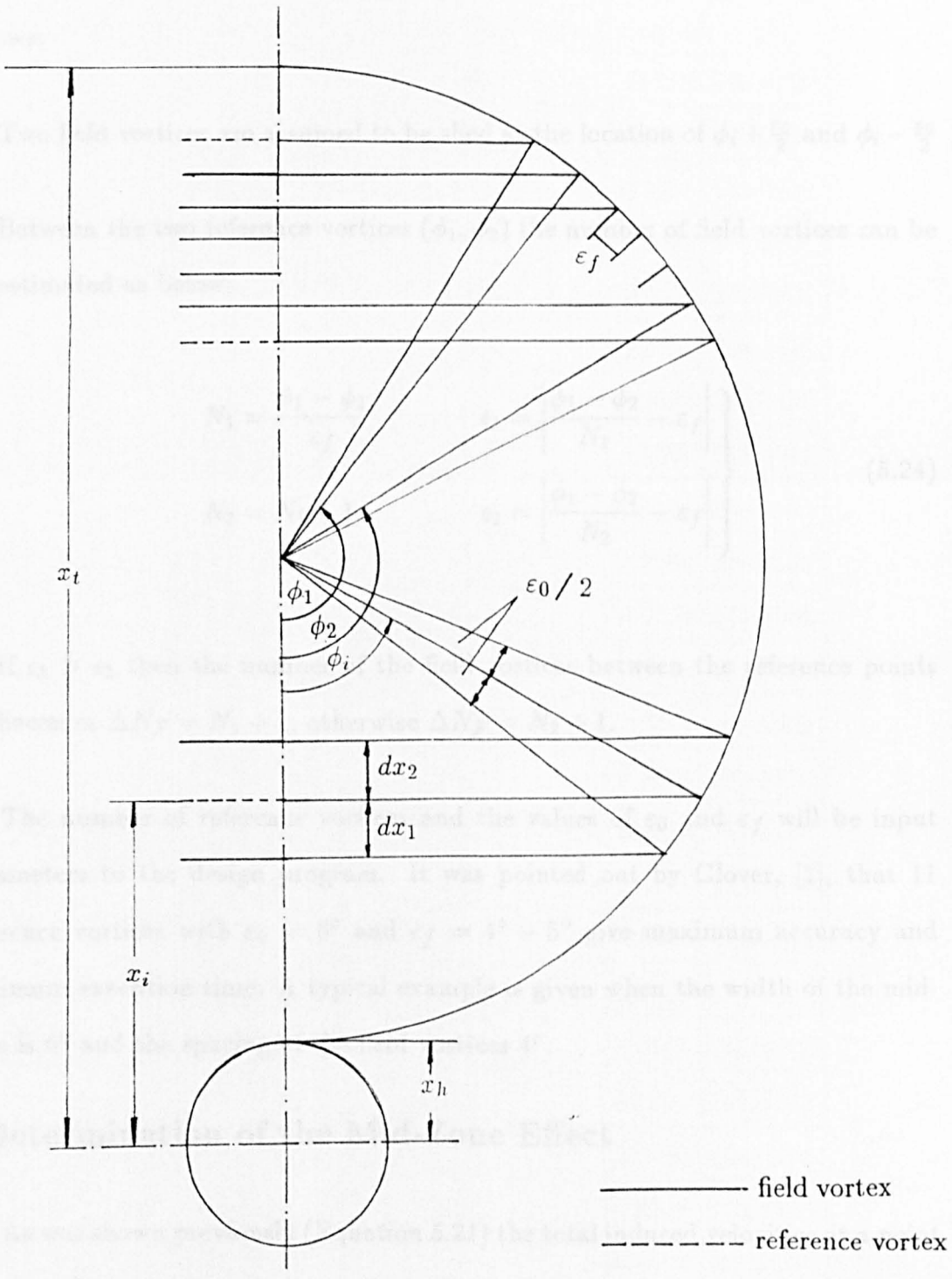

Figure 5.3 — Field and Reference Vortices

follows:

- Two field vortices are assumed to be shed at the location of $\phi_i + \frac{\varepsilon_0}{2}$ and $\phi_i - \frac{\varepsilon_0}{2}$

- Between the two reference vortices (ϕ_1, ϕ_2) the number of field vortices can be estimated as below:

$$\left.\begin{aligned} N_1 &= \frac{\phi_1 - \phi_2}{\varepsilon_f} & \epsilon_1 &= \left|\frac{\phi_1 - \phi_2}{N_1} - \varepsilon_f\right| \\ N_2 &= N_1 + 1 & \epsilon_2 &= \left|\frac{\phi_1 - \phi_2}{N_2} - \varepsilon_f\right| \end{aligned}\right\} \tag{5.24}$$

If $\epsilon_2 > \epsilon_1$ then the number of the field vortices between the reference points becomes $\Delta N_F = N_1 + 1$, otherwise $\Delta N_F = N_2 + 1$.

The number of reference vortices and the values of ε_0 and ε_f will be input parameters to the design program. It was pointed out by Glover, [1], that 11 reference vortices with $\varepsilon_0 = 6°$ and $\varepsilon_f = 4° - 5°$ give maximum accuracy and minimum execution time. A typical example is given when the width of the mid-zone is 6^o and the spacing of the field vortices 4^o.

5.6 Determination of the Mid-Zone Effect

As was shown previously (Equation 5.21) the total induced velocities at a point are given by

$$u = \int_{x_h}^{x_t} I\left(\frac{dG}{dx}\right)_k \frac{dx_k}{2(x_{ij} - x_{kj})} \tag{5.25}$$

Reference Vortex	No. of the Field Vortex	Radius	ϕ^0
11	40	1.0000	180.0000
	39	0.9991	176.3150
	38	0.9966	172.6250
	37	0.9926	168.9301
	36	0.9824	162.9301
	35	0.9721	158.4875
	34	0.9597	154.0450
10		0.9500	151.0449
	33	0.9394	148.0450
	32	0.9269	144.8177
	31	0.9134	141.5904
9		0.9000	138.5904
	30	0.8857	135.5904
	29	0.8645	131.3936
	28	0.8418	127.1968
	27	0.8179	123.0000
8		0.8000	120.0000
	26	0.7816	117.0000
	25	0.7514	112.2388
	24	0.7201	107.4775
7		0.7000	104.4775
	23	0.6796	101.4775
	22	0.6504	97.2388
	21	0.6209	93.0000
6		0.6000	90.0000
	20	0.5791	87.0000

Reference Vortex	No. of the Field Vortex	Radius	ϕ^0
	19	0.5496	82.7613
	18	0.5204	78.5225
5		0.5000	75.5225
	17	0.4799	72.5225
	16	0.4486	67.7612
	15	0.4184	63.0000
4		0.4000	60.0000
	14	0.3821	57.0000
	13	0.3582	52.8032
	12	0.3355	48.6064
	11	0.3143	44.4096
3		0.3000	41.4096
	10	0.2866	38.4096
	9	0.2731	35.1823
	8	0.2606	31.9550
2		0.2500	28.9550
	7	0.2403	25.9550
	6	0.2278	21.5124
	5	0.2176	17.0704
	4	0.2074	11.0702
	3	0.2023	7.3801
	2	0.2008	3.6900
1	1	0.2000	0.0000

Table 5.1 — A typical distribution of the field vortices

When x_{kj} approaches x_{ij}, the integrand tends to infinity. But this difficulty can be resolved by considering a narrow space on either side of the reference point within which the integrand assumes certain values. Using a similar procedure to that in [1], the numerical integration of the above equation is divided into three parts as follows:

$$\int_{x_h}^{x_t} = \int_{x_h}^{x_{ij}-dx_1} + \int_{x_{ij}-dx_1}^{x_{ij}+dx_2} + \int_{x_{ij}+dx_2}^{x_t} \tag{5.26}$$

The mid-zone effect is represented by the integral $\int_{x_{ij}-dx_1}^{x_{ij}+dx_2}$ and can be determined by expanding this as a Taylor series:

$$\left.\begin{aligned} \int_{x_{ij}-dx_1}^{x_{ij}+dx_2} F(x)\frac{dx}{2(x_{ij}-x_{kj})} &= F(x_{ij})\int_{x_{ij}-dx_1}^{x_{ij}+dx_2}\frac{dx}{2(x-x_{ij})} \\ &-F'(x_{ij})\int_{x_{ij}-dx_1}^{x_{ij}+dx_2} dx + \frac{1}{2!2}F''(x_{ij})\int_{x_{ij}-dx_1}^{x_{ij}+dx_2}(x-x_{ij})dx \\ -\frac{1}{3!2}F'''(x_{ij})\int_{x_{ij}-dx_1}^{x_{ij}+dx_2}(x-x_{ij})^2dx &+ \ldots \end{aligned}\right\} \tag{5.27}$$

Integrating each part of above equation, e.g.

$$\frac{1}{2}F(x_{ij})\int_{x_{ij}-dx_1}^{x_{ij}+dx_2}\frac{dx}{(x-x_{ij})} = \frac{F(x_{ij})}{2}ln|\frac{dx2}{dx1}| \tag{5.28}$$

$$\frac{F'(x_i)}{2}\int_{x_{ij}-dx_1}^{x_{ij}+dx_2} dx = (\frac{dx_2+dx_1}{2})F'(x_{ij}) \tag{5.29}$$

$$\frac{1}{2!2}F''(x_{ij})\int_{x_{ij}-dx_1}^{x_{ij}+dx_2}(x-x_{ij})dx = \frac{1}{2!2}F''(x_{ij})(dx_2^2-dx_1^2) \approx 0 \tag{5.30}$$

$$\frac{1}{3!2}F'''(x_{ij})\int_{x_{ij}-dx_1}^{x_{ij}+dx_2}(x-x_{ij})^2dx = \frac{1}{3!3.2}F'''(x_{ij})(dx_2^3-dx_1^3)\approx 0 \qquad (5.31)$$

Where $F(x) = I(\frac{dG}{dx})_k$ and dx_1 & dx_2 are small distances on either side of the reference vortex.

In order to obtain the above equations in angular coordinates, the following equations can be used.

The circulation G is written in terms of ϕ as follows:

$$\frac{dG}{dx}dx = \frac{dG}{d\phi}d\phi \qquad \frac{dG}{dx} = \frac{dG}{d\phi}\frac{d\phi}{dx}$$

$$\frac{d^2G}{dx^2} = \frac{d^2G}{d\phi^2}(\frac{d\phi}{dx})^2 + \frac{dG}{d\phi}\frac{d^2\phi}{dx^2} \qquad (5.32)$$

$$Dx = dx_1 + dx_2 \quad \text{and} \quad \varepsilon = \frac{\varepsilon_0}{2} = \frac{d\phi}{2} = \text{half width of the mid-zone} \qquad (5.33)$$

and therefore

$$\frac{d^2\phi}{dx^2} = 2\varepsilon Dx(\frac{1}{dx_1}-\frac{1}{dx_2}) \qquad (5.34)$$

and the final form of the mid-zone integral becomes

$$\int_{\phi_i-\varepsilon}^{\phi_i+\varepsilon} = -\frac{\varepsilon}{Dx}\left[(\frac{dG}{d\phi})_i\left[I\left[Dx(\frac{1}{dx_1}-\frac{1}{dx_2})-ln|\frac{dx_2}{dx_1}|\right]+dI\right]+2\varepsilon I(\frac{d^2G}{d\phi^2})_i\right] \qquad (5.35)$$

If dx_1 is assumed to be equal to dx_2 the above equation can be re-stated as follows

$$\int_{\phi_i-\varepsilon}^{\phi_i+\varepsilon} = -\frac{\varepsilon}{Dx}\frac{dG}{d\phi}dI + 2\varepsilon I\frac{d^2G}{d\phi^2} = -\frac{2\varepsilon^2}{Dx}[\frac{dG}{d\phi}\frac{dI}{2\varepsilon}+I\frac{d^2G}{d\phi^2}] \qquad (5.36)$$

The above equation can be simplified using the expressions of $2\varepsilon = d\phi$ and $\frac{Dx}{d\phi} = \frac{1-x_h}{2}\sin\phi_i$ and finally it becomes

$$\int_{\phi_i-\varepsilon}^{\phi_i+\varepsilon} = -\frac{\varepsilon}{\frac{1-x_h}{2}\sin\phi_i}\left[\frac{dG}{d\phi_i}dI + \frac{dI}{d\phi_i} + I\frac{d^2G}{d\phi_i^2}\right] \tag{5.37}$$

This is the resulting equation obtained as in [1] and accordingly the velocity induced at the j^{th} downstream of the i^{th} reference vortex by the k^{th} field vortex can be represented as follows.

$$u = -\int_0^{\phi-\varepsilon} I\frac{\sum_{n=1}^{9} A_n n\cos n\phi_k}{2(x_{ij}-x_{kj})}d\phi_k + \int_{\phi-\varepsilon}^{\phi+\varepsilon} - \int_{\phi+\varepsilon}^{\pi} I\frac{\sum_{n=1}^{9} A_n n\cos n\phi_k}{2(x_{ij}-x_{kj})}d\phi_k \tag{5.38}$$

5.7 Local Wake Velocities in the Slipstream

Detailed knowledge of the local wake velocity distribution in the slipstream is necessary for the establishment of a realistic model of the part of the trailing vortices which have a significant effect on the propeller design and final slipstream shape. This is the major difference between the present method and other conventional lifting line methods. In these conventional methods the radial wake velocity distribution at the propeller plane is assumed to be constant along the slipstream. But in reality this is not true, therefore it is essential to take account of the wake velocities behind the propeller for modelling the true shape of the slipstream.

In this procedure the wake velocities in the slipstream are calculated at a number of control points using the methods described in Chapter 3. The choice of the number of control points to be considered is a compromise between numerical accuracy and computing time. In the present work, 21 control points are distributed axially along each of 12 lines placed at various radial locations.

Of the radial control points, 11 are situated at the propeller design section radii and an extra point is placed below the propeller hub radius to allow the calculation of the wake velocities within the contracted propeller slipstream. The axial control points are placed at the following non-dimensional distances, Y/R, downstream of the propeller plane:

$$\frac{Y}{R} = 0.0,\quad 0.06,\quad ,0.20,\quad 0.40,\quad 0.60,\quad 0.80,\quad 1.0,\quad 1.2,\quad 1.4,\quad 1.6$$
$$1.8,\quad 2.0,\quad 4.0,\quad 6.0,\quad 8.0,\quad 10.0,\quad 12.0,\quad 14.0,\quad 16.0,\quad 18.0,\quad 20.0$$

The local wake velocities at the 252 control points are calculated and stored for later use in calculating the deformation of the slipstream. In the later calculation, the wake velocities at control points on the vortex lines are derived by linear interpolation within the stored values.

5.8 Deformation of the Slipstream

At a point x_{ij} a distance y_{ij} downstream from the lifting line, the slope of the vortex line is given by

$$\tan \alpha_{ij} = \frac{U_{r_{ij}} + u_{r_{ij}}}{U_{a_{ij}} + u_{a_{ij}}} \tag{5.39}$$

where $U_{a_{ij}}$, $U_{r_{ij}}$ are the local wake velocities in the axial and radial directions and $u_{a_{ij}}$, $u_{r_{ij}}$ propeller induced velocities in the axial and radial directions.

The radius of the vortex line can be then determined from the following equation:

$$x_{ij} = x_i + \int_0^{y_{ij}} \tan \alpha_{ij} d\alpha_i \tag{5.40}$$

The hydrodynamic pitch angle of the trailing vortices in the slipstream becomes

$$\beta_{ij} = tan^{-1}\Big[\frac{U_{a_{ij}} + u_{a_{ij}}}{\pi x_{ij} nD - u_{t_{ij}}}\Big] \tag{5.41}$$

As can be seen from Equations 5.39 and 5.41, the deformed slipstream shape depends on the total velocity on the vortex lines. The total velocity can be defined as the sum of velocities induced at the point by the trailing vortices in the slipstream, bound vortices at the lifting line and the local wake velocities. As long as the total velocity at the point is calculated correctly, the true shape of the slipstream can be obtained.

The components of the induced velocities or the local wake velocities can be calculated using previously mentioned procedures, except for the velocities induced by the trailing vortices at the hub and tip where the induction factors approach infinity. In order to overcome this difficulty the hub and tip radii are redefined as $x_{hub} = x_h + 0.012$, $x_{tip} = x_t - 0.012$. These sections are treated as the hub and tip radii within the all design calculations.

5.9 Convergence of Slipstream Shape

One of the main objectives of this section is to show how the helical slipstream shape gradually converges to a final stable form. In order to achieve this objective, the total velocities are calculated at each of the control points located on the reference vortex lines. Their location with respect to the lifting line is given as follows:

$$\theta = 0,\ \frac{\pi}{16},\ \frac{\pi}{8},\ \frac{\pi}{4},\ \frac{3\pi}{8},\ \frac{\pi}{2},\ \frac{3\pi}{4},\ \pi,\ \frac{5\pi}{4},\ \frac{3\pi}{2},\ \frac{7\pi}{4},\ 2\pi,\ 2.5\pi$$
$$3\pi,\ 3.5\pi,\ 4\pi,\ 4.5\pi,\ 5\pi,\ 6\pi,\ 7\pi \text{ and } 10\pi.$$

Hence, 231 control points are used for the representation of the slipstream. For the initial numerical calculation to define the trailing vortex shape, the local wake velocities only are used since the induced velocities are still unknown. Using this slipstream shape the bound circulation can be defined and provides the means for the calculation of the induced velocities. Having calculated the induced velocities related to the previously established bound circulation, a new slipstream shape is obtained. According to the new deformed helical slipstream shape, the induction factors and the bound circulation are redefined and consequently the velocities induced at control points are recalculated. This procedure are carried out until a satisfactory result is obtained with the aim of modelling a final stable irregular helical slipstream shape. The design also satisfies the power absorption condition. This convergence can be achieved by 3 or 4 iterations. At least 3 iterations are essential to ensure the accuracy of the results.

In the process of deriving the new slipstream shape, an over correction of the radii of the helices results in a fluctuation of the induced velocities when using Equation 5.40. Therefore, it is necessary to use a new approximation which is the arithmetic mean of the existing radius and that calculated by Equation 5.40. This procedure supplies a smooth change from an original form to deformed one.

5.10 Circumferential Mean Velocities by Trailing Vortices

In the regular helical slipstream case, the mean induced velocities due to trailing vortices can be calculated using elliptic integrals, whereas in the deformed helical slipstream case the use of elliptic integrals is impossible. Therefore, the most straight forward procedure for the calculation of mean velocities is to use the equations from the Biot-Savart's Law. The angle between the blades is divided

into a number of parts and velocities induced at these points are calculated. These velocities are then integrated numerically and divided by the blade angle to obtain the circumferential mean induced velocities. In this study the angle between the blades is divided into six parts resulting in seven points. On each point, the induction factors are calculated from a slightly different form of Equation 5.9, 5.10, 5.11 as stated below:

$$I_a = \sum_{1}^{z}(x_i - x_k) \int_{0}^{\infty} \tan\beta_{kj} \frac{x_{kj}}{a^3} \left[x_{kj} - x_i \cos(\theta_{kj} + \phi_z + \phi_f)\right] \theta_j \tag{5.42}$$

$$I_t = \sum_{1}^{z}(x_i - x_k) \int_{0}^{\infty} \tan\beta_{kj} \frac{x_{kj}}{a^3} \left[x_i - x_{kj}\cos(\theta_{kj}+\phi_z) - y_{kj}\cot\beta_{kj}\sin(\theta_{kj}+\phi_z+\phi_f)\right] d\theta_j \tag{5.43}$$

$$I_r = \sum_{1}^{z}(x_i - x_k) \int_{0}^{\infty} \tan\beta_{kj} \frac{x_{kj}}{a^3} \left[-y_{kj}\cot\beta_{kj}\cos(\theta_{kj}+\phi_z) + x_{kj}\sin(\theta_{kj}+\phi_z+\phi_f)\right] d\theta_j \tag{5.44}$$

where

$$a = \sqrt{y_{kj}^2 + x_i^2 + x_{kj}^2 - 2x_i x_{kj}\cos(\theta_{kj} + \phi_z + \phi_f)} \tag{5.45}$$

$$\phi_f = \frac{2\pi(K-1)}{Z(N-1)} \qquad K = 1, 2, ..., N$$

N: The number of the points between the blades

Z: The number of the blades.

The bound vortices also contribute to the circumferential mean induced velocities. Using a formal application of Biot-Savart's Law, one can show that the mean velocities induced by the bound vortices of the propeller are only tangential. Thus, the circumferential mean induced velocities include:

- Axial, tangential, radial circumferential mean velocities induced by trailing vortices.

- Tangential circumferential mean velocity induced by bound vortices.

Chapter VI

Propeller/Stator Combination

6.1 Introduction

Current design procedures, including optimisation of radial loading on the basis of the lifting line model, result in conventional propellers with the highest achievable efficiency. In recent years shipowners' requirements for improved fuel economy have led to the development and application of propulsive devices other than the conventional propeller.

Contrarotating propellers provide an effective means of reducing the rotational energy in the slipstream and will also remove the unbalanced torque reaction associated with the conventional propeller. However, their application involves increased capital cost and mechanical complications related to gear box and shafting. Largely for these reasons contrarotating propellers have not gained widespread use on commercial vessels and their use has been limited to torpedoes, where torque balance is essential.

Some of the benefits of contrarotation can be achieved at less cost and with reduced mechanical complication by the use of fixed guide vanes, i.e. stators, placed either upstream or downstream of the propeller. The stator can be designed to remove the unbalanced torque reaction and to reduce the rotational energy loss, but the gain in propulsor efficiency will be less than that achieved with contrarotation because of the increased drag of the stator.

As with other energy saving propulsors, the use of a stator is only worthwhile where the energy losses in the slipstream are significant i.e. the propeller loading is moderate to high. Where the propeller loading is light, as in the case of torpedo, the use of a stator may result in reduced propulsor efficiency, but they provide a cheap and effective means of removing the unbalanced torque.

6.2 Propeller with Downstream or Upstream Stator

Both downstream and upstream stators are designed such that the tangential velocities which they induce in the slipstream cancel those induced by the propeller, but the source of the efficiency gain is different in each case.

The downstream stator has a negligible effect on the propeller forces but, for appropriate propulsor loading, the stator produces a net positive thrust and the propulsor efficiency becomes greater than that of the equivalent conventional propeller.

On the other hand, the upstream stator produces a net negative thrust but modifies the flow to the propeller in such way that the propeller thrust is increased and, again in the right conditions, the propeller efficiency is increased.

Previous studies have shown, [3], that the use of a downstream stator is more effective than that of an upstream stator. Therefore the propeller with a downstream stator will be investigated more fully in the following sections.

6.3 Hydrodynamic Modelling of the Stator

The stator can be modelled by a system of lifting lines. The path of the trailing vortices behind the stator is different than that of the propeller. In the stator case,

the trailing vortices are no longer taken to be helical, but rather consist of semi-infinite line vortices. The velocities induced by each horseshoe vortex, consisting of a bound vortex segment and its accompanying trailing vortices, can be calculated by an application of the Biot-Savart Law.

Derivation of the equations from the Biot-Savart Law can be classified into two groups: equations for the stator induced velocities by non-deformed trailing vortices and those by deformed trailing vortices.

As shown in Figure 6.1 the velocities induced at a point $P(r_p, y_p, 0)$ by a short element of non-deformed vortex line located at $R(r\sin\theta, y, r\cos\theta)$ can be written as

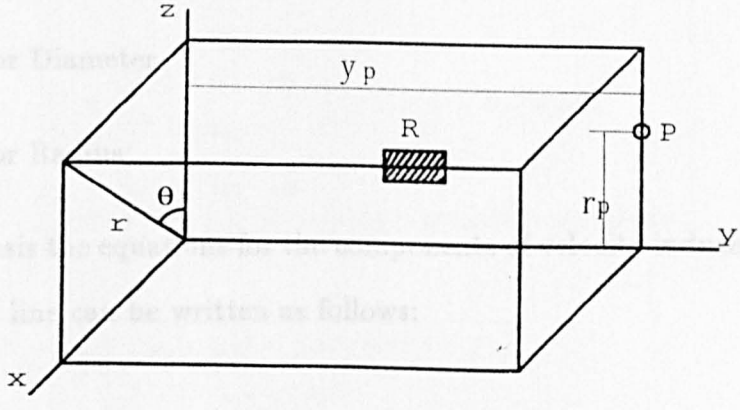

Figure 6.1 — Stator Modelling by Non-deformed Vortex Lines

$$d\vec{u} = \frac{\Gamma}{4\pi a^3} \begin{pmatrix} \vec{i} & \vec{j} & \vec{k} \\ 0 & 1 & 0 \\ -r\sin\theta & y_p - y & (r_p - r\cos\theta) \end{pmatrix} \tag{6.1}$$

or

$$\left.\begin{aligned} du_a &= 0 \\ du_r &= \frac{\Gamma}{4\pi a^3}[r\sin\theta]dy \\ du_t &= \frac{\Gamma}{4\pi a^3}[r_p - r\cos\theta]dy \end{aligned}\right\} \tag{6.2}$$

where $a = \sqrt{[r^2 + r_p^2 + (y_p - y)^2 - 2rr_p\sin\theta]}$

The use of Equation 6.2 is further simplified if it is put in non-dimensional form and for this purpose the following non-dimensional quantities are introduced: $\frac{u_a}{V_s}$, $\frac{u_t}{V_s}$, $\frac{u_r}{V_s}$, $x = \frac{r}{R_s}$, $x_p = \frac{r_p}{R_s}$, $G = \frac{\Gamma}{\pi D_s V_s}$

where

D_s= Stator Diameter

R_s= Stator Radius

On this basis the equations for the components of velocity induced at the point P by a vortex line can be written as follows:

$$\left.\begin{aligned} \frac{u_a}{V_s} &= 0 \\ \frac{u_r}{V_s} &= \frac{G}{2}\int_0^\infty \frac{1}{a^3}[x\sin\theta]dy \\ \frac{u_t}{V_s} &= \frac{G}{2}\int_0^\infty \frac{1}{a^3}[x_p - x\cos\theta]dy \end{aligned}\right\} \tag{6.3}$$

where

$$a = \sqrt{[x^2 + x_p^2 + (y_p - y)^2 - 2xx_p \sin\theta]}$$

For a stator having Z_s equally spaced blades, Z_s free vortex lines will start from the points on the blades corresponding to the radius r, the angular position of these lines in relation to the reference blade being given by

$$\phi_z = \frac{2\pi(n-1)}{Z_s} \tag{6.4}$$

where $n = 1, 2, 3, ...Z_s$ Then the total induced velocities can be determined by the simple summation of the individual velocities induced by the Z_s vortex lines from the hub (x_h) to tip (x_t) as follows:

$$\left.\begin{aligned} \frac{u_a}{V_s} &= 0 \\ \frac{u_r}{V_s} &= \sum_1^{Z_s} \frac{G}{2} \int_{x_h}^{x_t} \int_0^{\infty} \frac{1}{a^3}[x \sin(\theta + \phi_z)]dydx \\ \frac{u_t}{V_s} &= \sum_1^{Z_s} \frac{G}{2} \int_{x_h}^{x_t} \int_0^{\infty} \frac{1}{a^3}[x_p - x\cos(\theta + \phi_z)]dydx \end{aligned}\right\} \tag{6.5}$$

where $a = \sqrt{[x^2 + x_p^2 + (y_p - y)^2 - 2xx_p \sin(\theta + \phi_z)]}$

The above equations only give the effect of the vortices between $y = 0$ and $y = \infty$ and named as R.H.S. effect (explained in section 5.4). If a point is located between $y = 0$ and $y = y_p$, in addition to the R.H.S, the L.H.S effect is also calculated by integrating effect of the vortices between the $y = 0$ and $y = y_p$ as follows:

$$\left.\begin{aligned}
\frac{u_a}{V_s} &= 0 \\
\frac{u_r}{V_s} &= \sum_1^{Z_s} \frac{G}{2} \int_{x_h}^{x_t} \int_0^{y_p} \frac{1}{a^3}[x \sin(\theta + \phi_z)] dy dx \\
\frac{u_t}{V_s} &= \sum_1^{Z_s} \frac{G}{2} \int_{x_h}^{x_t} \int_0^{y_p} \frac{1}{a^3}[x_p - x \cos(\theta + \phi_z)] dy dx
\end{aligned}\right\} \tag{6.6}$$

The total induced velocities at the point P from the lifting line can be obtained by the summation of the effect of R.H.S and L.H.S for the tangential and axial induced velocities and the subtraction of the effect L.H.S and R.H.S for the radial induced velocities.

With a finite number of stator blades, the self-induced velocities around the circle at any radius of the stator will fluctuate cyclically. To design the stator it is necessary to use the mean values of these fluctuations. These mean velocities can easily be calculated in terms of the elliptic integrals of the first, second and third kind and written with the effect of the free vortices placed from the boss and the tip as follows:

$$u_{a,t,r} = -\int_{x_h}^{x_t} \delta u_{(a,t,r)_i} \frac{Z_s(\frac{\partial G}{\partial x})_i}{x_i} dx \tag{6.7}$$

When x is replaced by the angular coordinate ϕ , the above equation becomes

$$u_{a,t,r} = -Z_s \int_0^{\pi} \frac{\delta u_{(a,t,r)_i}}{x_i} \sum_{n=1}^{9} A_n n \cos n\phi_i d\phi \tag{6.8}$$

where $u_{(a,t,r)_i}$ are the axial, tangential and radial mean induced velocity components given by Equation 4.37 to 4.39.

The equation for the velocities induced at the point $P(0, y_p, r_p)$, Figure 6.2, by a deformed trailing vortex located at a general point $(r \sin\theta, y, r \cos\theta)$ can be

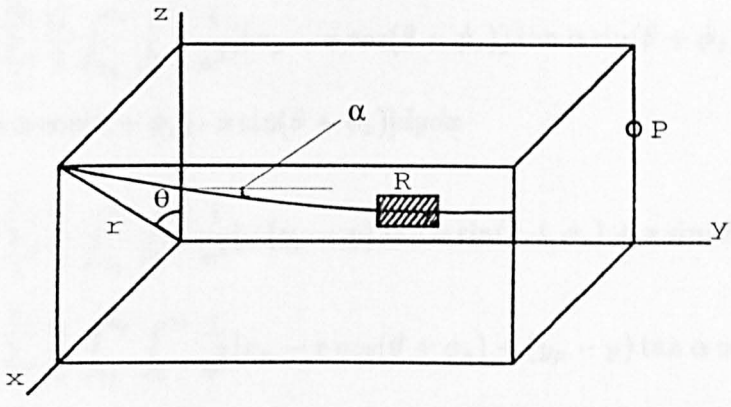

Figure 6.2 — Stator Modelling by Deformed Vortex Lines

formulated as follows:

$$d\vec{u} = \frac{\Gamma}{4\pi a^3} \begin{pmatrix} i & j & k \\ -\tan\alpha \sin\theta & 1 & -\tan\alpha\cos\theta \\ -r\sin\theta & y_p - y & (r_p - r\cos\theta) \end{pmatrix} \tag{6.9}$$

or

$$\left.\begin{aligned} du_a &= \frac{\Gamma}{4\pi a^3}[(r_p - r\cos\theta)\tan\alpha\sin\theta + \tan\alpha\cos\theta \cdot r\sin\theta]dy \\ du_r &= \frac{\Gamma}{4\pi a^3}[-(y_p - y)\tan\alpha\sin\theta + r\sin\theta]dy \\ du_t &= \frac{\Gamma}{4\pi a^3}[r_p - r\cos\theta + (y_p - y)\tan\alpha\cos\theta]dy \end{aligned}\right\} \tag{6.10}$$

When integration of the trailing vortices downstream from the lifting line and from the hub to the tip for each blade are considered, the following equations are

obtained in non-dimensional form:

$$\left.\begin{aligned} u_a &= \sum_1^{Z_s} \frac{G}{2} \int_{x_h}^{x_t} \int_0^{\infty} \frac{1}{a^3}[(x_p - x\cos(\theta+\phi_z))\tan\alpha\sin(\theta+\phi_z) + \\ &\quad \tan\alpha\cos(\theta+\phi_z)\cdot x\sin(\theta+\phi_z)]dydx \\ u_r &= \sum_1^{Z_s} \frac{G}{2} \int_{x_h}^{x_t} \int_0^{\infty} \frac{1}{a^3}[-(y_p - y)\tan\alpha\sin(\theta+\phi_z) + x\sin(\theta+\phi_z)]dydx \\ u_t &= \sum_1^{Z_s} \frac{G}{2} \int_{x_h}^{x_t} \int_0^{\infty} \frac{1}{a^3}[x_p - x\cos(\theta+\phi_z) + (y_p - y)\tan\alpha\cos(\theta+\phi_z)]dydx \end{aligned}\right\} \quad (6.11)$$

6.4 Design Consideration of Downstream Stator

The design variables for the stator are the number of blades and the axial separation of the propeller and stator. It is desirable to keep the tip of the stator within the propeller slipstream and for that reason the tip radius of the stator is set equal to the radius of the contracted propeller slipstream at the plane of the stator, as shown in Figure 6.3.

The following assumptions are also made in designing a downstream stator:

- The blades of the stator are considered to have an equal angular spacing.
- The stator is assumed to have zero skew and rake.
- The blades are represented by straight, radial lifting lines.

Having established the stator hub and tip radii from the propeller slipstream shape, 37 field points are distributed between the hub and tip with 5^o spacing between the points in angular coordinate. As in the case of the propeller, this spacing was found to give good accuracy and acceptable computation time. The

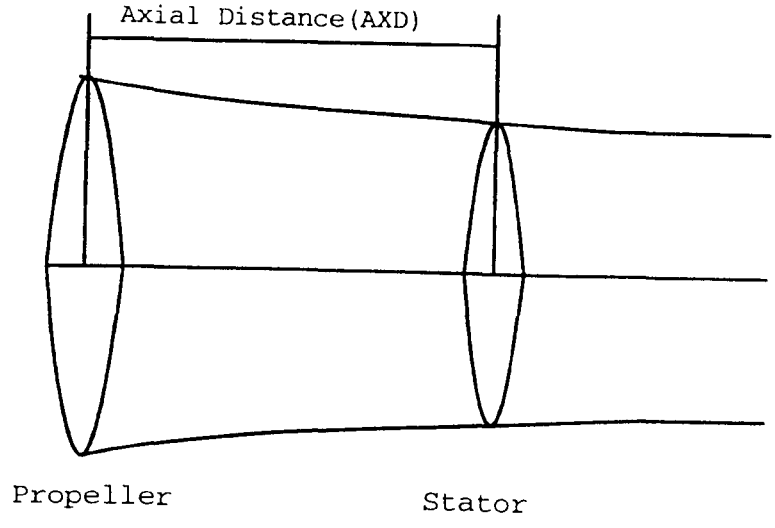

Figure 6.3 — Downstream Stator

locations of the field points are determined by following equation,

$$x_f(i) = x_h + 0.5(1 - x_t)(1 - \cos\theta_i) \tag{6.12}$$

where $\theta_i = \frac{\pi}{36}(N-1)$ $\qquad (N = 1, 2, 3, ..., 37)$

Since there are no rotational induced velocities downstream of the stator, the free vortex lines shed by the stator are directed axially downstream on the surfaces of cylinders which contract with the propulsor slipstream. On each of the trailing vortex lines shed from the stator 30 vortex elements and control points are considered and the non-dimensional axial location of these points is determined as below:

$$y_i = 5(1 - cos\theta_i) \tag{6.13}$$

where $\theta_i = \frac{\pi}{60}N \qquad N = 1,2,3,...,30$

Having done this, 1110 points are obtained to model the slipstream shape behind the stator. The next step is to determine the bound vortices of the stator in order to achieve the design of the stator. Once the bound circulation of the stator is established, the velocity induced by the stator can be calculated in axial, radial and tangential directions using Equation 6.11.

6.5 Determination of Bound Vortices of the Stator

In order to determine the induced velocities, first the circulation of the stator must be calculated. As stated earlier, the principle of the downstream stator design was to balance out the tangential velocities in the slipstream. Therefore the mean tangential velocities induced by the propeller should be cancelled out by those of the stator at infinity downstream where the trailing vortices shed from the propeller or the stator have significant effect while the bound vortices do not have any effect. The tangential velocities induced by the stator can be written in terms of the unknown circulation coefficients, A_n's as follows

$$u_t = \sum_{1}^{Z_s} \int_0^{\pi} \sum_{n=1}^{9} A_n \cdot \sin n\phi_i \int_0^{\infty} \frac{[x_p - x\cos(\theta+\phi_z) + (y_p - y)\tan\alpha\cos(\theta+\phi_z)]}{2[x^2 + x_p^2 + (y_p - y)^2 - 2xx_p\sin(\theta+\phi_z)]^{3/2}} dy d\phi \tag{6.14}$$

In order to calculate the mean tangential induced velocity at any radial location, the blade angle is divided into five parts and the above equation is applied at the resulting six points. The induced velocities are calculated and integrated at these points, then divided by the blade angle to give the mean induced velocity at that radial location.

The total mean tangential velocities induced by propeller are calculated on

each of 9 radii at infinity and those by stator are also determined at the same locations in terms of the unknown A_n's. Then a system of nine simultaneous equations is formed. The solution of this resulting matrix gives the unknown bound circulation coefficients of the stator. Having established the bound circulation, the induced velocities are calculated using Equation 6.11. An earlier experiment with the method indicated that the induced velocities in axial and radial directions are very small and they are ignored in this work.

6.6 Stator Torque and Thrust

As can be seen from Figure 6.4, the thrust and torque can be formulated for each blade section as below:

$$dT = dL\cos\beta_i - dD\sin\beta_i \tag{6.15}$$

$$dQ = (dL\sin\beta_i + dD\cos\beta_i)\ r \tag{6.16}$$

where $\beta_i = \frac{U_a + u_{apm}}{u_{tpm} - u_{ts}}$, u_{apm} and u_{tpm} are the axial and tangential mean velocities induced by the propeller, u_{ts} is the tangential velocity induced by the stator and U_a is the local wake velocity.

The resultant velocity, lift coefficient, drag coefficient, and lift-length coefficient can also be expressed as below respectively:

$$V_r = \frac{u_{apm} + U_a}{\sin\beta_i}$$

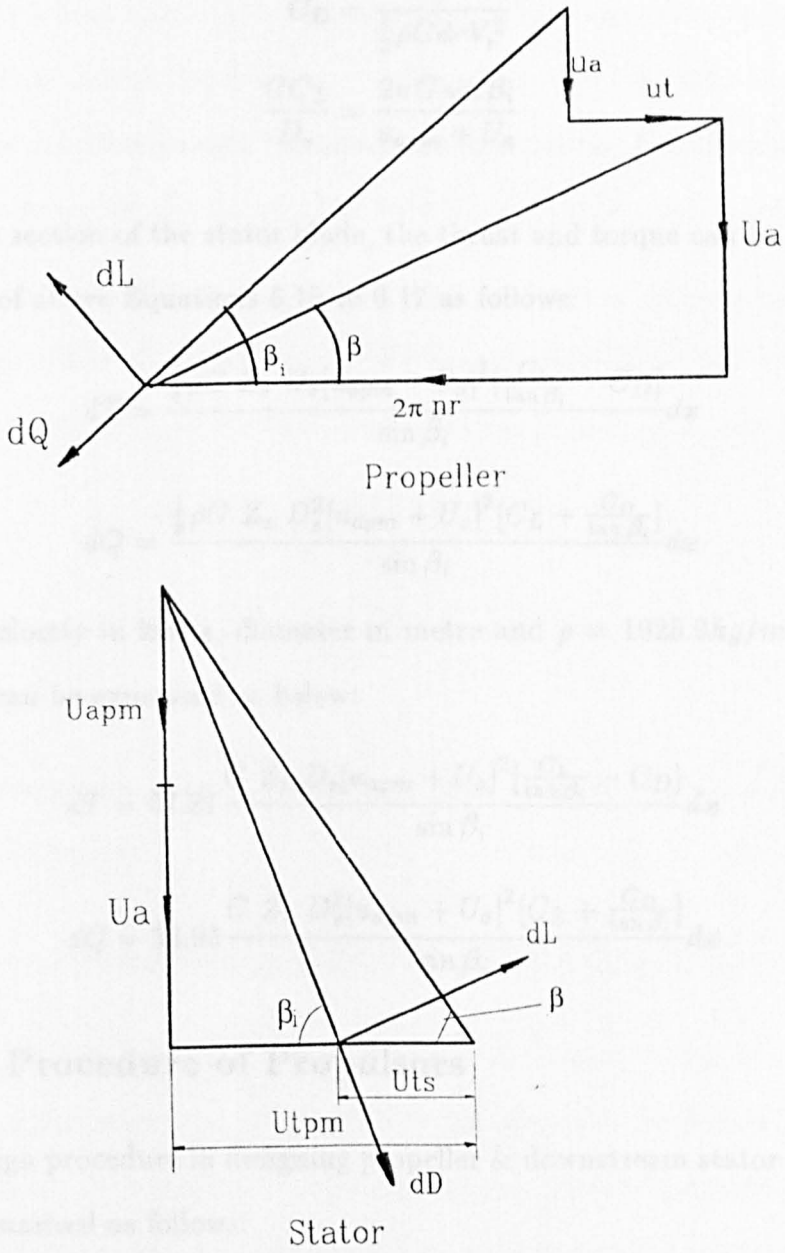

Figure 6.4 — Forces at Section of the Propeller and Downstream Stator

$$C_L = \frac{dL}{\frac{1}{2}\rho C dr V_r^2}$$

$$C_D = \frac{dD}{\frac{1}{2}\rho C dr V_r^2} \tag{6.17}$$

$$\frac{CC_L}{D_s} = \frac{2\pi G \sin\beta_i}{u_{apm} + U_a}$$

For each section of the stator blade, the thrust and torque can be obtained by making use of above Equations 6.15 to 6.17 as follows:

$$dT = \frac{\frac{1}{4}\rho C\ Z_s\ D_s[u_{apm} + U_a]^2[\frac{C_L}{\tan\beta_i} - C_D]}{\sin\beta_i} dx \tag{6.18}$$

$$dQ = \frac{\frac{1}{8}\rho C\ Z_s\ D_s^2[u_{apm} + U_a]^2[C_L + \frac{C_D}{\tan\beta_i}]}{\sin\beta_i} dx \tag{6.19}$$

When the velocity in knots, diameter in metre and $\rho = 1025.9 kg/m^3$ the thrust and torque can be expressed as below:

$$dT = 67.87\frac{C\ Z_s\ D_s[u_{apm} + U_a]^2[\frac{C_L}{\tan\beta_i} - C_D]}{\sin\beta_i} dx \tag{6.20}$$

$$dQ = 33.93\frac{C\ Z_s\ D_s^2[u_{apm} + U_a]^2[C_L + \frac{C_D}{\tan\beta_i}]}{\sin\beta_i} dx \tag{6.21}$$

6.7 Design Procedure of Propulsors

The design procedure in designing propeller & downstream stator combination can be summarised as follows:

- The propeller is designed by the method given in Chapter 5. The tangential mean velocities induced by the propeller are also calculated at infinity in the slipstream.

- The stator diameter is established as the diameter of the slipstream at the given axial distance.

- The stator bound circulation is calculated such that the stator induced tangential velocities cancel those due to the propeller. Consequently the thrust and torque are calculated using the stator characteristics. The calculations of the stator geometry, which are adopted from [3], are carried out as follows:

The initial width of the stator blade is taken as 25 % of the propeller diameter. The thickness of the blades section tapers linearly from $\frac{t}{C} = 0.20$ at the hub to $t = 0.003D_S$ at the tip and the thickness, t_i, of the section at x_i becomes

$$t_i = \frac{(0.20C_h - 0.003D_s)(x_t - x_i)}{(x_t - x_h)} + 0.003D_s \tag{6.22}$$

where C_h is the chord width at the hub, D_s the stator diameter, x_h the hub radius and x_t the tip radius.

The section drag coefficient can be written in terms of the blade thickness and chord length as below:

$$C_{D_i} = 2(1 + 2\frac{t_i}{C_i})[1.89 + 1.62log(\frac{C_i}{30 \times 10^{-6}})]^{-2.5} \tag{6.23}$$

Using the initial values of the stator geometry the stator design is made for the cancellation of the rotational velocity due to the propeller. Since it is unlikely that the stator blades will experience cavitation, the only limit which need be placed on the lift developed by the blade sections is that they should not have excessive form drag. On completion of the initial stator design calculations the section chords are adjusted to give lift coefficient values between 0.55 and 0.65, while at the same time maintaining a fair blade outline. The section thicknesses and drag coefficients are

given new values appropriate to the new chord lengths. The design of the stator is repeated with these new values and the process continued until convergence. In this way, cancellation of the rotational induced velocities is achieved with minimum stator drag.

Chapter VII

Application

7.1 Introduction

The purpose of this chapter is to illustrate the numerical application of the theoretical procedures given in the earlier sections and to discuss the results of the application. For the most appropriate application of the procedures, the calculations were carried out for a torpedo shaped body which was assumed to be deeply submerged.

Initially, the flow analysis around the body were carried out for the body without an operating propeller, for which the flow was assumed to consist of two parts: potential flow and boundary layer flow. The free surface effect was not taken into account since the body was assumed to be deeply submerged. The theoretical procedures described earlier were used to calculate the potential and boundary layer flows around the body and, in particular, to produce the nominal velocity distribution in the plane of the propeller.

The next step was the achievement of the propeller design using the newly obtained nominal velocity distribution. When the body was investigated with an operating propeller, essential interactions between the body and propeller had to be taken into account and simultaneously the propeller design should be redone. This procedure could provide the effective wake. Due to the slender body and the complexity of the mathematical modelling of the wake, the interaction between

the body&the propeller and the propeller&the boundary layer are ignored, as will be explained in a later section. Therefore the nominal velocities were used in all calculations. The use of the nominal wake would also provide the possibility of comparing the results for the propeller design.

Having obtained the final design of the propeller with a balanced slipstream shape, a stator device was placed downstream of the propeller. Based upon the assumption that the stator had no effect on the body, the performance of this combination was investigated for the variation in the number of the blades of the stator and for the variation in the axial distance between the stator and propeller.

In order to perform the above computations miscellaneous computer programs were written in Fortran 77 programming language for the propeller and stator design and some of the existing softwares were modified for flow calculations. These programs were set up to be run on an unix based Sun workstation.

7.2 Flow Analysis

In order to analyse the flow around the body, the potential flow calculation was carried out using Hess-Smith method [17]. The existing computer program based on this method was enhanced and used for computing the flow velocities around the torpedo shape body.

The input data file to the program contained the necessary information to control the flow of the computations, geometry of the body surface and off-body points. The body surface was defined by offset points in three dimensional space. The coordinate system, which these points were referred to, was designated as the reference coordinate system. The offset input had to be distributed in such a

way that an efficient representation of the body in terms of minimum CPU time could be achieved. In particular, the input points were increased in regions where the curvature of the body surface was large and the flow velocity was expected to change rapidly, while the input points were distributed sparsely in regions where neither the body geometry nor the the flow properties were varying significantly.

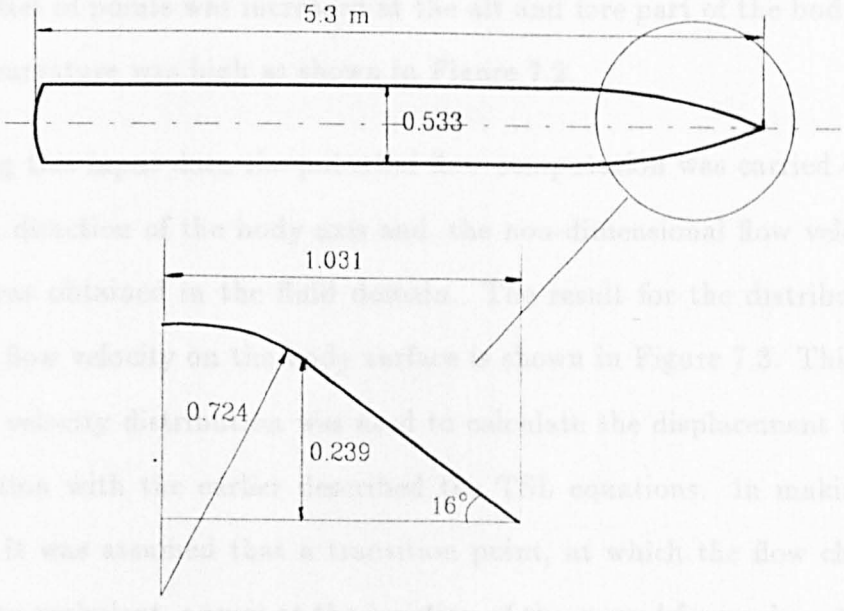

Figure 7.1 — The Geometry of the Body

The body surface was approximated by joining the input offset points which formed a set of plane quadrilateral panels. It was easy to organise the input offset points in such a way that the body was divided by rows and columns so that these points could easily be entered either in row direction or in column direction. The body, whose geometric characteristics as shown in Figure 7.1, was initially defined by 3952 input points. Nevertheless, this number was found to be high as it required

very large amount of CPU time. Therefore a set of preliminary calculations was carried out to find the optimum number of of input points for the same accuracy and consequently the number of input points was reduced to 1000. Although the body was approximated by 1000 input points, only 250 of them were entered to the computer program because of the axisymmetric nature of the body geometry. The details of the offset points are given in Appendix B for information. The density of the offset of points was increased at the aft and fore part of the body where the surface curvature was high as shown in Figure 7.2.

Using this input data the potential flow computation was carried out for unit inflow in direction of the body axis and, the non-dimensional flow velocity distribution was obtained in the fluid domain. The result for the distribution of the external flow velocity on the body surface is shown in Figure 7.3. This computed external velocity distribution was used to calculate the displacement thickness in combination with the earlier described the TSL equations. In making this calculation it was assumed that a transition point, at which the flow changes from laminar to turbulent, occurs at the junction of the curved forward portion and the parallel body. This seems a reasonable assumption to make because of the sudden change in body curvature which occurs at that point. Based upon this assumption the boundary layer calculation was performed. The resulting displacement and boundary layer (B.L.) thicknesses normal to the body surface are shown in Figure 7.4 at speeds of 50 and 15 knots. These speeds were considered as the design speed of the propellers as corresponding to lightly and heavily loaded operation conditions respectively. It can be seen from this figure that the change in speed does not result in much change in displacement thickness, but in a significant change in boundary layer thickness.

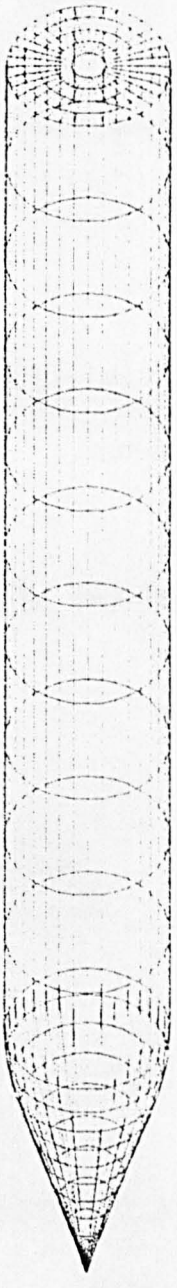

Figure 7.2 — Discretisation of the Body

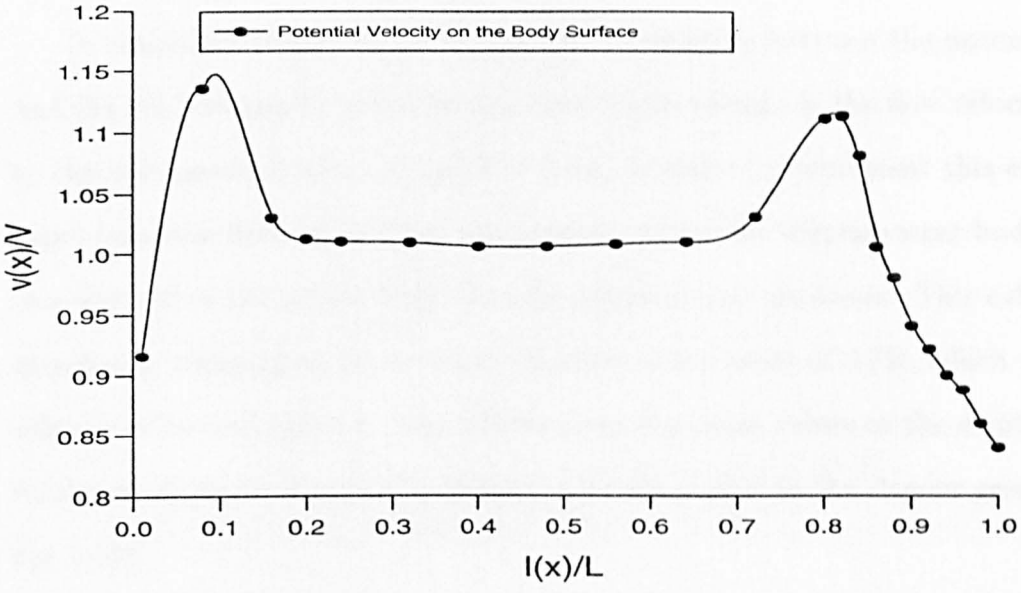

Figure 7.3 — The velocity on the Body surface

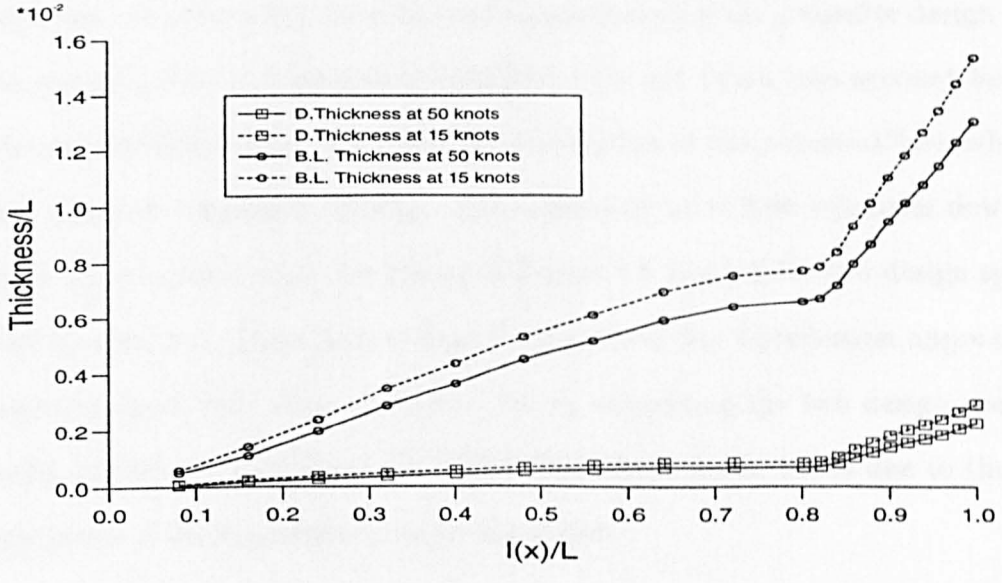

Figure 7.4 — Boundary Layer Thickness on the Body

In simplified terms, the hydrodynamic interaction between the potential flow and the BL flow can be taken into account by the change in the flow velocities due to the displacement effect of the flow field. In order to implement this effect the same potential flow calculation was carried out for the displacement body which was defined as the actual body plus the displacement thickness. This calculation resulted in a change in the external velocities of the order of 0.7%, which was considered to be insignificant. This follows from the small values of the displacement thickness shown in Figure 7.4, which can be attributed to the slender geometry of the body.

The next stage was to calculate the velocities inside the boundary layer by using Equation 3.32. Having performed the calculation of the local flow velocities at the control points of the slipstream in the axial and radial directions, the necessary input data for the wake distribution became ready for the propeller design process. As noticed, the local tangential velocities were not taken into account because of the slender shape of the body and the assumption of the potential flow, which does not create a tangential velocity. The computed axial flow velocities downstream from the propeller plane are shown in Figure 7.5 and 7.6 for two design speeds. It can be seen from these figures that the axial velocity distribution approaches the uniform onset flow value at $Y/R = 2.0$ In comparing the two design speeds, the axial velocities for 50 knots are higher than those for 15 knots due to the greater thickness of the boundary layer at low speed.

The radial components of the flow at points within the boundary layer were calculated on the assumption that the ratio of the radial components to the axial components (U_r/U_a) derived from the potential flow calculation remained constant

and could be applied to the axial velocities derived from the boundary layer calculation. Although it could be argued that this effect should be calculated on a more sound basis, the assumption was considered to be satisfactory in relation to the flow associated with the slender torpedo body. The radial velocities have small values at the propeller plane and approach zero rapidly in the downstream direction. They are shown in Figure 7.7 and Figure 7.8 for the two design speeds.

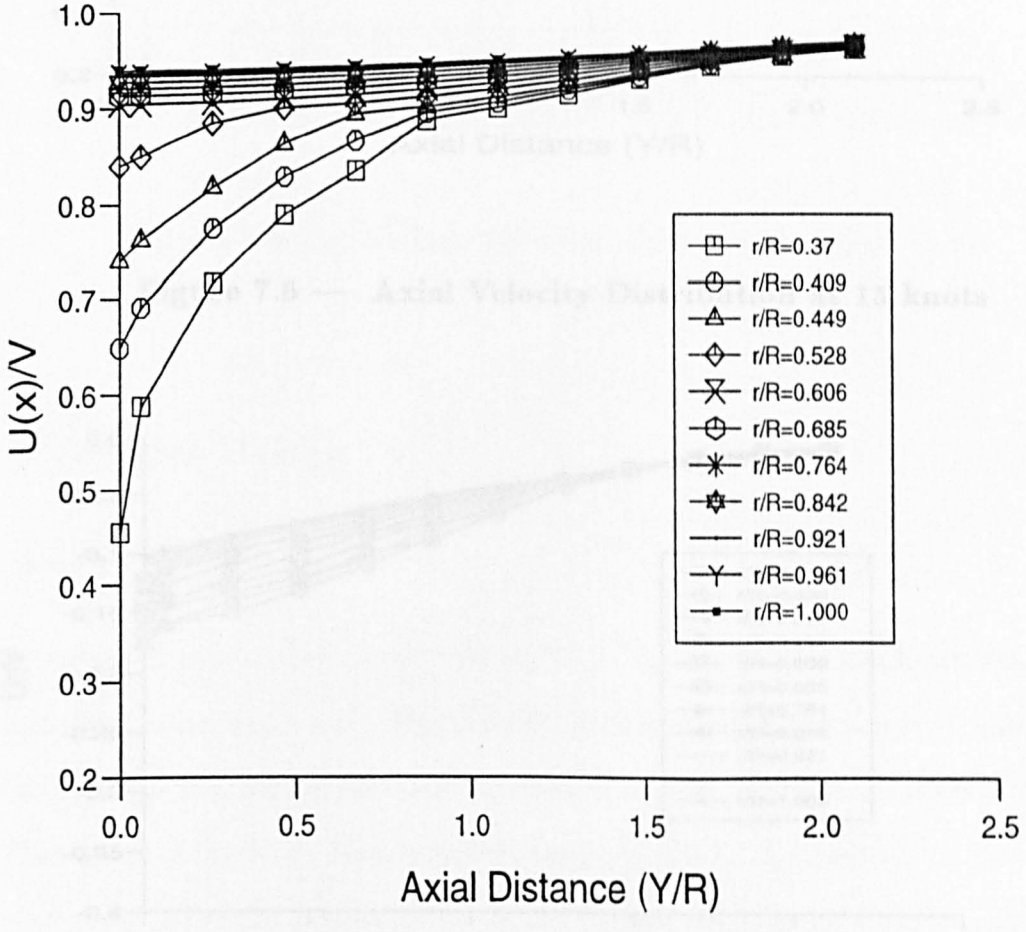

Figure 7.5 — Axial Velocity Distribution at 50 knots

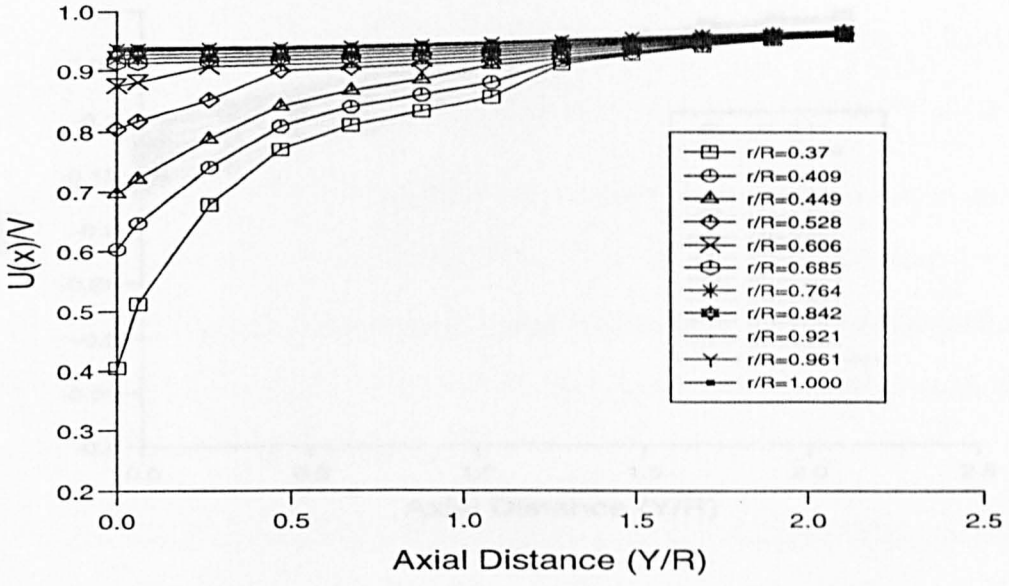

Figure 7.6 — Axial Velocity Distribution at 15 knots

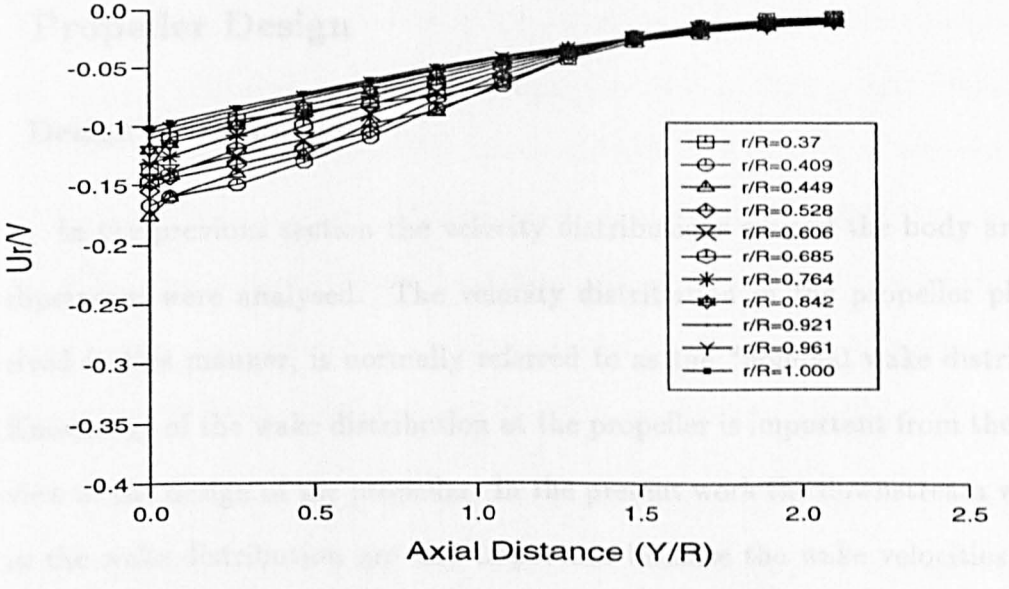

Figure 7.7 — Radial Velocity Distribution at 50 knots

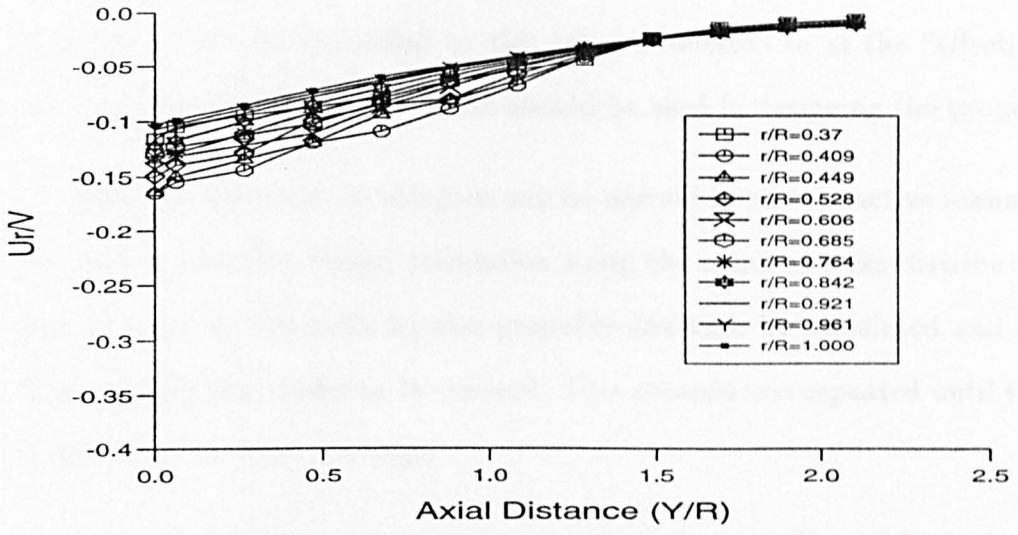

Figure 7.8 — Radial Velocity Distribution at 15 knots

7.3 Propeller Design

7.3.1 Design Methodology

In the previous section the velocity distributions around the body and in the slipstream were analysed. The velocity distribution in the propeller plane, derived in this manner, is normally referred to as the "nominal wake distribution". Knowledge of the wake distribution at the propeller is important from the point of view of the design of the propeller. In the present work the downstream variations in the wake distribution are also important because the wake velocities must be accounted for in modelling the paths of the trailing vortices.

In fact, with a propeller working behind the body, the flow around the body and in its wake, will be modified by the action of the velocities induced by the

propeller. The wake modified by this effect is referred to as the "effective wake" and the effective wake distribution should be used in designing the propeller.

The effective wake distribution can be derived in an interactive manner, starting with a propeller design calculation using the nominal wake distribution. The flow induced on the body by this propeller can then be calculated and the body flow and effective wake can be derived. This procedure is repeated until the values of the effective wake converge.

In the above process the important point is the modelling of the hydrodynamic interaction effect between the flows around the body and the propeller. The influence of the propeller induced flow on the potential flow around the body was found to be negligible for the most of the propeller loadings considered here. The effect on the boundary layer flow could be more important but cannot be represented easily. The author attempted to quantify this effect using an available computer program based on a semi-empirical methodology proposed by Huang [43]. Unfortunately, it was not possible to achieve a stable solution and this effect was not included in the present procedure. This omission was not considered important because, with the thin boundary layer associated with the torpedo shape body, the influence of boundary layer flow on the wake distribution at the propeller was small. In summary, the nominal wake distribution was used in designing the propeller.

The major steps of the propeller design methodology based on the theory given in Chapter 5 is shown in Figure 7.9 and a Fortran computer program was written, based on this methodology.

The basic input data required by the present propeller design method can be

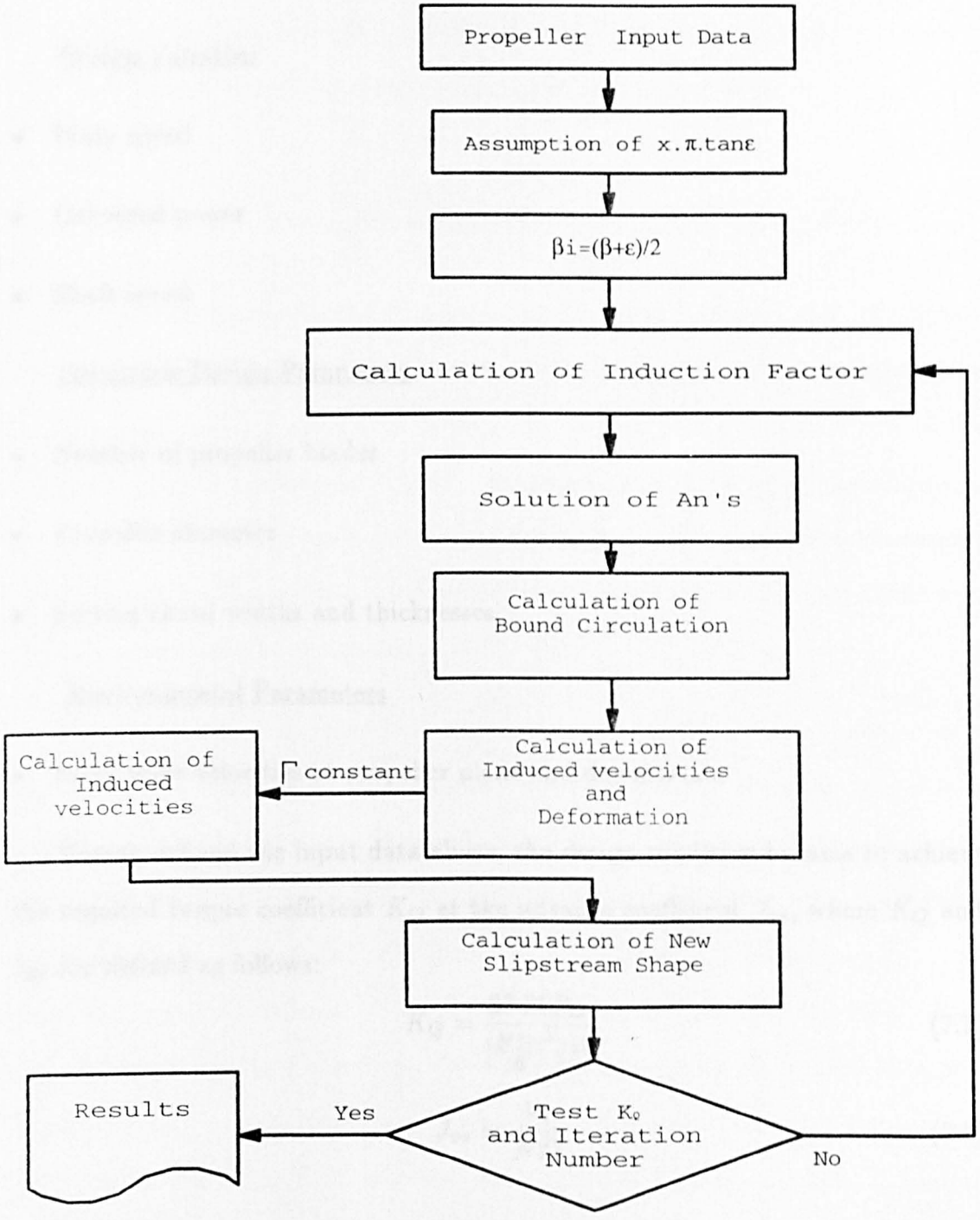

Figure 7.9 — Propeller Design Procedure

listed as follows:

Design Variables

- Body speed
- Delivered power
- Shaft speed

Geometric Design Parameters

- Number of propeller blades
- Propeller diameter
- Section chord widths and thicknesses

Environmental Parameters

- Body wake velocities at propeller plane and downstream

Having defined the input data above, the design condition became to achieve the required torque coefficient K_Q at the advance coefficient J_{vs}, where K_Q and J_{vs} are defined as follows:

$$K_Q = \frac{33.55 P_D}{[\frac{ND}{10}]^3 D^2} \tag{7.1}$$

$$J_{vs} = \frac{V_s}{ND} \tag{7.2}$$

In order to calculate the induction factors using Equations 5.9 to 5.11, the initial value of the vortex pitch angle of the trailing vortices should be determined. The advance angle β_y at the propeller plane and downstream is calculated from

the rotational speed of the propeller, N, and the wake velocities. An initial value of $x\pi \tan\varepsilon$, the pitch ratio of the vortex sheets in the ultimate wake is assumed and the initial values of the vortex pitch angles are derived from

$$\beta_{iy} \doteq \frac{(\beta_y + \varepsilon)}{2} \tag{7.3}$$

Using these values the initial slipstream geometry is defined and the induction factors are calculated to determine expressions for the velocities induced by the propeller vortex system at 9 radial points on the lifting line, in terms of the unknown Fourier coefficients. These expressions are introduced to the minimum energy loss condition $x\pi \tan\varepsilon = constant$ and a system of nine simultaneous equation is formed. The solution of these equations gives the circulation coefficients A_n and hence the bound circulation Γ.

Having calculated the bound circulation the induced velocities in the slipstream are calculated. Using these calculated induced velocities and the wake velocities, a deformed slipstream shape is obtained. Based on this deformed slipstream shape, the calculation of the induction factors is carried out. Keeping the bound circulation constant, the induced velocities and consequently the deformation of the slipstream are re-calculated. This is the completion of the first iteration. Having completed the first iteration, the next iteration starts using that deformed slipstream to calculate the bound circulation. The expressions for the induced velocities at the lifting line are determined and the resulting equations are solved as before to give the new circulation. This procedure is continued until the slipstream shape is converged. It was found by early experiments with the method that at least 3 iterations would be necessary for the convergence of the slipstream

shape and to achieve the required torque coefficient. During each iteration the elementary torque coefficients $\frac{dK_Q}{dx}$ for eleven sections are calculated, the values at the hub and tip being set equal to zero. Integration of these coefficients gives the calculated torque coefficient, K_{Q_o}. If $|K_{Q_o} - K_Q| < 0.0001$ and the slipstream shape is properly converged, the design is considered to be completed. The final propeller characteristics such as hydrodynamic pitch angle, β_i, the lift-length coefficient $\frac{cC_l}{D}$, the lift coefficient C_L, and the elementary thrust coefficient $\frac{dK_T}{dx}$ are then calculated for each nine sections.

7.3.2 Illustrative Examples

In this section a propeller design based upon the above methodology was performed for verification and comparison with results of other methods. Since the slipstream deformation was expected to be a function of load coefficient C_T, it was decided to select two types of loading condition: lightly and heavily loaded cases with the same propeller geometric characteristics at different advance speeds and rates of rotation. Details of the design data which are referred to as DATA1 for the lightly loaded case are as follows:

Design Characteristics for DATA1

Delivered Power, P_D= 260 KW

Design Speed, V= 50 $Knots$

Rate of Rotation, N= 3000 rpm

Propeller Diameter, D= 0.490 $metre$

Number of Blades, Z= 3

Radius	0.37	0.409	0.449	0.528	0.606	0.685	0.764	0.842	0.921	0.961	1.0
C (m)		0.1725	0.1800	0.1925	0.2080	0.2122	0.2045	0.1840	0.1420	0.1050	0
C_D		0.0095	0.0093	0.0092	0.0091	0.0090	0.0089	0.0088	0.0087	0.0086	

The input wake velocities (U(x)/V) computed from the previous procedure is shown in Table 7.1

$\frac{Radius}{Y/R}$	0.37	0.409	0.449	0.528	0.606	0.685	0.764	0.842	0.921	0.961	1.0
0.00	0.455	0.649	0.740	0.841	0.904	0.912	0.920	0.927	0.933	0.936	0.938
0.06	0.588	0.691	0.763	0.851	0.904	0.913	0.920	0.927	0.933	0.936	0.938
0.26	0.716	0.775	0.819	0.885	0.906	0.914	0.922	0.928	0.934	0.937	0.939
0.46	0.790	0.830	0.864	0.900	0.909	0.917	0.924	0.930	0.936	0.938	0.940
0.67	0.836	0.867	0.893	0.904	0.913	0.921	0.927	0.933	0.938	0.940	0.943
0.87	0.888	0.895	0.900	0.910	0.919	0.926	0.932	0.937	0.942	0.944	0.946
1.08	0.900	0.905	0.910	0.919	0.926	0.932	0.937	0.942	0.946	0.948	0.949
1.28	0.914	0.918	0.922	0.929	0.934	0.939	0.943	0.947	0.950	0.952	0.954
1.48	0.930	0.933	0.935	0.939	0.943	0.947	0.950	0.953	0.956	0.957	0.958
1.69	0.944	0.946	0.947	0.949	0.952	0.954	0.956	0.959	0.960	0.961	0.962
1.89	0.955	0.955	0.956	0.958	0.959	0.961	0.962	0.964	0.965	0.966	0.967
2.10	0.962	0.963	0.963	0.964	0.965	0.966	0.967	0.968	0.969	0.970	0.970
4.14	0.988	0.988	0.988	0.988	0.988	0.988	0.988	0.989	0.989	0.989	0.989
6.18	0.994	0.994	0.994	0.994	0.994	0.994	0.994	0.994	0.994	0.994	0.994
8.22	0.996	0.996	0.996	0.996	0.996	0.996	0.996	0.996	0.996	0.996	0.996
10.26	0.997	0.997	0.997	0.997	0.997	0.997	0.997	0.997	0.997	0.997	0.997
12.30	0.998	0.998	0.998	0.998	0.998	0.998	0.998	0.998	0.998	0.998	0.998
14.34	0.998	0.998	0.998	0.998	0.998	0.998	0.998	0.998	0.998	0.998	0.999

16.38	0.999	0.999	0.999	0.999	0.999	0.999	0.999	0.999	0.999	0.999	0.999
18.42	0.999	0.999	0.999	0.999	0.999	0.999	0.999	0.999	0.999	0.999	0.999
20.46	0.999	0.999	0.999	0.999	0.999	0.999	0.999	0.999	0.999	0.999	0.999

Table 7.1 — Wake Velocities for DATA1

For DATA1, the propeller design was carried out using the above values. The results of the application of the design method were rather encouraging. The slipstream shape seemed to converge at all control points but there were a few control points at which some irregularities in the magnitude of the velocities were observed. The irregularities occurred at the hub and tip and in the region immediately downstream of the lifting line. This was attributed to the close radial spacing of the field and reference vortices which resulted in unrealistic values. This problem was overcome by increasing the spacing of the field vortices without significant influence on the overall accuracy of the calculation.

Convergence of the deformed slipstream shape was achieved in three iterations. The downstream variations of the induced velocity components and of the slipstream radius for the mid-section of the propeller blade are shown in Figure 7.10 to 7.14. The figures represent the computations for each iteration process. As can be seen from these figures the velocities converge very rapidly. In fact, after the second iteration the values remain virtually unchanged.

In Table 7.2 the results are shown in comparison with those from the methods of Glover and Koumbis [2, 6]. It must be borne in mind that in these methods only the local velocities on the propeller plane were used as input wake values

whereas in the present method the variation of the flow velocities in the slipstream was taken into account. In Glover's method the non-deformed helical slipstream shape is used for the hydrodynamic modelling of the propeller, while a deformed slipstream shape is considered in Koumbis' method.

Lightly Loaded Case (DATA1)			
	Glover's Method	Koumbis' Method	Pr. Method
K_Q	0.1143	0.01143	0.1143
K_T	0.0502	0.0503	0.0500
η	0.647	0.648	0.646
C_T	0.149	0.149	0.148

Table 7.2 — Comparison of the Methods

As can be seen from Table 7.2, there is not much difference between the calculated results. This may suggest that for this design case (i.e. loading) the effect of the variation in flow velocities in the slipstream does not have a significant effect on the propeller design.

The calculated bound circulation, hydrodynamic pitch angle, lift-length coefficient are shown in Figures 7.15 to 7.17 respectively in comparison with other methods (i.e Glover's method and Koumbis' method).

The results for the reference helices shed at the characteristic non-dimensional radii of the lifting line with variation of axial distance downstream and iterations

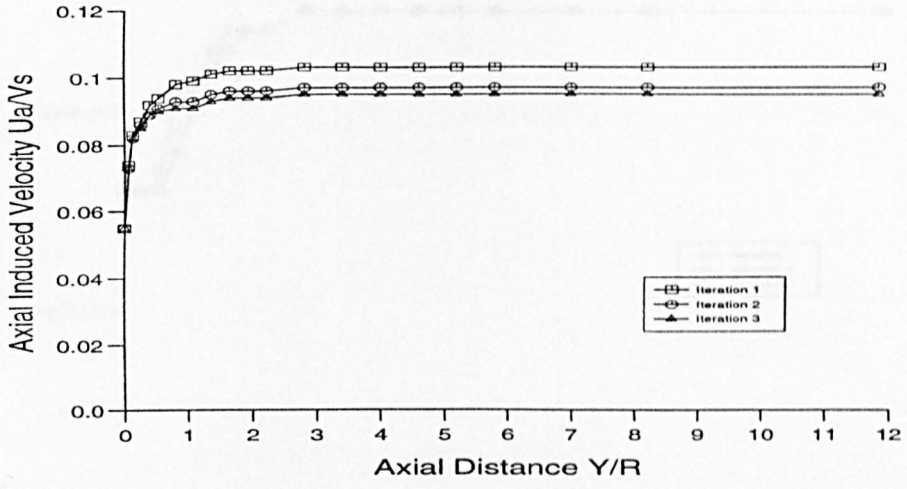

Figure 7.10 — Variation of Axial Induced Velocity at x=0.61 for DATA1

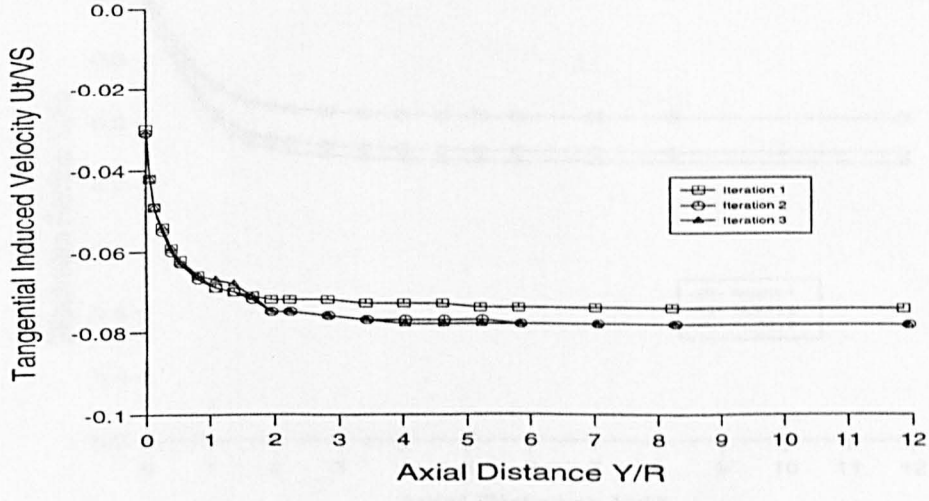

Figure 7.11 — Variation of Tangential Induced Velocity at x=0.61 for DATA1

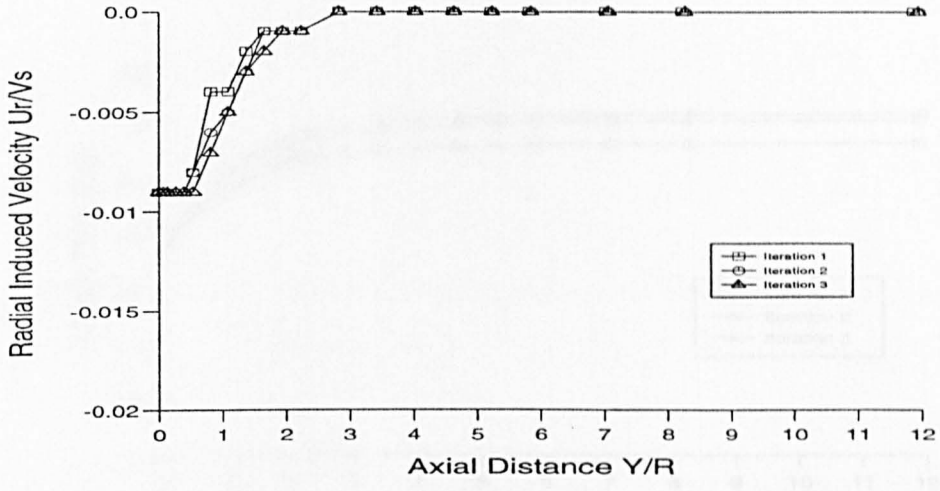

Figure 7.12 — Variation of Radial Induced Velocity at x=0.61 for DATA1

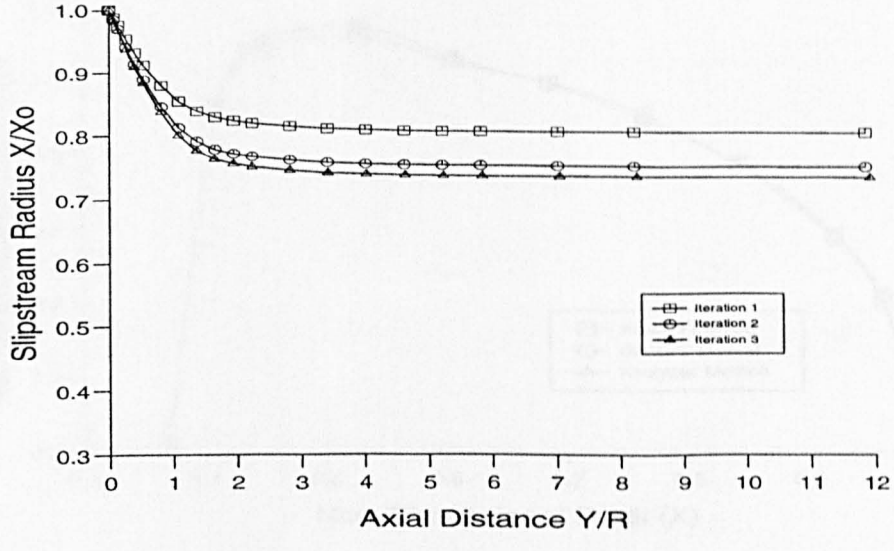

Figure 7.13 — Variation of Radius at x=0.61 for DATA1

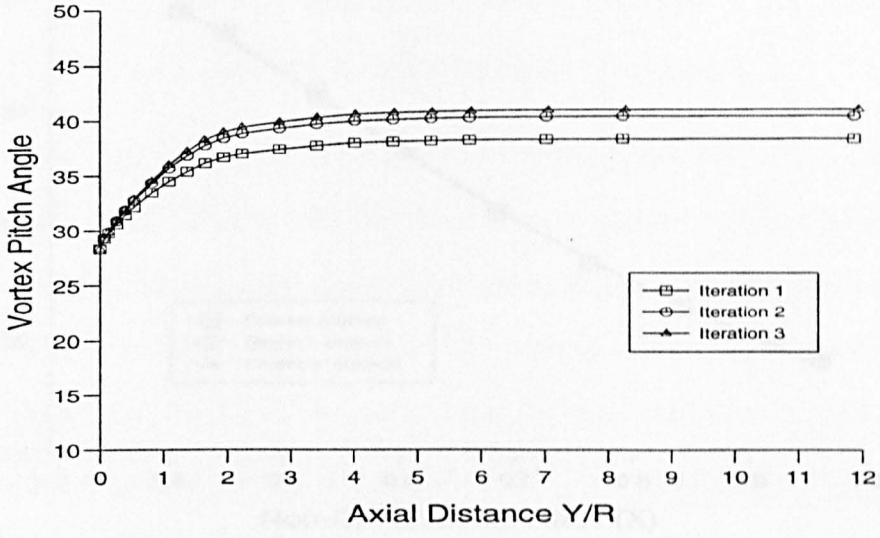

Figure 7.14 — Vortex Pitch Variation at x=0.61 for DATA1

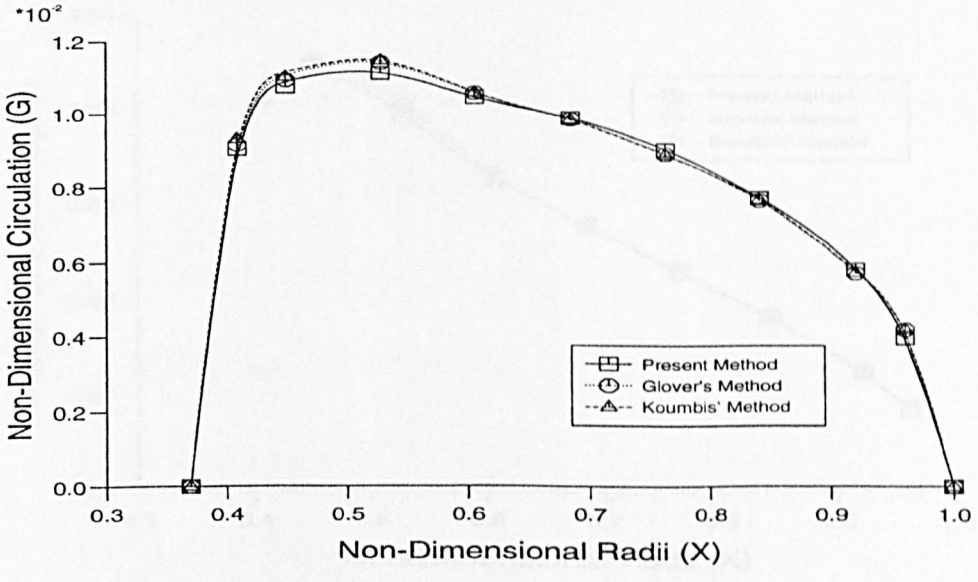

Figure 7.15 — Circulation Distribution (DATA1)

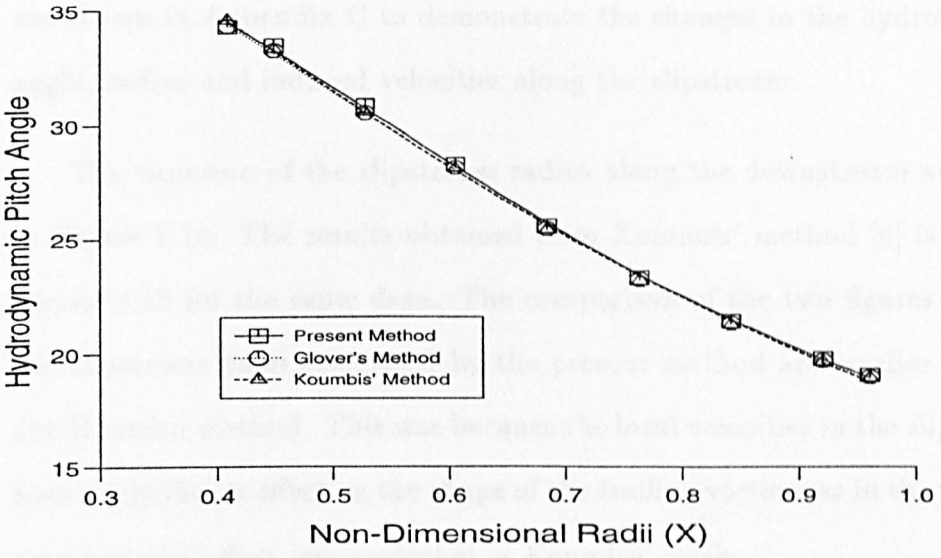

Figure 7.16 — Hydrodynamic Pitch Angle (DATA1)

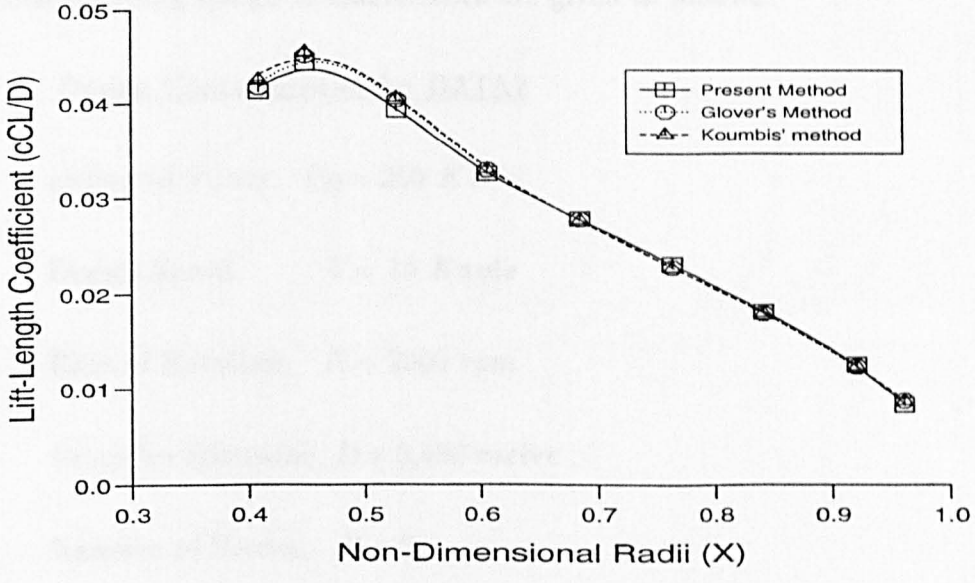

Figure 7.17 — Lift-Length Coefficient (DATA1)

are shown in Appendix C to demonstrate the changes in the hydrodynamic pitch angle, radius and induced velocities along the slipstream.

The variation of the slipstream radius along the downstream are also plotted in Figure 7.18. The results obtained from Koumbis' method [6] is also shown in Figure 7.19 for the same data. The comparison of the two figures indicates that the slipstream radii calculated by the present method are smaller than those by the Koumbis method. This was because the local velocities in the slipstream would have a significant effect on the shape of the trailing vortices as in the real slipstream case and this effect was neglected in Koumbis' work.

7.3.3 Design Calculations for DATA2

The set of design data for the heavily loaded case is referred to as DATA2 and corresponding design characteristics are given as follows:

Design Characteristics for DATA2

Delivered Power, P_D= 260 KW

Design Speed, V= 15 $Knots$

Rate of Rotation, N= 2000 rpm

Propeller Diameter, D= 0.490 $metre$

Number of Blades, Z= 3

The chord widths and thicknesses of the propeller blade corresponding to each of the section radii are taken the same as DATA1. The wake velocities at the propeller plane and downstream are given in Table 7.3:

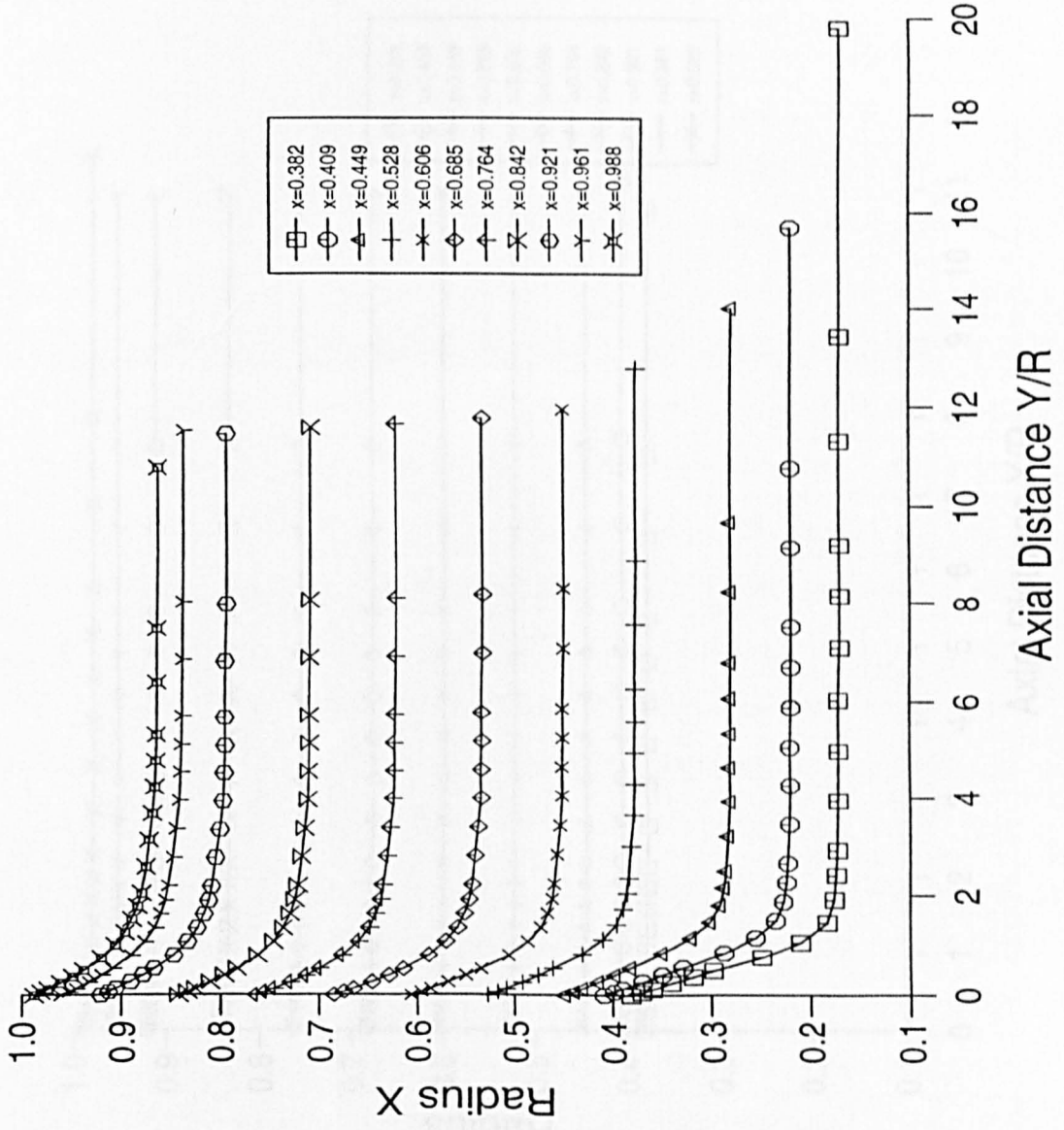

Figure 7.18 — Slipstream Shape by Present Method for DATA1

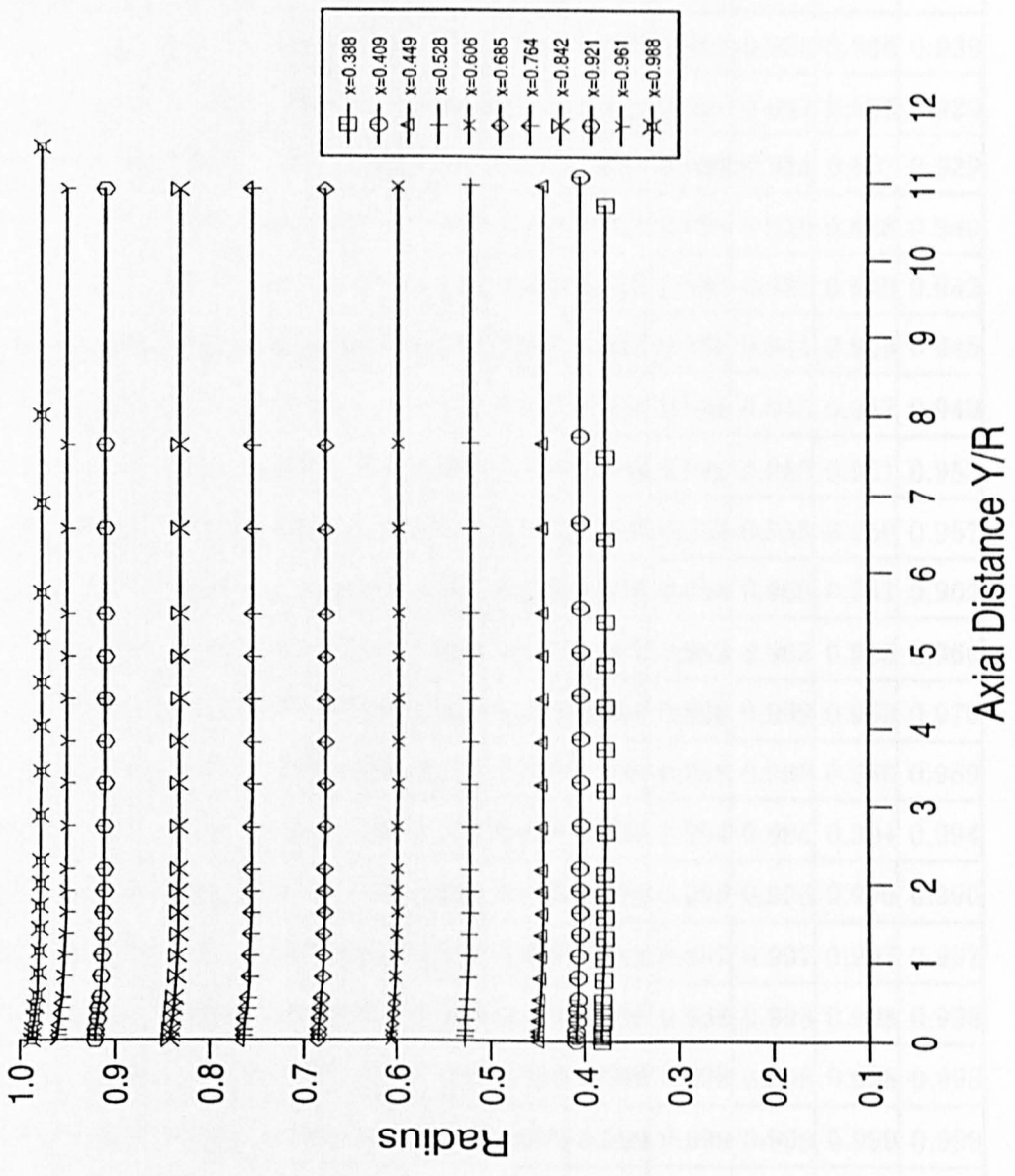

Figure 7.19 — Slipstream Shape by Koumbis' Method for DATA1

$\frac{Radius}{Y/R}$	0.37	0.409	0.449	0.528	0.606	0.685	0.764	0.842	0.921	0.961	1.0
0.00	0.405	0.603	0.697	0.805	0.875	0.913	0.920	0.927	0.933	0.936	0.939
0.06	0.512	0.647	0.722	0.817	0.881	0.913	0.921	0.927	0.933	0.936	0.939
0.26	0.678	0.740	0.788	0.852	0.906	0.915	0.922	0.928	0.934	0.937	0.939
0.46	0.770	0.808	0.841	0.899	0.909	0.917	0.924	0.930	0.935	0.938	0.940
0.67	0.810	0.840	0.867	0.903	0.912	0.920	0.927	0.933	0.938	0.940	0.942
0.87	0.833	0.860	0.885	0.909	0.918	0.925	0.931	0.936	0.941	0.943	0.945
1.08	0.856	0.880	0.908	0.917	0.925	0.931	0.936	0.941	0.945	0.947	0.949
1.28	0.911	0.916	0.920	0.927	0.933	0.938	0.942	0.946	0.950	0.951	0.953
1.48	0.928	0.931	0.933	0.938	0.942	0.946	0.949	0.952	0.955	0.956	0.957
1.69	0.943	0.944	0.946	0.948	0.951	0.953	0.956	0.958	0.960	0.961	0.962
1.89	0.954	0.954	0.955	0.957	0.958	0.960	0.961	0.963	0.965	0.965	0.966
2.10	0.961	0.962	0.962	0.963	0.964	0.965	0.966	0.968	0.969	0.969	0.970
4.14	0.988	0.988	0.988	0.988	0.988	0.988	0.988	0.988	0.988	0.989	0.989
6.18	0.994	0.994	0.994	0.994	0.994	0.994	0.994	0.994	0.994	0.994	0.994
8.22	0.996	0.996	0.996	0.996	0.996	0.996	0.996	0.996	0.996	0.996	0.996
10.26	0.997	0.997	0.997	0.997	0.997	0.997	0.997	0.997	0.997	0.997	0.997
12.30	0.998	0.998	0.998	0.998	0.998	0.998	0.998	0.998	0.998	0.998	0.998
14.34	0.998	0.998	0.998	0.998	0.998	0.998	0.998	0.998	0.998	0.998	0.998
16.38	0.999	0.999	0.999	0.999	0.999	0.999	0.999	0.999	0.999	0.999	0.999
18.42	0.999	0.999	0.999	0.999	0.999	0.999	0.999	0.999	0.999	0.999	0.999
20.46	0.999	0.999	0.999	0.999	0.999	0.999	0.999	0.999	0.999	0.999	0.999

Table 7.3 — Wake Velocities for DATA2

The design calculations were carried out as for the previous lightly loaded case, the similar results are shown in Table 7.4 and in Figures from 7.20 to 7.27. As shown in Table 7.4 the present method with this set of data (DATA2) indicates slightly higher efficiency value in comparison with the methods of Glover and Koumbis. The comparison of the lightly and heavily loaded design cases are discussed in the following section.

Heavily Loaded Case (DATA2)			
	Glover's Method	Koumbis' Method	Pr. Method
K_Q	0.03858	0.03858	0.03858
K_T	0.2636	0.2706	0.2754
η	0.448	0.458	0.466
C_T	3.94	4.05	4.11

Table 7.4 — Comparison of the Methods

7.3.4 Discussion

In the previous sections, it was shown the influence of the helical slipstream upon itself with the local velocities results in change in the slipstream so that it gradually converges to a fixed deformed form. The slipstream deformations for each of flow cases, such as potential flow, wake flow without a propeller and wake flow with a propeller, are shown in Figures 7.29 and 7.30 for DATA1 and DATA2 respectively.

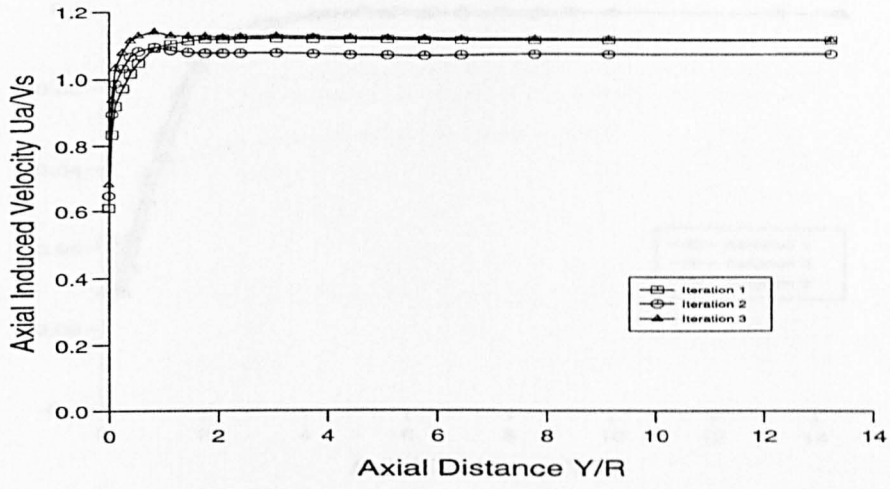

Figure 7.20 — Variation of Axial Induced Velocity at x=0.61 for DATA2

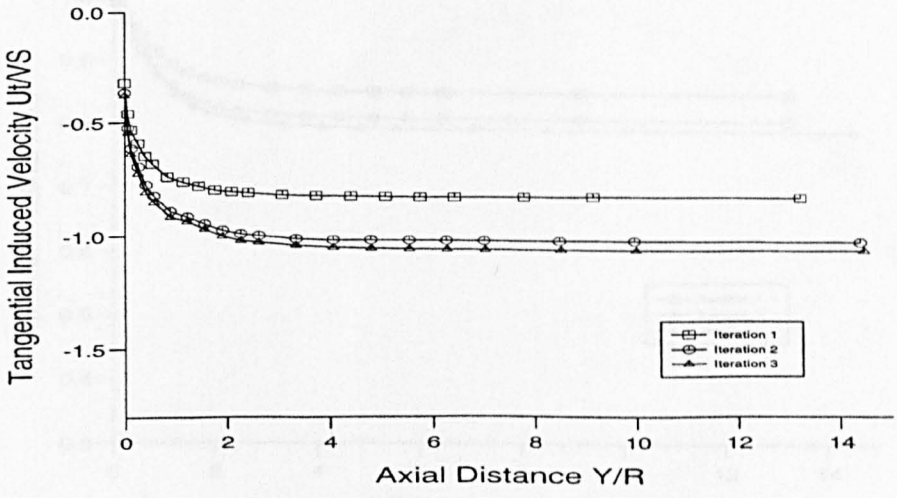

Figure 7.21 — Variation of Tangential Induced Velocity at x=0.61 for DATA2

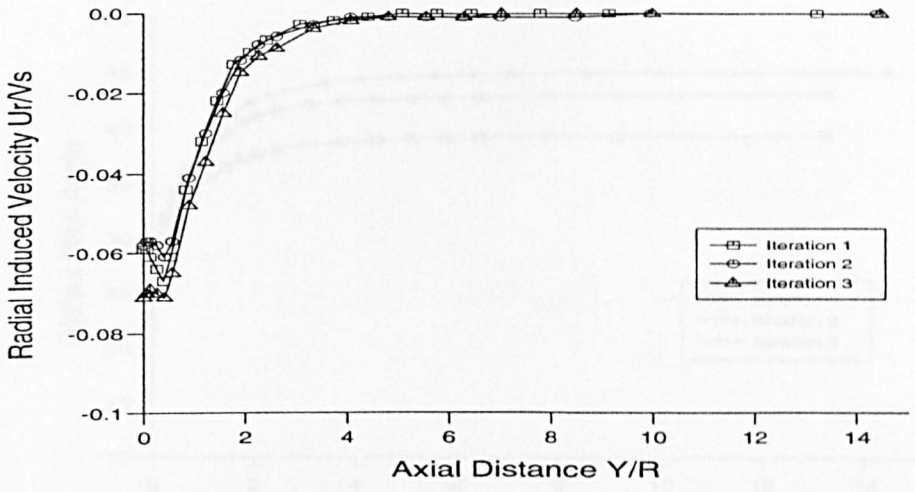

Figure 7.22 — Variation of Radial Induced Velocity at x=0.61 for DATA2

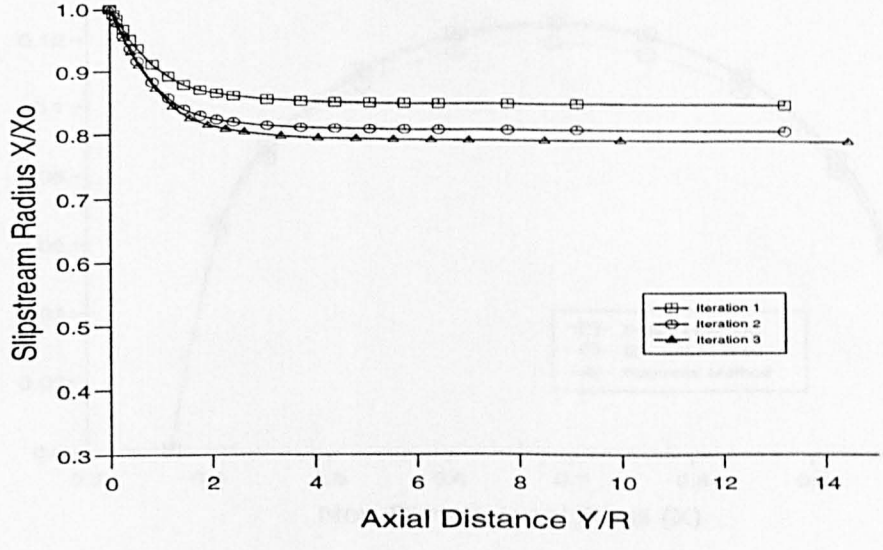

Figure 7.23 — Variation of Radius at x=0.61 for DATA2

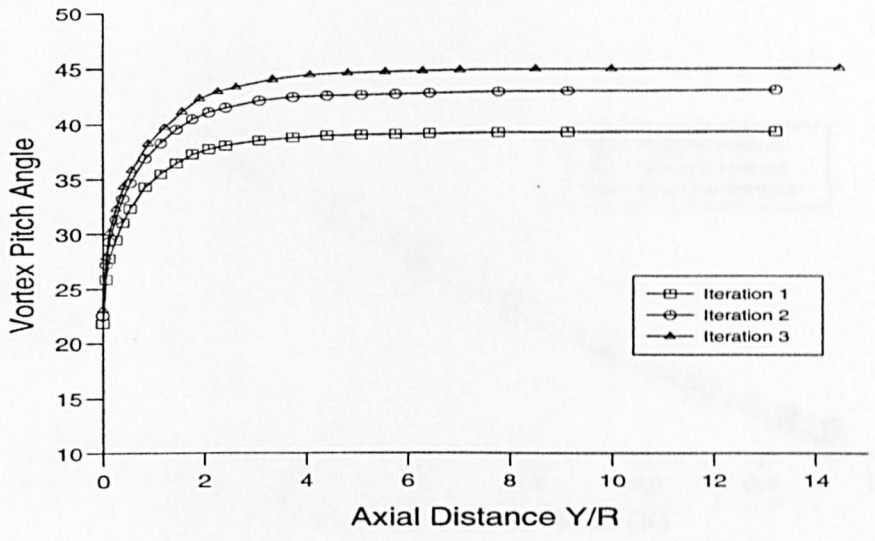

Figure 7.24 — Vortex Pitch Variation at x=0.61 for DATA1

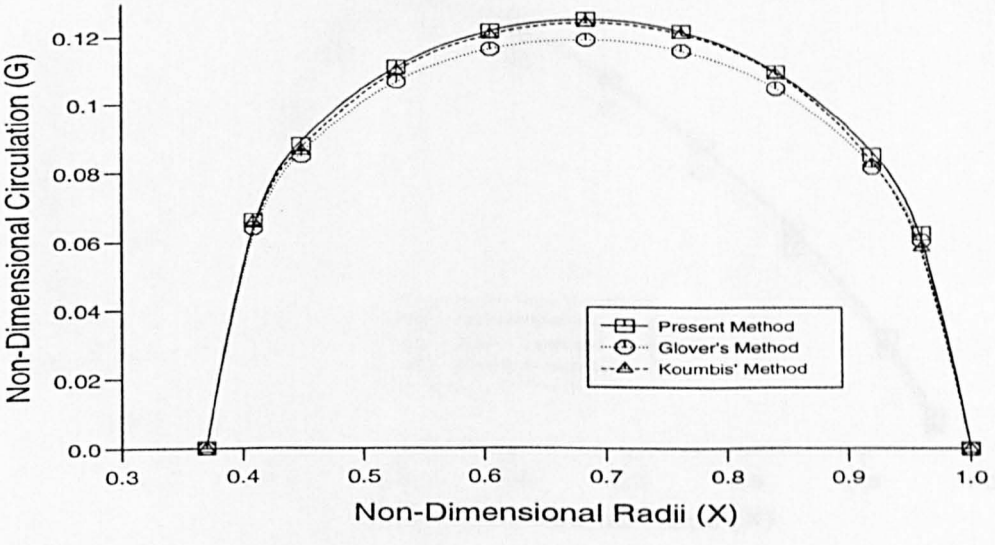

Figure 7.25 — Circulation Distribution (DATA2)

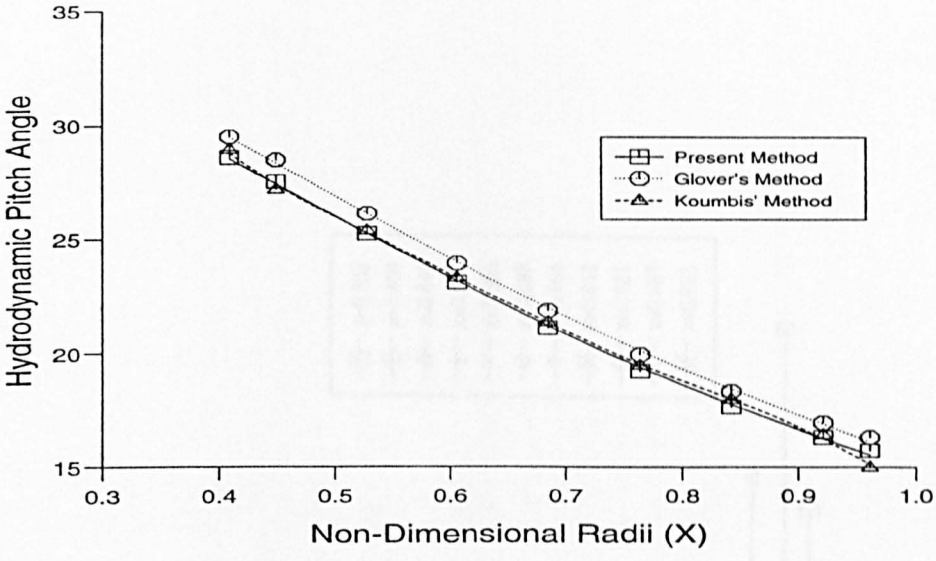

Figure 7.26 — Hydrodynamic Pitch Angle (DATA2)

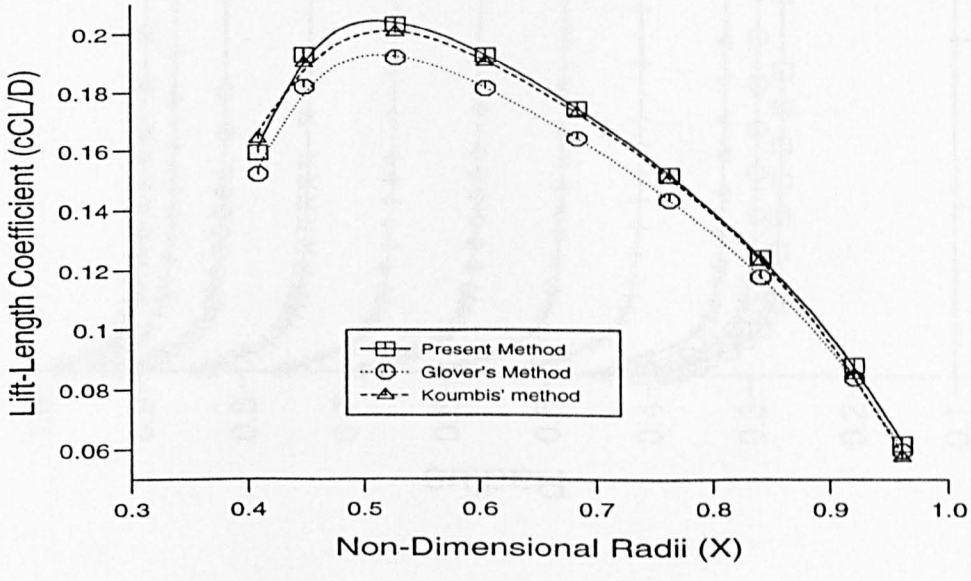

Figure 7.27 — Lift-Length Coefficient (DATA2)

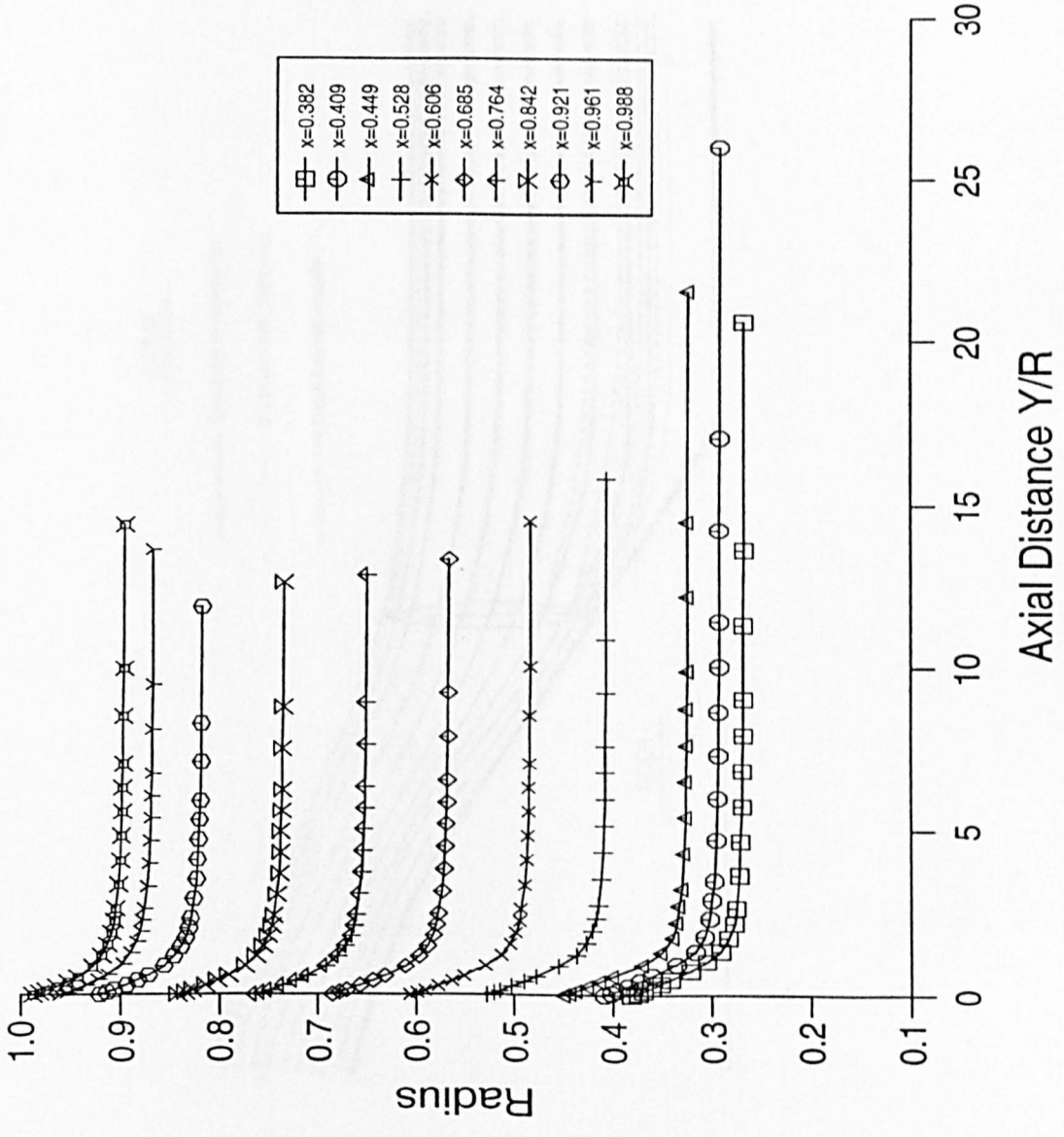

Figure 7.28 — Slipstream Shape by Present Method for DATA2

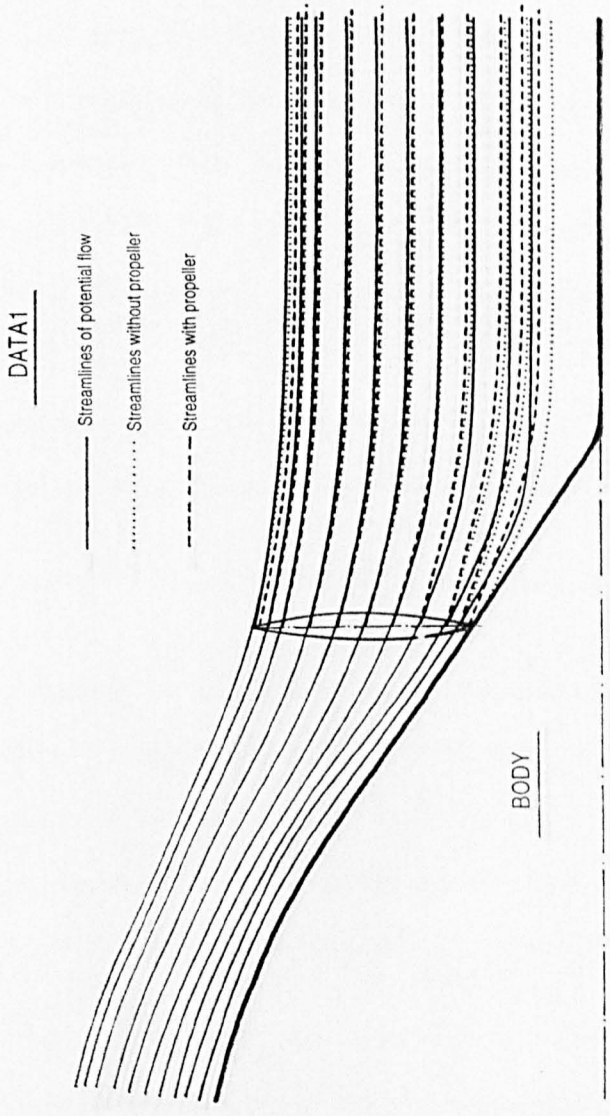

Figure 7.29 — Flow behind the Body for DATA1

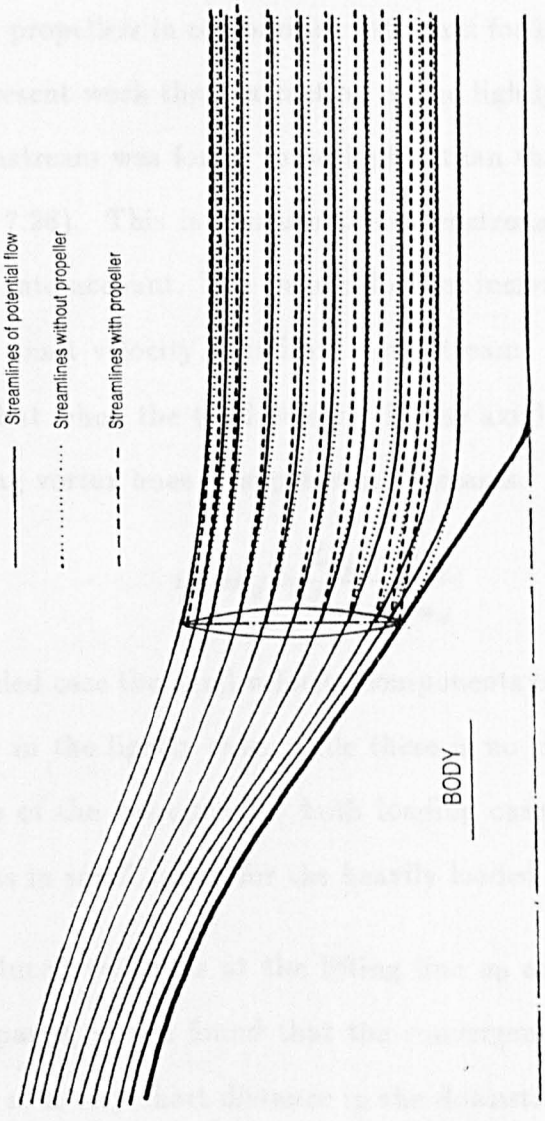

Figure 7.30 — Flow behind the Body for DATA2

The ratio of the slipstream contraction is a function of the thrust load coefficient. In classical methods, in which the wake velocities are assumed to remain constant along the slipstream, more contraction of the slipstream could be seen for the heavily loaded propellers in comparison with that for lightly loaded propellers. However in the present work the contraction of the lightly loaded propeller (Figure 7.18) far downstream was found to be higher than that of the heavily loaded propeller (Figure 7.28). This is because the downstream variation of the wake velocities is taken into account. The wake velocities increase along the slipstream and approach the onset velocity at infinity downstream. It can be seen from following equation that when the total velocity in the axial direction increases, the slope of the trailing vortex lines or slipstream decreases.

$$\tan \alpha_{ij} = \frac{U_{r_{ij}} + u_{r_{ij}}}{U_{a_{ij}} + u_{a_{ij}}}$$

In the heavily loaded case the axial velocity components of each vortex were much bigger than those in the lightly case, while there is no significant change on the other components of the velocities for both loading cases. Therefore, the above formulation results in small values for the heavily loaded case.

When the induced velocities at the lifting line u_0 and at infinity u_∞ downstream were compared, it was found that the convergence in magnitude from u_0 to u_∞ took place at a very short distance in the downstream as seen from Figure 7.10, 7.11, 7.12, 7.20, 7.21 and 7.22. According to the classical lifting line theory the magnitude of the induced velocities at the blade sections (u_0) are half of the velocities at the far downstream. This is valid for the axial and tangential velocity components whilst the radial components becomes zero as can be seen from Figure 7.12 and 7.22 for two different design cases.

If one investigates the behaviour of the axial and tangential induced velocity components, it can be seen that, the rate of convergence of the induced velocity magnitude (u_0) to the velocity magnitude at the far downstream (u_∞) is relatively high as shown in Figures 7.10, 7.11 ,7.20 and 7.21. In other words, the change in magnitude from (u_0) to (u_∞) takes place at very short distance from the blade section along the downstream.

Another interesting aspect of the behaviour of these induced velocities is that the ratio of the magnitude of the induced velocities far downstream to that at the lifting line ($\frac{u_\infty}{u_0}$) does not equal 2.0 as expected from the simple theory and varies dependent upon the loading conditions. As can be seen from Figures 7.10 and 7.11 for the lightly loaded case, $\frac{u_\infty}{u_0}$ equals to 1.74 for the axial induced velocity and 2.48 for the tangential induced velocity. A similar trend is also observed for the heavily loaded case, as seen from Figure 7.20 and 7.21, for which the associated velocity ratios take values of 1.62 and 2.76 respectively for the axial and tangential components. The differences in the velocity ratio with respect to the classical lifting line theory value (i.e. $\frac{u_\infty}{u_0} = 2.0$) is due to the effect of the trailing vortex lines defined as follows.

Let an "External Field" vortex be defined as a vortex line located at a point above that at which the induced velocities are to be calculated and similarly let an "Internal Field" vortex be defined as the one below that point. With a non-deformed helical slipstream shape, which is used in the classical lifting line theory, the behaviour of the vortex line does not change along the slipstream, so that it remains in the external or the internal field in relation to reference point.

However, when the slipstream deformation is accounted for, a vortex line,

which is initially in the External Field in relation to a particular reference point, contracts and moves into Internal Field at some distance downstream from the lifting line. This results in a reduction in the axial velocity induced by the vortex line at the reference point and an increase in the tangential velocity.

7.4 Propeller with Downstream Stator

In this section the results of design calculations for propulsors comprising a propeller and a downstream stator will be described.

The theoretical basis of the stator design method was described in Chapter 6. Based on this theory, an appropriate software module which contained a group of subroutines was written and combined with the main propeller design program.

The input data to the stator design program consists of the number of the blades, the chord lengths, the axial distance between the propeller and the stator and the axial distance along the slipstream at which the tangential velocities induced by the propeller are to be cancelled out. This location was taken as $Y/R = 15.0$.

Designs were made for 5 sets of data. As stated in the Introduction, a major motivation for the present work was to develop a design method for propeller/stator propulsors driving torpedo shape bodies. DATA1 represents a typical set of torpedo propulsor design data and DATA2 represents a fictional heavily-loaded version of the same propulsor. Propeller/stator propulsors were designed for both these sets of data.

In Reference 3, Glover presented results from the application of a propeller/stator

design method applied to 3 sets of surface ship data. For these ships there was no knowledge of the downstream variations in the wake and Glover's did not account for the deformation of the propulsor slipstream. Results for these data sets derived from the current method are included here to demonstrate the effects of slipstream deformation. Details of these data are shown below.

Design Characteristics for DATA3

Delivered Power, P_D= 33880.0 *KW*

Design Speed, V= 26.5 *Knots*

Rate of Rotation, N= 98.7 *rpm*

Propeller Diameter, D= 7.555 *metre*

Wake Fraction, w= 0.177

Number of Blades, Z= 6

x	0.20	0.25	0.30	0.40	0.50	0.60	0.70	0.80	0.90	0.95	1.0
1-w	0.464	0.484	0.533	0.644	0.795	0.858	0.891	0.905	0.908	0.909	0.910
C (m)		1.892	1.981	2.160	2.305	2.410	2.453	2.387	2.081	1.689	
C_D		0.0083	0.0081	0.0077	0.0074	0.0072	0.0070	0.0069	0.0070	0.0073	

Design Characteristics for DATA4

Delivered Power, P_D= 19985.0 *KW*

Design Speed, V=15.0 *Knots*

Rate of Rotation, N= 85.0 *rpm*

Propeller Diameter, D= 8.340 *metre*

Wake Fraction, w= 0.443

Number of Blades, Z= 4

x	0.20	0.25	0.30	0.40	0.50	0.60	0.70	0.80	0.90	0.95	1.0
1-w	0.308	0.332	0.363	0.435	0.561	0.715	0.792	0.847	0.869	0.874	0.878
C (m)		2.002	2.103	2.285	2.439	2.550	2.596	2.526	2.202	1.787	
C_D	-	0.0088	0.0085	0.0080	0.0076	0.0074	0.0072	0.0070	0.0071	0.0073	-

Design Characteristics for DATA5

Delivered Power, P_D= 28540.0 *KW*

Design Speed, V=19.6 *Knots*

Rate of Rotation, N= 105.0 *rpm*

Propeller Diameter, D= 7.56 *metre*

Wake Fraction, w= 0.390

Number of Blades, Z= 5

x	0.20	0.25	0.30	0.40	0.50	0.60	0.70	0.80	0.90	0.95	1.0
1-w	0.627	0.595	0.547	0.462	0.400	0.386	0.501	0.657	0.822	0.891	0.947
C (m)		2.342	2.460	2.674	2.853	2.984	3.037	2.955	2.576	2.090	
C_D		0.0079	0.0077	0.0073	0.0071	0.0069	0.0067	0.0067	0.0067	0.0069	

In investigating the performance characteristics of the propeller/stator combination, two parameters were considered to be important and were therefore systematically varied. These parameters were the number of stator blades and the

axial distance between the propeller and the stator.

In order to investigate the effect of the number of stator blades, the stator blade number was varied from 3 to 15 in steps of 3 for all data, except for DATA4 which involved a 4 bladed propeller and for which the number of stator blades was varied from 4 to 14 in steps of 2. In varying the number of blades, the objective was to determine the blade number beyond which the gain in performance becomes practically insignificant.

The axial distance (AXD) between the lifting line of the propeller and the stator results in changes in the stator diameter and the propeller induced velocities. For each set of design data the axial spacing was varied from Y/R=0.2 to 0.8 in steps of 0.2, where Y/R is the ratio of axial distance to the propeller radius.

Calculation of the mean velocities induced by the propeller, at the stator and in the slipstream, is essential for the design of the stator. These calculations were carried out using Equations 5.42 - 5.44 and results from DATA1 & DATA2 are shown in Figures 7.31 to 7.36 for the axial, tangential and radial components, respectively. The axes of these figures are self explanatory and each figure represents the variations during one revolution of the propeller of the velocities induced on a stator blade, which in this case was situated a distance $Y/R = 0.5$ downstream of the propeller.

The main objective of the application of propeller/stator propulsors to torpedos is the cancellation of the unbalanced torque reaction. Design of the stator to cancel the rotational velocities in the slipstream results in a stator torque which is less than that of the propeller because of the smaller frictional drag of the stator. This

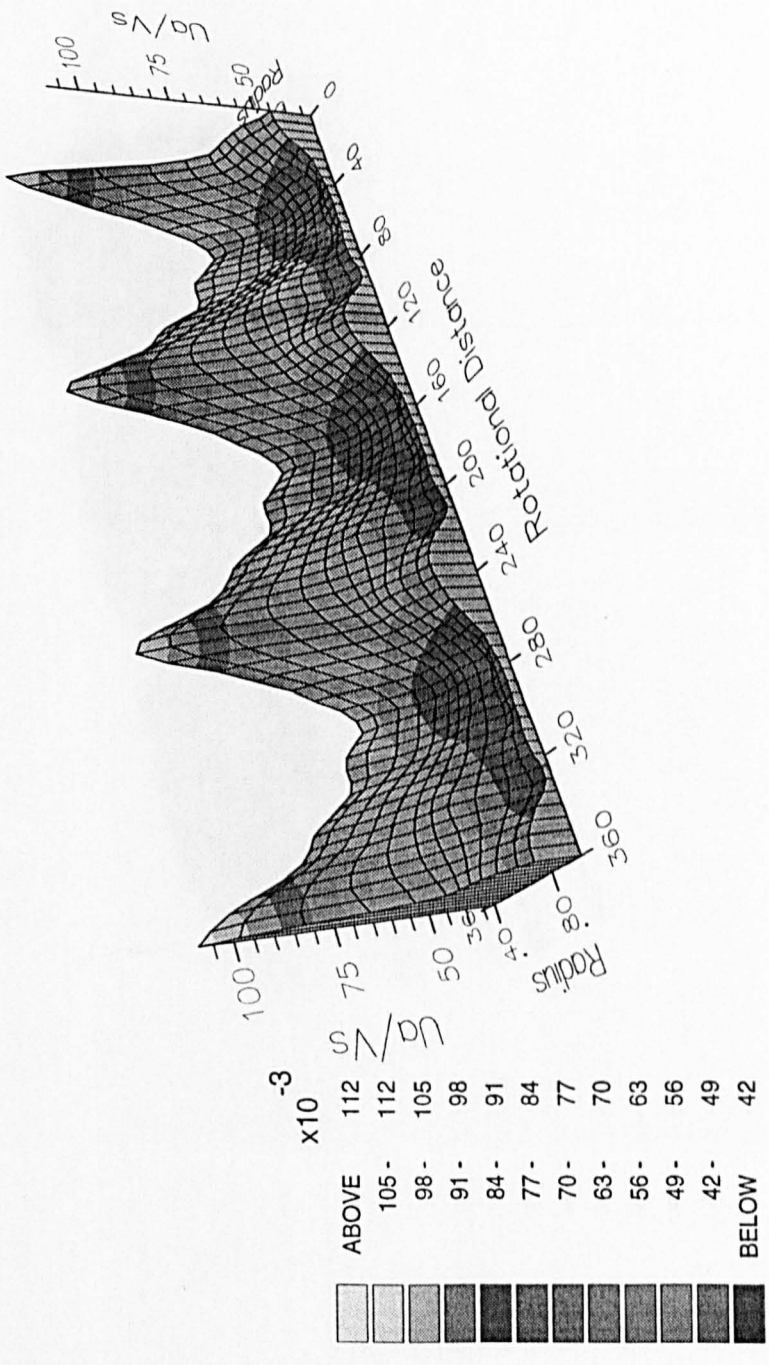

Figure 7.31 — Axial Induced Velocities at Y/R=0.5 for DATA1

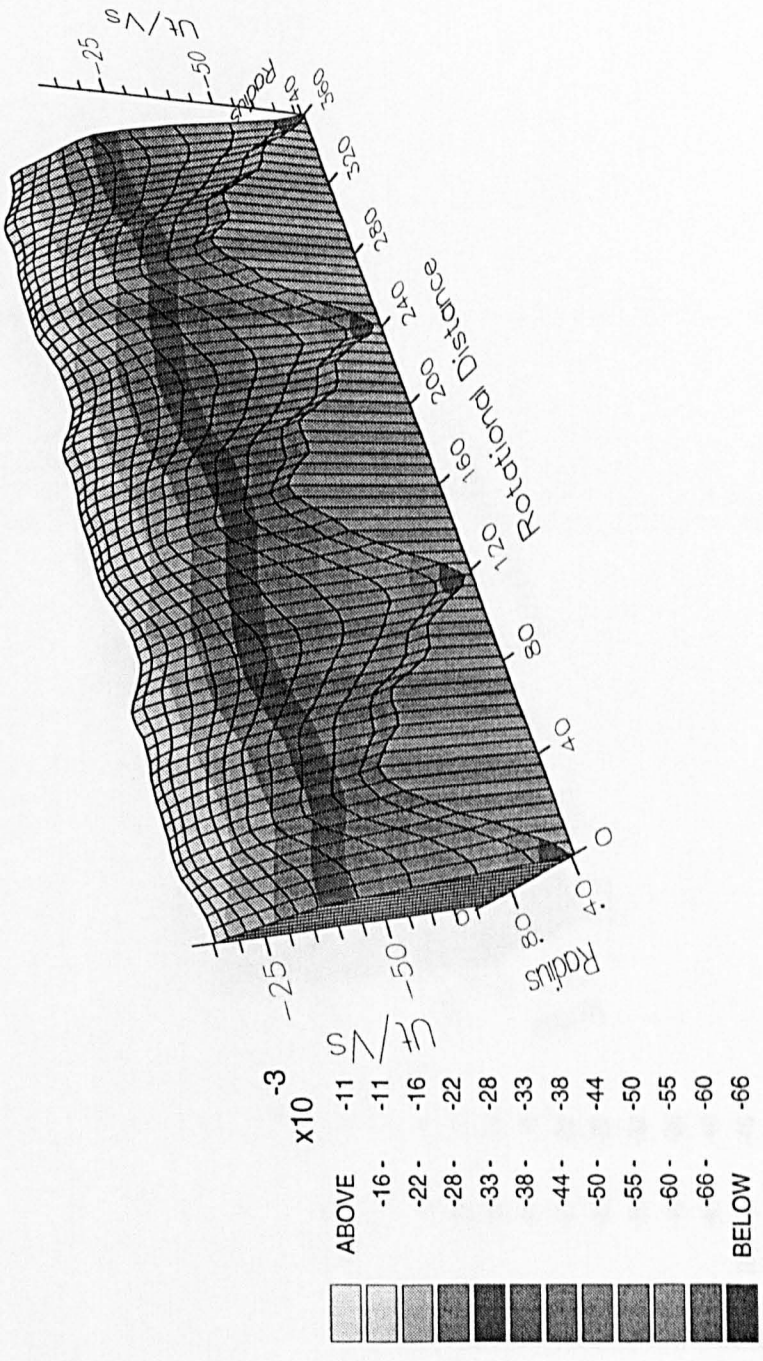

Figure 7.32 — Tangential Induced Velocities at Y/R=0.5 for DATA1

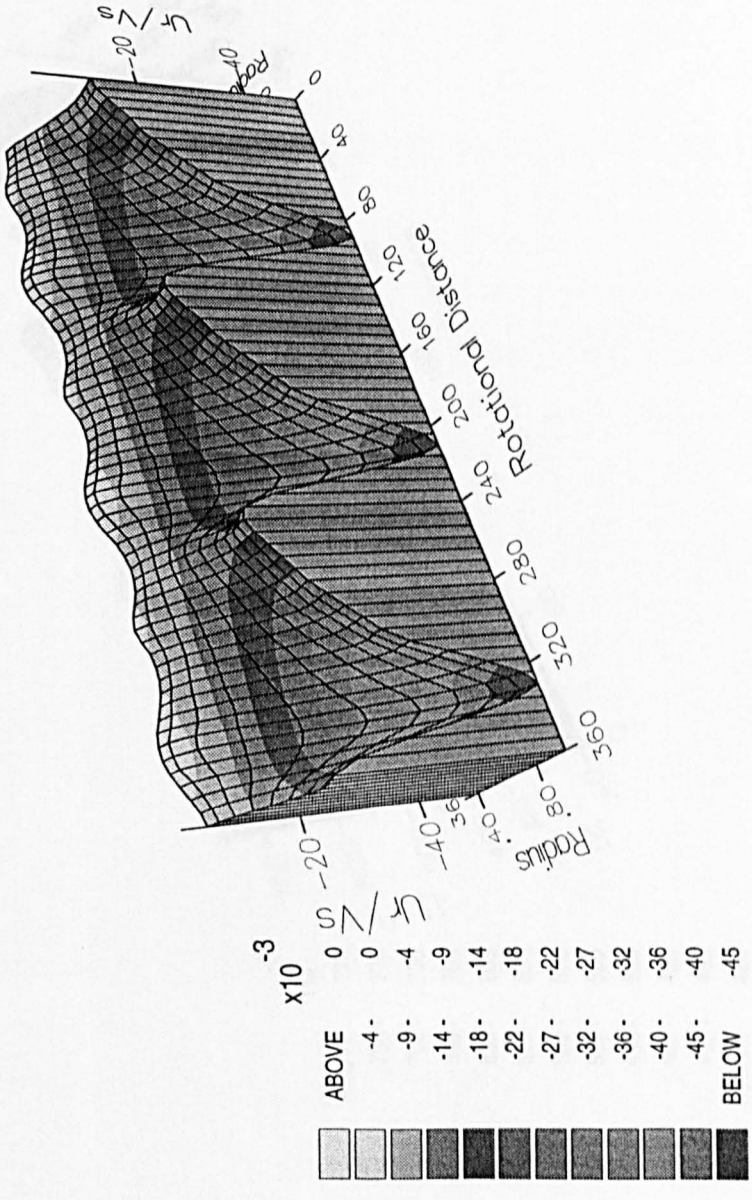

Figure 7.33 — Radial Induced Velocities at Y/R=0.5 for DATA1

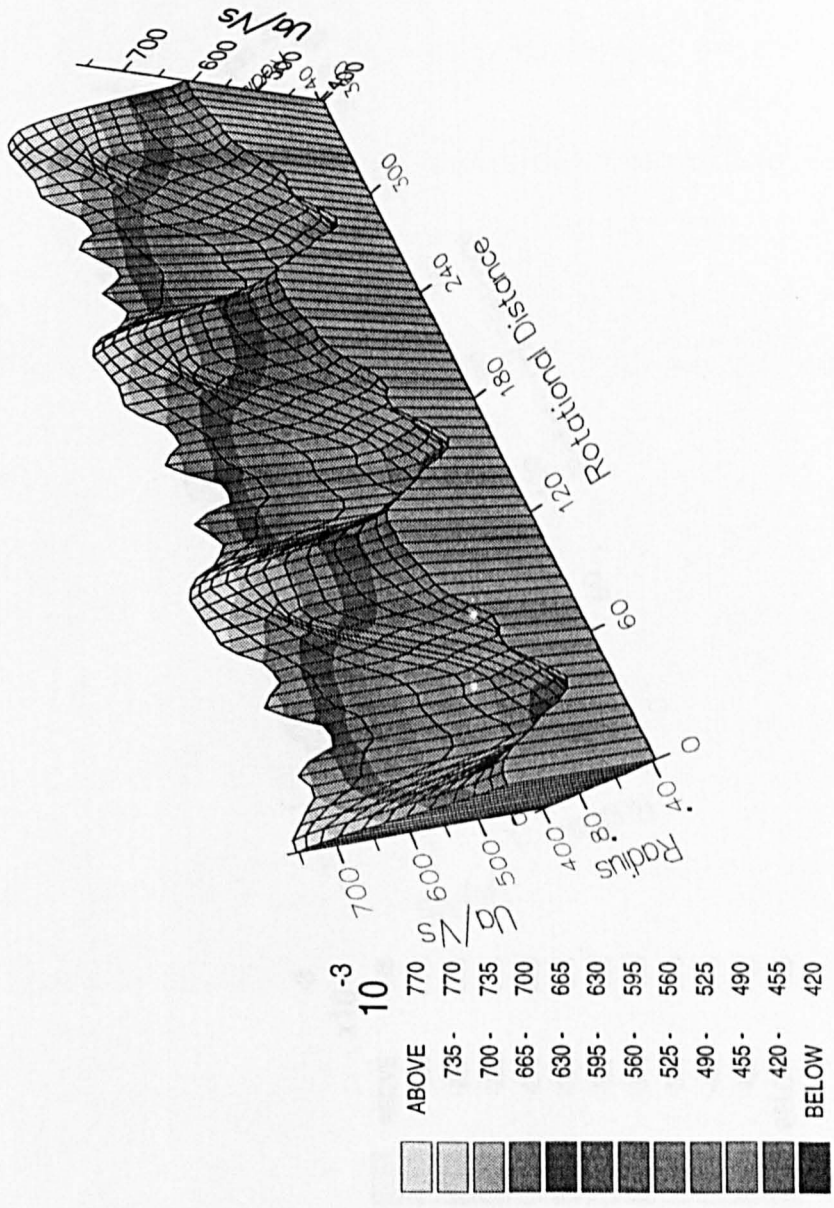

Figure 7.34 — Axial Induced Velocities at Y/R=0.5 for DATA2

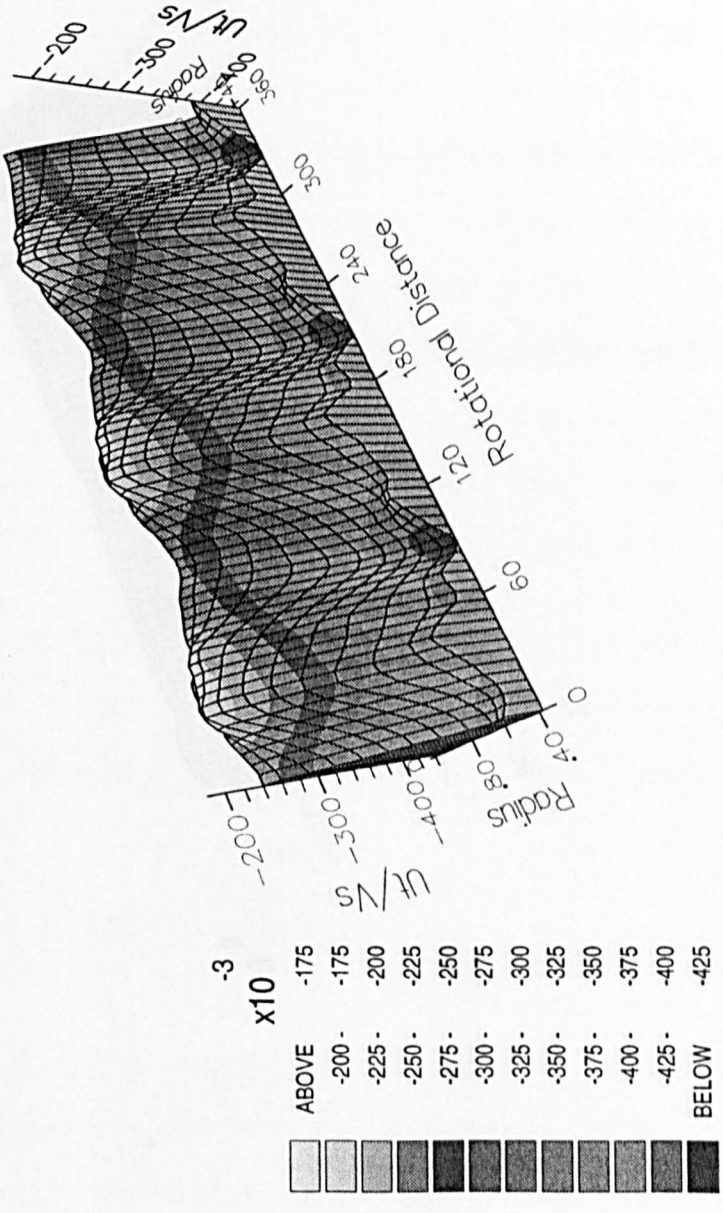

Figure 7.35 — Tangential Induced Velocities at Y/R=0.5 for DATA2

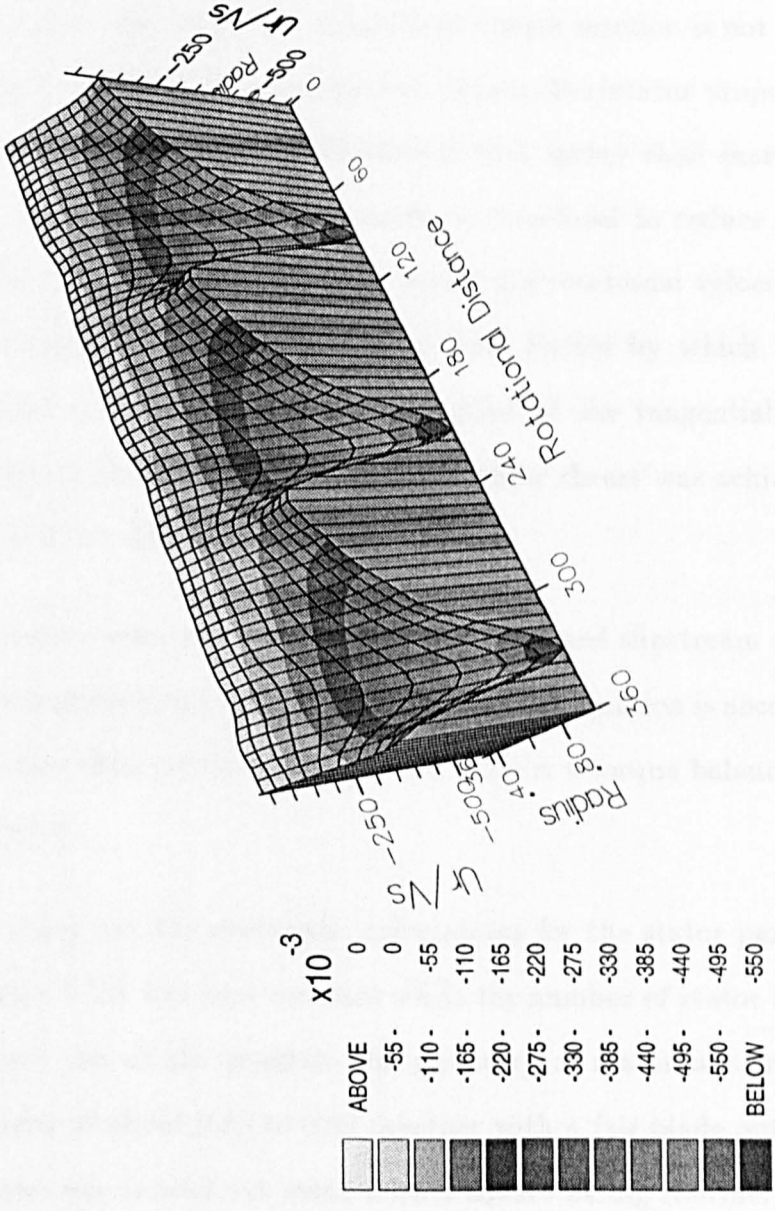

Figure 7.36 — Radial Induced Velocities at Y/R=0.5 for DATA2

is overcome by increasing the stator circulation to achieve torque balance, this increase in circulation being coupled with a decrease in stator thrust.

In the case of the surface ship the unbalanced torque reaction is not important and the purpose of considering the application of propeller/stator propulsors is to increase propulsor efficiency. Glover [3] showed that rather than increasing the circulation to achieve torque balance, it could be beneficial to reduce the stator circulation slightly below that necessary to cancel the rotational velocities in the slipstream. Glover introduced the idea of a Load Factor by which the stator circulation derived on the basis of the cancellation of the tangential velocities should be multiplied. He showed that maximum stator thrust was achieved when this factor had a value of about 0.9.

However, Glover's work was based on the non-deformed slipstream model and the present work demonstrated that, when slipstream deformation is accounted for, maximum propulsor efficiency is achieved when there is a torque balance between propeller and stator.

In order to carry out the systematic calculations for the stator performance, firstly the distance AXD was kept constant while the number of stator blades was changed. At each run of the program the geometry of stator was modified to give lift coefficients of about 0.55 to 0.65 together with a fair blade outline. This smoothing process was carried out using a least square fitting routine. Following this process, for each sets of design data, 200 different stator designs were generated and the respective gains due to the application of a stator behind the propellers were computed. The results of the computation are presented in Figure 7.37 to 7.46 in terms of the gain in propulsor efficiency against the number of stator blades

for varying AXD.

As can be seen seen from Figure 7.37 to 7.46, the general trend of the results in such that as the number of stator blades increases the efficiency increases at a high rate for a practical number of blades (about 9-10) and converges to a maximum value. Moreover, as AXD increases the gain also increases. This trend is valid for all the design data except for the lightly loaded case (DATA1) which displayed no dramatic gain with the varying number of blades. If one compares the effect of the number of the stator blades on the heavily loaded (i.e. Figures 7.39-40) and lightly loaded (Figures 7.37-38) cases respectively two distinct trends can be observed: the first one is such that the gain for the heavily loaded case is much more than for lightly loaded case. Secondly, in general, the gain decreases as the number of stator blades increases for the lightly load case while the trend is opposite for the heavily loaded case. The reason behind the above defined trends can be partly explained by investigating the following thrust equation of the stator blade element:

$$dT = \frac{\frac{1}{4}\rho C\ Z_s\ D_s[u_{apm} + U_a]^2[\frac{C_L}{\tan\beta_i} - C_D]}{\sin\beta_i} dx$$

According to the above equation the negligible gain in the lightly loaded case can be attributed to the negative thrust generated by the stator partly due to small lift relative large drag forces on the stator. In the lightly loaded case the value of $[\frac{C_L}{\tan\beta_i} - C_D]$ becomes less than zero for some blade sections. Therefore these blade sections produce a negative thrust which results in a decrease in propulsor efficiency. For the second trend it is difficult to analyse the contribution of each parameters (i.e. C_L, C, β_i, etc.) in above equation. Even if one could investigate the effect of each parameter, to draw a conclusion for an entire stator would be

difficult due to the large number of parameters to be investigated. Therefore it is author's belief that the second trend is also the direct result of this equation.

As mentioned earlier, since the maximum gain is reached with a practical number of stator blades, there will be no point in further increasing the number of blades which is also a handicap from the manufacturing point of view (i.e. labour, material etc.)

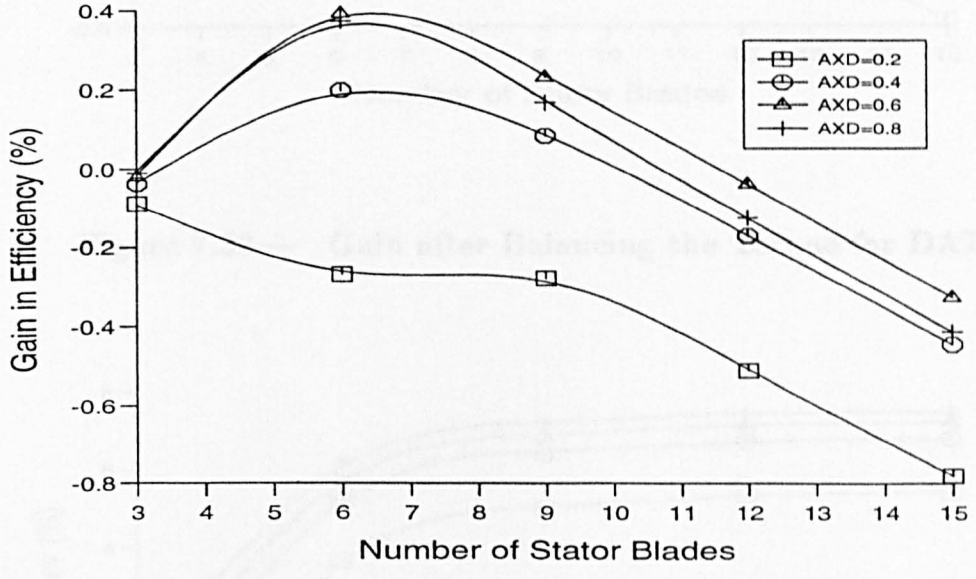

Figure 7.37 — Variation of Stator Blades for DATA1

Similarly, as the axial separation was increased the gain also increased at a high rate for practical value of AXD and this rate became smaller for the large AXD values. This also suggested that, from the design point of view, there will be no point in locating the stator far behind the propeller for high efficiency values. On the other hand, based upon the non-deformed slipstream assumption, Glover

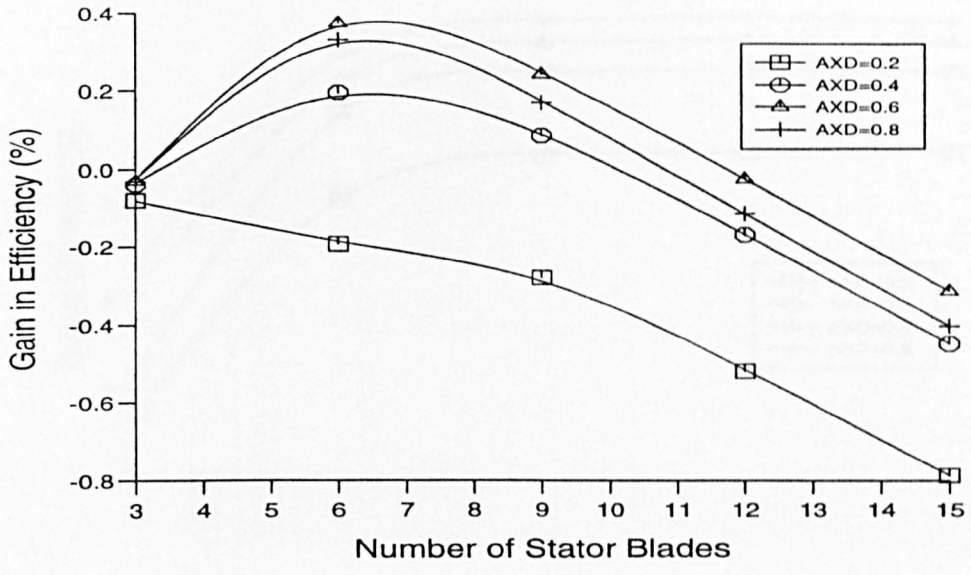

Figure 7.38 — Gain after Balancing the Torque for DATA1

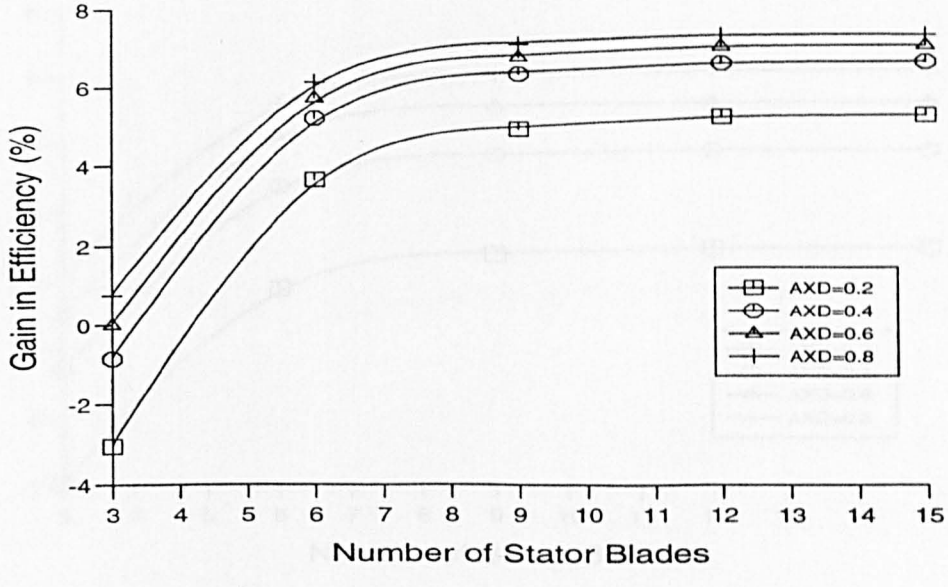

Figure 7.39 — Variation of Stator Blades for DATA2

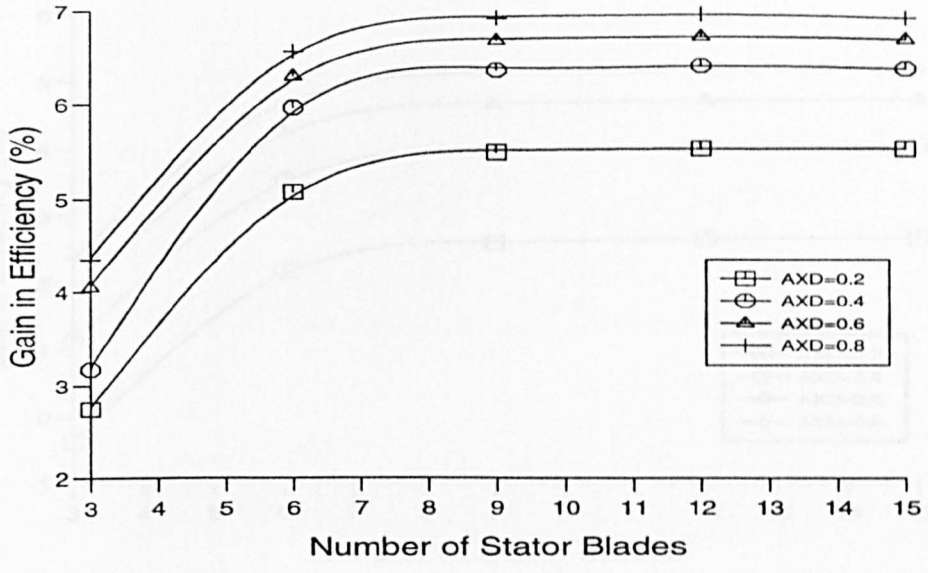

Figure 7.40 — Gain after Balancing the Torque for DATA2

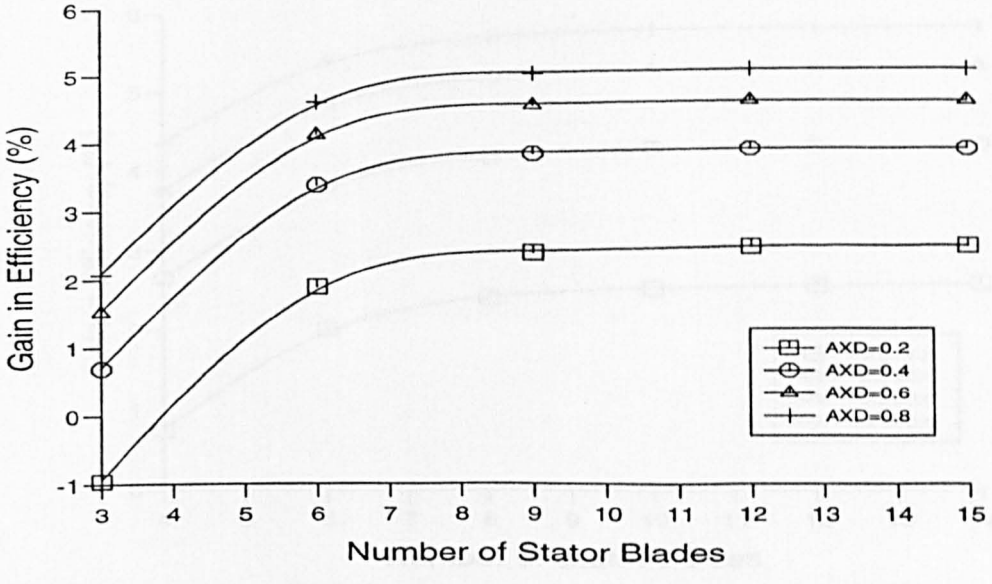

Figure 7.41 — Variation of Stator Blades for DATA3

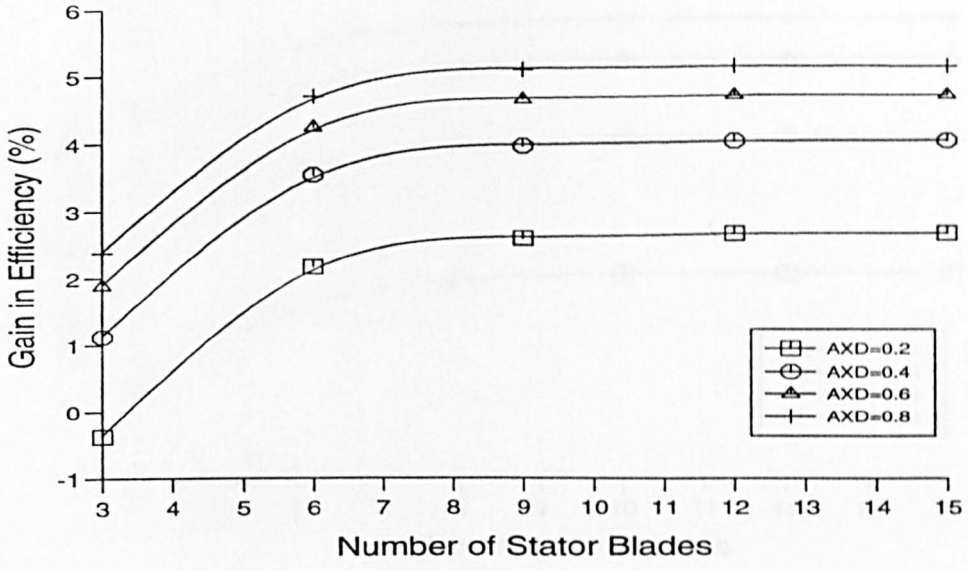

Figure 7.42 — Gain after Balancing the Torque for DATA3

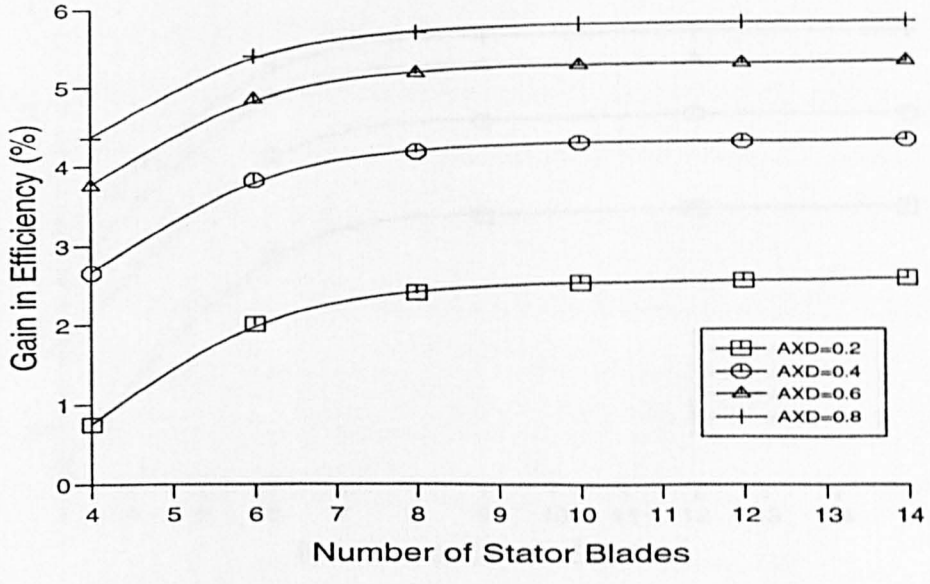

Figure 7.43 — Variation of Stator Blades for DATA4

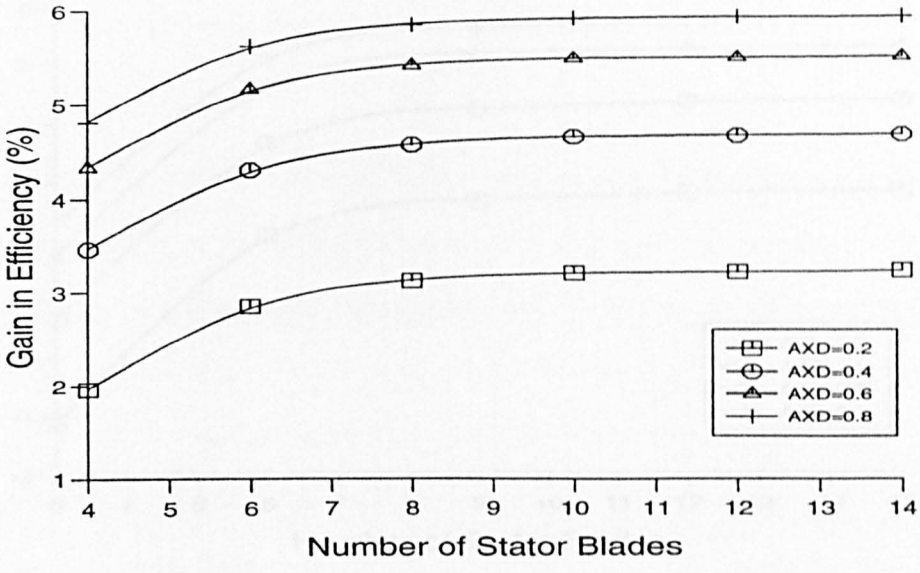

Figure 7.44 — Gain after Balancing the Torque for DATA4

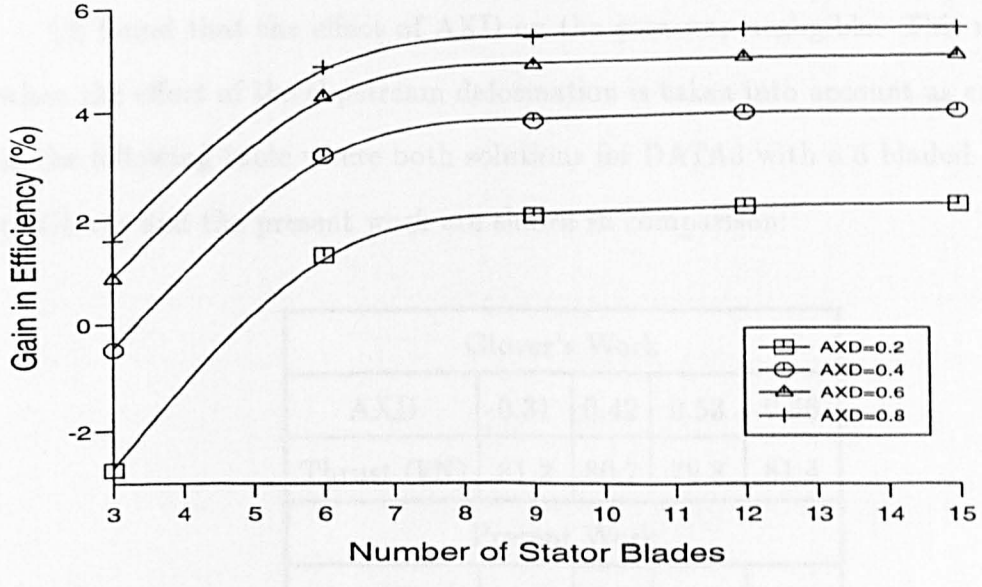

Figure 7.45 — Variation of Stator Blades for DATA5

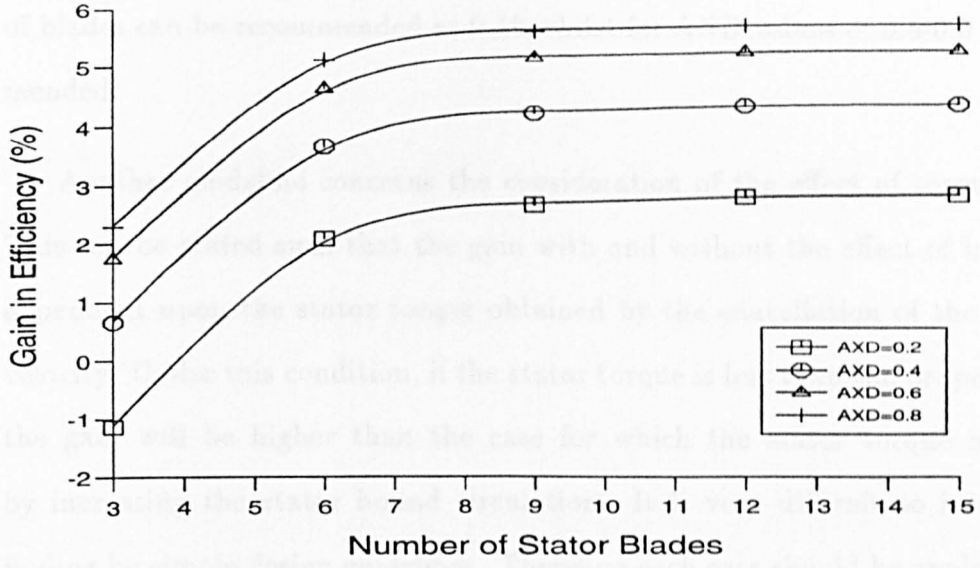

Figure 7.46 — Gain after Balancing the Torque for DATA5

[3] found that the effect of AXD on the gain was negligible. This is not true when the effect of the slipstream deformation is taken into account as can be seen in the following table where both solutions for DATA3 with a 6 bladed stator due to Glover and the present work are shown in comparison:

Glover's Work				
AXD	0.31	0.42	0.53	0.66
Thrust (kN)	81.2	80.7	79.8	81.4
Present Work				
AXD	0.2	0.4	0.6	0.8
Thrust (kN)	43.77	84.7	108.7	121.9

By taking into account the above findings a design guideline for the number

of blades can be recommended as 9-10 whilst for AXD values of 0.5-0.6 are recommended.

Another guideline concerns the consideration of the effect of torque balance. This can be stated such that the gain with and without the effect of balancing is dependent upon the stator torque obtained by the cancellation of the tangential velocity. Under this condition, if the stator torque is less than the propeller torque the gain will be higher than the case for which the stator torque is balanced by increasing the stator bound circulation. It is very difficult to interpret this finding by simple design guidelines. Therefore each case should be analysed by the computer program and the optimum gain found.

	DATA1	DATA2	DATA3	DATA4	DATA5
Number of Stator Blades	6	9	9	10	10
Axial Distance (AXD)	0.600	0.500	0.600	0.600	0.600
Stator Diameter (m)	0.456	0.462	7.308	7.879	7.090
Stator Thrust (KN)	0.040	1.310	107.5	126.9	145.9
% Gain by Present Method	0.500	6.706	4.775	5.595	5.349
% Gain by Glover's Method	-	-	4.730	5.020	5.590

Table 7.5 — Stator Design for each of Design Sets

Based upon the above analyses and the derived design recommendations, some sample design cases were selected for optimum gain and computations were carried out using the earlier defined design data for the balanced case. The results of the

computations are presented in Table 7.5 in comparison with the Glover data [3]. The full details of the computation for the propellers and stators are included in Appendix D for further information.

Chapter VIII

General Conclusion

One of the most significant advances in propeller design has been the great increase in the use of computer. As computer technology has advanced, the computational procedures for propeller design have been improved to take advantage of this new technology. The simple Momentum Theory has evolved into today's Lifting Surface Theory.

During the evolution of the design procedures between the above mentioned two extremes, the lifting line design procedure has occupied the screw propeller designers more than any other method. Therefore today lifting line methods still have the most respected place amongst the others. This is not only because they are modest in terms of the computational demands, but also they have the advantage of being widely used and well established procedure due to their long service history.

From the above point of view, it could be well justified to seek for the further improvements in the present lifting line procedures. Indeed if one investigates the earlier lifting line models, it is found that a number of simplifying assumptions were necessary in order to derive a solution with the available computational tools. One of these assumptions is that the propeller is moderately loaded and that the downstream variation in induced velocities and the resulting slipstream deformation can be neglected. Later development of the lifting line methods has tackled the slipstream deformation by taking into account the self induced veloci-

ties. But none of these methods included the effect of the local inflow velocities in the slipstream which would contribute to the deformation of the slipstream.

Therefore it was thought that the objective of this thesis should be the further improvement of the lifting line procedure with an emphasis on more realistic representation of the slipstream deformation. As this deformation is one of the key parameters in the design of the performance improvement devices, the secondary objective of the thesis has been set to design a stator behind the propeller and analyse the performance characteristics of the combined propulsor system.

In order to justify the above objectives, in the first chapter of the thesis an introductory section has been included and objectives and the layout of the thesis also presented. The second chapter of the thesis involved the review of the three key issues involved in the propeller design as well as in the objectives of the thesis. These issues were the propeller design procedures, propeller/stator combination and flow around the body and propeller. Based upon this review work, in the third chapter of the thesis, the flow prediction around a slender body was presented by using a "Three-dimensional Panel Technique" for the potential flow and the "Thin Shear Layer Equations" for viscous flow. This provided the necessary wake data to develop the propeller design theory. In the fourth chapter, a description was given of the basic theory which led to the development of the Classical Lifting Line theory which assumes a regular helical slipstream downstream of the propeller. The fifth chapter described the development of the Advanced Lifting Line method in which the deformed nature of the trailing vortex system was determined using the "Free Slipstream Analysis Method".

In this method the slipstream geometry was allowed to deform and to align

with the local velocity field which comprised the inflow velocities and the velocities induced by the trailing vortices. In the sixth chapter this design procedure was combined with that of a stator device placed behind the propeller. Therefore the necessary formulation for the induced velocities of the stator was presented. The seventh chapter involved the illustration of the numerical application of the design procedure and discussion of the results deducted from this application for different loading cases. Finally in the present chapter, overall conclusions drawn from the work are discussed and recommendations for future work are given.

During the computational implementation of the above methodology a set of computer programs was used. Some of them were developed by the author and some were modified or enhanced versions of software available in the department. The software can be classified into three major groups; flow calculation, propeller design and stator design software. The first group of software was available in the department and was further enhanced for the present use, the rest of software was developed by the author during the course of the work.

Based upon the work carried out in this thesis the following overall conclusions can be drawn:

- In spite of the advances in numerical methods and computers, the lifting line based propeller design procedures still play an important role in propeller design methodology and there is still room to further improve these procedures.

- One of the simplifying assumptions of the conventional lifting line method is that the propeller is moderately loaded and that the resulting slipstream shape is regular. This may not be true, particularly, for the heavily loaded propeller

due to the effect of the inflow velocities and the induced velocities of the trailing vortices on themselves which would result in a contracted slipstream tube and a downstream increase in vortex pitch.

- Rational design of the stator device requires accurate information on the slipstream geometry for determining the stator diameter. This can be provided by the improved procedure presented in this thesis.

- In determining the slipstream shape geometry an iterative solution was implemented such that the bound circulation obtained from first iteration of the lifting line solution remained constant and the form of the trailing vortex lines was modified corresponding to the local inflow velocities and the induced velocities due to trailing vortex system. This procedure was employed until a balanced slipstream shape was obtained. In this iterative process it was found that the slipstream form was stabilised well within a distance of 3.5R downstream of the propeller.

- The analysis of the slipstream deformation indicated that the rate of contraction was very high in the above specified region and the contribution due to the local inflow velocities played a significant role in this contraction.

- As a result of more realistic slipstream shape, the hydrodynamic pitch angle (β_i) increased very rapidly downstream of the propeller and the hydrodynamic pitch angle on the lifting line were found to be smaller than those obtained by the regular helical slipstream model (i.e. conventional lifting line model) for heavily loaded propeller.

- Effort put in to this thesis for the improvement of the actual slipstream repre-

sentation indicated that the classical lifting line methods would underestimate the propeller efficiency for the heavily loaded propeller about 4% whilst for the lightly loaded propeller the use of the regular slipstream assumption can be justified.

- The improved design methodology presented in this thesis would provide more sound design for the performance improvement devices, e.g stator, contrarotating propellers, Grim vane wheels etc, due to more realistic representation of the slipstream details.

- The performance analysis of the propeller combined with the stator located behind the propeller indicated that the undesirable effect of the propeller torque can be avoided by the use of the stator. This is an important design requirement for the directional stability of the high speed submerged bodies like submarines, torpedos, Autonomous Underwater Vehicles (AUV's).

- It is a known fact that the number of the blades is one of the important parameters in the design of the stator devices. The parametric analysis of the number of blades of the stator indicated as the number of blade increased, the efficiency increased at a high rate over a practical number of blades and converges to a maximum value. Therefore there will be no point in further increasing the number of blades beyond certain number which will increase the manufacturing costs.

- Another important design parameter of the stator device was its longitudinal separation from the propeller. The systematic investigation of this design parameter indicated that the gain would increase at high rate for practical values

of this separation whilst it would be negligible beyond a certain range.

- By taking into account the above two findings, a design guideline for the number of blades was recommended as 9-10 whilst for the stator separation a value of 0.5 or 0.6R was recommended.

- The gain obtained by the application of the stator device was dependent upon the load case and the torque balance of the propeller. In general the maximum gain which was about 6.5% was obtained for the heavily loaded case.

- It was found that the absolute torque balance and the maximum gain cannot be achieved simultaneously. Therefore the stator designer should make a design decision depending upon his design objectives or should search for a compromise design solution by using the stator design software.

The majority of the above conclusions were drawn from the computation carried out by using the earlier mentioned design software developed during this research work. The theoretical procedure and the associated software for the flow prediction neglects the effect of the free surface. Therefore, the implemented software for the flow prediction can cater only for the wake values of deeply submerged bodies. However overall design software is general and also applicable to surface ships provided that the wake data are available.

- Within the above limitations it is believed that the procedure and the associated software provided in this thesis would provide the designers with the capability for more sound propeller and stator design in particular for submerged ships like submarines, torpedos and AUV's.

Apart from the immediate application to the naval submerged bodies (i.e. tor-

pedo, submarines), today one of the major applications of the present work could be to AUV's which have considerable promise as a major tool for gathering scientific data in the deep ocean. Their use in combination with more efficient remote sensing techniques for the determination of sea floor characteristics and local water column properties has been a major attraction for the underwater technologists. The accuracy of the sensor performance and maintenance of the intended trajectories is very much dependent on the superior motion performance of the vehicle, in particular its stability. Moreover, they require efficient propulsion systems due to long data gathering time spent under water with limited fuel/battery space in their bodies. Within this context, the existing design tool would be very appropriate as it could be used for balancing the torque as well as improving propulsive efficiency.

Another potential application area for the present design tool would be the Small Water Area Twin Hull (SWATH) ships. These vessels have slender submerged hulls which are ideal for the application of the performance improvement devices. They suffer from higher frictional drag due to a large wetted surface area and they are payload limited due to large structural weight. Therefore energy efficient systems like propeller/stator combination would be very much appropriate.

- However the improvement gained by the present procedure will be offset by the increase in the computer time, the ratio of the CPU of the present propeller design method in comparison with that of the classical lifting line method is about 30. This is not expected to be a major problem considering the enormous power of existing computers. In fact this has been the major source of encouragement for the recommendation to improve the present procedure by using the "Lifting Surface Method" as a natural extension of the Lifting Line

Methods.

- It should be borne in mind that throughout this work no consideration has be given to cavitation and noise. Generally, due to its low speed, there should be no danger of cavitation occurring on the stator blades but the influence of propeller cavitation on the stator performance may need to be considered.

- The flow prediction module of the existing design software neglects the effect of the free surface. As a result the present software has restricted application to surface ships if the wake data is not available. Therefore it is recommended to combine this effect in the present wake prediction software by using state of the art methods.

- Because of the novelty of the system there is not much detailed data on the performance characteristics of the stators. Therefore it would be useful to perform model propeller testing to verify and validate the present design tool.

References

1. Glover, E.J. " Slipstream Deformation and its Influence on Marine propeller Design", *Ph.D. Thesis, University of Newcastle upon Tyne, 1970*

2. Glover, E.J. " A Design Method For the Heavily Loaded Marine Propellers ", *Trans.RINA, Vol.116, pp.111,124, 1973*

3. Glover, E.J. " Rotor /Stator Propulsors - Parametric Studies , " *Hydronav'91, Gdansk, 1991*

4. Glover, E.J. " Free Slipstream Analysis of Propeller Slipstream Deformation , " *International Symposium on Hydro and Aerodynamics in Marine Engineering, HADMAR'91, Volume.1, 28 October-1 November, Varna Bulgaria, 1991*

5. Koumbis, A. " An Improved Mathematical Model of The Action of Open Propellers and Ducted Thrusters," *PhD Thesis, University of Newcastle upon Tyne, 1981*

6. Koumbis, A. " On the Effect of the Slipstream on the Representation of Open Propellers", *Trans-RINA, 1983*

7. Strscheletzky, M. " Hydrodynamische Grundlagen zur Berechnung der Schiffschrauben ", *G. Braun, Karlsruhe, 1950*

8. Burrill, L.C. " Calculation of Marine Propeller Performance Characteristics, " *Trans. N.E.C.I.E.S. Vol.60, 1943-44*

9. Burrill, L.C. " The Optimum Diameter of Marine Propellers," *Trans. N.E.C.I.E.S. Vol.72, 1955-56*

10. Ryan P.G. and Glover, E.J. " A Ducted Propeller Design Method: A new Approach Using Surface Vorticity Distribution Techniques and Lifting Line Theory", *Trans-RINA 1972, pp.545,563*

11. Rankine, W.J.M. " On the Mechanical Principles of the Action of Propellers", *Trans. I.N.A., Vol. 6, 1865*

12. Froude, R.E. " On the Part Played in the Operation of Propulsion by Differences in Fluid Pressure", *Trans. I.N.A., Vol. 30, 1889*

13. Lanchester, F.W. " Aerodynamics " *Constable & Co., London, 1907*

14. Prandtl, L. and Betz, A. " Vier Abhandlungen zur Hydro-und Aerodynamik", *Gottingen, 1927*

15. Eckhart, M.K. and Morgan W.B., " A Propeller Design Method ", *Trans. SNAME, Vol.63, 1955*

16. Lerbs, H.W," Moderately Loaded Propellers with a Finite Numbers of Blades and an Arbitrary Distribution of Circulation", *Trans SNAME, vol.60, 1952*

17. Hess, J.L. and Smith, A.M.O. "Calculation of Non-Lifting Potential Flow about Arbitrary Three-Dimensional Bodies," *Douglas Aircraft Company Inc, Report No:ES40622 , 1962*

18. Smith, A. M. O and Pierce, J. " Exact Solution of the Neumann Problem, Calculation of Non-Circulatory Plane and Axially Symmetric Flow About or Within Arbitrary Boundaries," *Douglas Aircraft Co. Report ES-26988, 1958*

19. Hess, J.L. and Smith, A.M.O. "Calculation of Potential Flow about Arbitrary Bodies ," *Pergamen Press Series, Progress in Aeronautical Science , Vol.8, 1966*

20. Hess, J.L. and Smith, A.M.O. "Calculation of Potential Flow about Arbitrary Three-Dimensional Lifting Bodies," *Douglas Aircraft Company Inc, Report No:MDC J5679-01, Oct.1972*

21. Hess, J.L. " Status of a Higher-Order Panel method for Non-Lifting Three Dimensional Potential Flow," *Douglas Aircraft Company Inc, Report No:NACS-76118-30, 1977*

22. Kerwin, J.E., Coney, W.B. and Hsin, C.Y. " Hydrodynamic Aspects of Propeller/Stator Design", *Propeller'88 Symposium, Virginia, Paper No.3, 1988*

23. Patience, G. " Developments in Marine Propellers," *Stone Manganese Marine Limited, Technical Paper No.22, January 1991*

24. Van Gent W. and Van Oossanen P. " Influence of Wake on Propeller Loading and Cavitation", *ISP, p.279-321, 1973*

25. Van Manen, J. D. et al. "The Design of Wake-adapted Screws and Their Behaviour Behind the Ship," *ISP , Vol.2 No:7, 1955.*

26. Cummings, D.E. " The Effect of Propeller Wake Deformation on Propeller Design", *ISP, July, 1976*

27. Greeley, D. C. and Kerwin J. E. "Numerical Methods For Propeller Design and Analysis in Steady-Flow" *Trans SNAME , Vol.90, 1982, p.415-453*

28. Hoshino, T. " A Surface Panel Methods with a Deformed Wake Model to Analyze Hydrodynamic Characteristics of Propellers in Steady Flow," *MTB195, April, 1991*

29. Mautner, T.S., Nelson, D.M. and Gillcrist, M.C. " Investigation of the SISUP (Swirl Including Stator Upstream of Propeller) Concept for Marine Propulsion", *SNAME, Propellers'88 Symposium, Paper No.2 , Virginia,1988*

30. Hughes, J. M. and Kinnas, S.A " A analysis Method for a ducted Propeller with Pre-Swirl Stator Blades", *SNAME, Propellers/Shafting'91 Symposium, Virginia, 1991*

31. Gaafary, M.M. and Mosaad, M.A. " Pre-Swirl Stator and Propeller/Stator Efficiency", *SNAME Propellers/Shafting'91 symposium, Virginia, USA, 1991*

32. Coney, W.B. " Optimum Circulation Distributions for a Class of Marine Propulsors ," *Journal of Ship Research , Vol.36 No.3, 1992*

33. Ikehata M and Chanda S. " Theoretical Calculation of Propulsive Performances of Stator-Propeller in Uniform Flow by Vortex Lattice Method", *Journal of The Society of Naval Architects of Japan, Vol. 166, 1989*

34. Chen, B.Y.H. " Postswirl Propulsors - A Design Method and an Application ," *International Symposium on Propulsors and Cavitation , Hamburg, Germany, June, 1992*

35. Brard, R. " The Representation of a Given Ship Form by Singularity Distribu-

tions when the Boundary Condition on the Free Surface is Linearised," *Journal of Ship Research, Vol.16, 1972*

36. Webster, W. C. "The Flow about Arbitrary Three-Dimensional Smooth Bodies," *Journal of Ship Research , Vol.19, No.4, Dec. 1975, pp. 206-218.*

37. Gomez, G.P., Linares, F.G and Briones I.B. " Some Improvements of Traditional Lifting Line Theory For Ship Propellers", *ISP, 1983, pp.154,175*

38. Froude, W. " On the Elementary Relation between Pitch, Slip and Propulsive Efficiency ", *Trans. I.N.A., Vol. 19, 1878*

39. Cebeci, T. and Bradshaw, P."Momentum Transfer in Boundary layers," *McGraw-Hill Book Co.,Inc.,New York, 1977*

40. Caracostas N. " Off-Design Performance Analysis of Ducted Propellers", *SNAME Propellers'78, Virginia , paper:3, pp.3.1-3.18*

41. Dyne, G. "A Method for the Design of Ducted Propellers in a Uniform Flow," *Publication of the Swedish State Shipbuilding Experimental Tank, No.62, 1967.*

42. McCormick, B. M., Eisenhuth J. J. and Lynn, J. E. " A Study of Torpedo Propellers -Part I ," *Ordnance Research Lab., Pennsylvania State Univ., Rept. No: 16597-5 , March 1956.*

43. Huang, T. T., Wang, H. T., Santelli, W. and Groves, N. C " Propeller/Stern/Boundary-Layer Interaction on Axisymmetric Bodies: Theory and Experiment," *DTNSRDC Report 76-0113, David W. Taylor Naval Ship Research and Development Centre , Bethasda, Md., 1976.*

44. Koronowicz, T. " A Theoretical Model of the Propeller and its Slipstream taking into account the deformation of the Free vortex System," *Proceedings of the symposium on Advances in Propeller Research and Design , Gdansk, 1981*

45. Loukakis, T.A. " On the Design of Highly Skewed Propellers, " *Proceedings of the symposium on Advances in Propeller Research and Design , Gdansk, 1981*

46. Gibson, I.S and Lewis, R.I " Ducted Propeller Analysis by Surface Vorticity and Actuator Disc theory," *Symposium on Ducted Propellers, RINA, 1973*

47. Glover, E.J. "Lifting Surface Analysis of High Speed Propeller Performance," *Symposium on High Speed Marine Vehicles, Naples Castel del'Ovo, Italy, 14-15 February 1991, Italy*

48. Loukakis, T.A. " A New Theory for the Wake of Marine Propellers," *Ph.D Thesis, M.I.T. Report No. 71-1 May 1971*

49. Anderson, P. " Lifting Line Theory and Calculation For supercavitating Propellers", *ISP, 1976*

Appendix A

Propeller Characteristics

Advance Coefficient

$$J = \frac{V_s}{ND}$$

Torque Coefficient

$$K_Q = \frac{Q}{\rho N^2 D^5}$$

Thrust Coefficient

$$K_T = \frac{T}{\rho N^2 D^4}$$

Thrust Loading Coefficient

$$C_T = \frac{8K_T}{\pi J_s^2 (1 - W_T)^2}$$

Hydrodynamic Pitch Angle

$$\beta_i = \tan^{-1} \frac{V_a + u_a}{\pi x_i n D - u_t}$$

Thrust Coefficient of the Blade Section

$$(\frac{K_T}{dx})_i = \frac{(\frac{C.C_l}{D})_i [\frac{\pi x}{J} - u_{t_i}]^2 J^2 (1 - \frac{C_D}{C_L} \tan \beta_i)}{4 \cos \beta_i}$$

Torque Coefficient of the Blade Section

$$(\frac{K_Q}{dx})_i = \frac{x_i (\frac{C.C_l}{D}) [(1 - W_T) + u_{a_i}]^2 J^2 (1 - \frac{C_D}{C_L} \tan \beta_i)}{8 \sin \beta_i}$$

Efficiency

$$\eta = \frac{J(1 - W_T)}{2\pi} \frac{K_T}{K_Q}$$

Lift-Lenght Coefficient

$$(\frac{cC_L}{D})_i = \frac{2\pi G_i \sin \beta_i}{(1 - W_t) + u_{a_i}}$$

where

$$G_i = \frac{\Gamma_i}{\pi D V_s}$$

Appendix B

Body Input Points

Body Input Points Coordinates

x(m)	y(m)	z(m)	x(m)	y(m)	z(m)
0.00000	0.000000	0.053300	0.00000	0.009255	0.052490
0.00000	0.018230	0.050086	0.00000	0.026650	0.046159
0.00000	0.034261	0.040830	0.00000	0.040830	0.034261
0.00000	0.046159	0.026650	0.00000	0.050086	0.018230
0.00000	0.052490	0.009255	0.00000	0.053300	0.000000
0.00000	0.000000	0.106600	0.00000	0.018511	0.104980
0.00000	0.036459	0.100171	0.00000	0.053300	0.092318
0.00000	0.068521	0.081660	0.00000	0.081660	0.068521
0.00000	0.092318	0.053300	0.00000	0.100171	0.036459
0.00000	0.104980	0.018511	0.00000	0.106600	0.000000
0.00000	0.000000	0.159900	0.00000	0.027766	0.157471
0.00000	0.054689	0.150257	0.00000	0.079950	0.138477
0.00000	0.102782	0.122490	0.00000	0.122490	0.102782
0.00000	0.138477	0.079950	0.00000	0.150257	0.054689
0.00000	0.157471	0.027766	0.00000	0.159900	0.000000
0.00000	0.000000	0.213200	0.00000	0.037022	0.209961
0.00000	0.072919	0.200342	0.00000	0.106600	0.184637
0.00000	0.137042	0.163321	0.00000	0.163321	0.137042
0.00000	0.184637	0.106600	0.00000	0.200342	0.072919
0.00000	0.209961	0.037022	0.00000	0.213200	0.000000
0.00500	0.000000	0.266500	0.00500	0.046277	0.262451
0.00500	0.091148	0.250428	0.00500	0.133250	0.230796
0.00500	0.171303	0.204151	0.00500	0.204151	0.171303
0.00500	0.230796	0.133250	0.00500	0.250428	0.091148
0.00500	0.262451	0.046277	0.00500	0.266500	0.000000
0.42500	0.000000	0.266500	0.42500	0.046277	0.262451
0.42500	0.091148	0.250428	0.42500	0.133250	0.230796
0.42500	0.171303	0.204151	0.42500	0.204151	0.171303
0.42500	0.230796	0.133250	0.42500	0.250428	0.091148
0.42500	0.262451	0.046277	0.42500	0.266500	0.000000
0.85000	0.000000	0.266500	0.85000	0.046277	0.262451
0.85000	0.091148	0.250428	0.85000	0.133250	0.230796
0.85000	0.171303	0.204151	0.85000	0.204151	0.171303
0.85000	0.230796	0.133250	0.85000	0.250428	0.091148
0.85000	0.262451	0.046277	0.85000	0.266500	0.000000
1.27500	0.000000	0.266500	1.27500	0.046277	0.262451
1.27500	0.091148	0.250428	1.27500	0.133250	0.230796
1.27500	0.171303	0.204151	1.27500	0.204151	0.171303
1.27500	0.230796	0.133250	1.27500	0.250428	0.091148
1.27500	0.262451	0.046277	1.27500	0.266500	0.000000
1.70000	0.000000	0.266500	1.70000	0.046277	0.262451

1.70000	0.091148	0.250428	1.70000	0.133250	0.230796
1.70000	0.171303	0.204151	1.70000	0.204151	0.171303
1.70000	0.230796	0.133250	1.70000	0.250428	0.091148
1.70000	0.262451	0.046277	1.70000	0.266500	0.000000
2.12500	0.000000	0.266500	2.12500	0.046277	0.262451
2.12500	0.091148	0.250428	2.12500	0.133250	0.230796
2.12500	0.171303	0.204151	2.12500	0.204151	0.171303
2.12500	0.230796	0.133250	2.12500	0.250428	0.091148
2.12500	0.262451	0.046277	2.12500	0.266500	0.000000
2.55000	0.000000	0.266500	2.55000	0.046277	0.262451
2.55000	0.091148	0.250428	2.55000	0.133250	0.230796
2.55000	0.171303	0.204151	2.55000	0.204151	0.171303
2.55000	0.230796	0.133250	2.55000	0.250428	0.091148
2.55000	0.262451	0.046277	2.55000	0.266500	0.000000
2.97500	0.000000	0.266500	2.97500	0.046277	0.262451
2.97500	0.091148	0.250428	2.97500	0.133250	0.230796
2.97500	0.171303	0.204151	2.97500	0.204151	0.171303
2.97500	0.230796	0.133250	2.97500	0.250428	0.091148
2.97500	0.262451	0.046277	2.97500	0.266500	0.000000
3.40000	0.000000	0.266500	3.40000	0.046277	0.262451
3.40000	0.091148	0.250428	3.40000	0.133250	0.230796
3.40000	0.171303	0.204151	3.40000	0.204151	0.171303
3.40000	0.230796	0.133250	3.40000	0.250428	0.091148
3.40000	0.262451	0.046277	3.40000	0.266500	0.000000
3.82500	0.000000	0.266500	3.82500	0.046277	0.262451
3.82500	0.091148	0.250428	3.82500	0.133250	0.230796
3.82500	0.171303	0.204151	3.82500	0.204151	0.171303
3.82500	0.230796	0.133250	3.82500	0.250428	0.091148
3.82500	0.262451	0.046277	3.82500	0.266500	0.000000
4.25000	0.000000	0.266500	4.25000	0.046277	0.262451
4.25000	0.091148	0.250428	4.25000	0.133250	0.230796
4.25000	0.171303	0.204151	4.25000	0.204151	0.171303
4.25000	0.230796	0.133250	4.25000	0.250428	0.091148
4.25000	0.262451	0.046277	4.25000	0.266500	0.000000
4.35500	0.000000	0.260000	4.35500	0.045148	0.256050
4.35500	0.088925	0.244320	4.35500	0.130000	0.225167
4.35500	0.167125	0.199172	4.35500	0.199171	0.167125
4.35500	0.225167	0.130000	4.35500	0.244320	0.088925
4.35500	0.256050	0.045149	4.35500	0.260000	0.000000
4.46000	0.000000	0.242000	4.46000	0.042023	0.238323
4.46000	0.082769	0.227406	4.46000	0.121000	0.209578
4.46000	0.155555	0.185383	4.46000	0.185383	0.155555
4.46000	0.209578	0.121000	4.46000	0.227406	0.082769
4.46000	0.238323	0.042023	4.46000	0.242000	0.000000
4.56500	0.000000	0.213000	4.56500	0.036987	0.209764
4.56500	0.072850	0.200154	4.56500	0.106500	0.184463
4.56500	0.136914	0.163167	4.56500	0.163167	0.136914
4.56500	0.184463	0.106500	4.56500	0.200154	0.072850
4.56500	0.209764	0.036987	4.56500	0.213000	0.000000
4.67000	0.000000	0.182000	4.67000	0.031604	0.179235

4.67000	0.062248	0.171024	4.67000	0.091000	0.157617
4.67000	0.116987	0.139420	4.67000	0.139420	0.116987
4.67000	0.157617	0.091000	4.67000	0.171024	0.062248
4.67000	0.179235	0.031604	4.67000	0.182000	0.000000
4.77500	0.000000	0.150000	4.77500	0.026047	0.147721
4.77500	0.051303	0.140954	4.77500	0.075000	0.129904
4.77500	0.096418	0.114907	4.77500	0.114907	0.096418
4.77500	0.129904	0.075000	4.77500	0.140954	0.051303
4.77500	0.147721	0.026047	4.77500	0.150000	0.000000
4.88000	0.000000	0.120000	4.88000	0.020838	0.118177
4.88000	0.041042	0.112763	4.88000	0.060000	0.103923
4.88000	0.077134	0.091925	4.88000	0.091925	0.077134
4.88000	0.103923	0.060000	4.88000	0.112763	0.041042
4.88000	0.118177	0.020838	4.88000	0.120000	0.000000
4.98500	0.000000	0.090000	4.98500	0.015628	0.088633
4.98500	0.030782	0.084572	4.98500	0.045000	0.077942
4.98500	0.057851	0.068944	4.98500	0.068944	0.057851
4.98500	0.077942	0.045000	4.98500	0.084572	0.030782
4.98500	0.088633	0.015628	4.98500	0.090000	0.000000
5.09000	0.000000	0.060000	5.09000	0.010419	0.059088
5.09000	0.020521	0.056382	5.09000	0.030000	0.051962
5.09000	0.038567	0.045963	5.09000	0.045963	0.038567
5.09000	0.051962	0.030000	5.09000	0.056382	0.020521
5.09000	0.059088	0.010419	5.09000	0.060000	0.000000
5.19500	0.000000	0.030000	5.19500	0.005209	0.029544
5.19500	0.010261	0.028191	5.19500	0.015000	0.025981
5.19500	0.019284	0.022981	5.19500	0.022981	0.019284
5.19500	0.025981	0.015000	5.19500	0.028191	0.010261
5.19500	0.029544	0.005209	5.19500	0.030000	0.000000
5.30000	0.000000	0.005000	5.30000	0.000868	0.004924
5.30000	0.001710	0.004698	5.30000	0.002500	0.004330
5.30000	0.003214	0.003830	5.30000	0.003830	0.003214
5.30000	0.004330	0.002500	5.30000	0.004698	0.001710
5.30000	0.004924	0.000868	5.30000	0.005000	0.000000

Off Point Coordinates

4.98500	0.000000	0.090600	5.00000	0.000000	0.086020
5.05000	0.000000	0.071680	5.10000	0.000000	0.057340
5.15000	0.000000	0.043011	5.20000	0.000000	0.028670
5.25000	0.000000	0.014330	5.30000	0.000000	0.000100
5.35000	0.000000	0.000000	5.40000	0.000000	0.000000
5.45000	0.000000	0.000000	5.50000	0.000000	0.000000
6.00000	0.000000	0.000000	6.50000	0.000000	0.000000
7.00000	0.000000	0.000000	7.50000	0.000000	0.000000
8.00000	0.000000	0.000000	8.50000	0.000000	0.000000
9.00000	0.000000	0.000000	9.50000	0.000000	0.000000
10.00000	0.000000	0.000000	4.98500	0.000000	0.090650
5.00000	0.000000	0.090650	5.05000	0.000000	0.090650
5.10000	0.000000	0.090650	5.15000	0.000000	0.090650
5.20000	0.000000	0.090650	5.25000	0.000000	0.090650
5.30000	0.000000	0.090650	5.35000	0.000000	0.090650

5.40000	0.000000	0.090650	5.45000	0.000000	0.090650
5.50000	0.000000	0.090650	6.00000	0.000000	0.090650
6.50000	0.000000	0.090650	7.00000	0.000000	0.090650
7.50000	0.000000	0.090650	8.00000	0.000000	0.090650
8.50000	0.000000	0.090650	9.00000	0.000000	0.090650
9.50000	0.000000	0.090650	10.00000	0.000000	0.090650
4.98500	0.000000	0.100205	5.00000	0.000000	0.100205
5.05000	0.000000	0.100205	5.10000	0.000000	0.100205
5.15000	0.000000	0.100205	5.20000	0.000000	0.100205
5.25000	0.000000	0.100205	5.30000	0.000000	0.100205
5.35000	0.000000	0.100205	5.40000	0.000000	0.100205
5.45000	0.000000	0.100205	5.50000	0.000000	0.100205
6.00000	0.000000	0.100205	6.50000	0.000000	0.100205
7.00000	0.000000	0.100205	7.50000	0.000000	0.100205
8.00000	0.000000	0.100205	8.50000	0.000000	0.100205
9.00000	0.000000	0.100205	9.50000	0.000000	0.100205
10.00000	0.000000	0.100205	4.98500	0.000000	0.110005
5.00000	0.000000	0.110005	5.05000	0.000000	0.110005
5.10000	0.000000	0.110005	5.15000	0.000000	0.110005
5.20000	0.000000	0.110005	5.25000	0.000000	0.110005
5.30000	0.000000	0.110005	5.35000	0.000000	0.110005
5.40000	0.000000	0.110005	5.45000	0.000000	0.110005
5.50000	0.000000	0.110005	6.00000	0.000000	0.110005
6.50000	0.000000	0.110005	7.00000	0.000000	0.110005
7.50000	0.000000	0.110005	8.00000	0.000000	0.110005
8.50000	0.000000	0.110005	9.00000	0.000000	0.110005
9.50000	0.000000	0.110005	10.00000	0.000000	0.110005
4.98500	0.000000	0.129360	5.00000	0.000000	0.129360
5.05000	0.000000	0.129360	5.10000	0.000000	0.129360
5.15000	0.000000	0.129360	5.20000	0.000000	0.129360
5.25000	0.000000	0.129360	5.30000	0.000000	0.129360
5.35000	0.000000	0.129360	5.40000	0.000000	0.129360
5.45000	0.000000	0.129360	5.50000	0.000000	0.129360
6.00000	0.000000	0.129360	6.50000	0.000000	0.129360
7.00000	0.000000	0.129360	7.50000	0.000000	0.129360
8.00000	0.000000	0.129360	8.50000	0.000000	0.129360
9.00000	0.000000	0.129360	9.50000	0.000000	0.129360
10.00000	0.000000	0.129360	4.98500	0.000000	0.148470
5.00000	0.000000	0.148470	5.05000	0.000000	0.148470
5.10000	0.000000	0.148470	5.15000	0.000000	0.148470
5.20000	0.000000	0.148470	5.25000	0.000000	0.148470
5.30000	0.000000	0.148470	5.35000	0.000000	0.148470
5.40000	0.000000	0.148470	5.45000	0.000000	0.148470
5.50000	0.000000	0.148470	6.00000	0.000000	0.148470
6.50000	0.000000	0.148470	7.00000	0.000000	0.148470
7.50000	0.000000	0.148470	8.00000	0.000000	0.148470
8.50000	0.000000	0.148470	9.00000	0.000000	0.148470
9.50000	0.000000	0.148470	10.00000	0.000000	0.148470
4.98500	0.000000	0.167825	5.00000	0.000000	0.167825
5.05000	0.000000	0.167825	5.10000	0.000000	0.167825

5.15000	0.000000	0.167825	5.20000	0.000000	0.167825
5.25000	0.000000	0.167825	5.30000	0.000000	0.167825
5.35000	0.000000	0.167825	5.40000	0.000000	0.167825
5.45000	0.000000	0.167825	5.50000	0.000000	0.167825
6.00000	0.000000	0.167825	6.50000	0.000000	0.167825
7.00000	0.000000	0.167825	7.50000	0.000000	0.167825
8.00000	0.000000	0.167825	8.50000	0.000000	0.167825
9.00000	0.000000	0.167825	9.50000	0.000000	0.167825
10.00000	0.000000	0.167825	4.98500	0.000000	0.187180
5.00000	0.000000	0.187180	5.05000	0.000000	0.187180
5.10000	0.000000	0.187180	5.15000	0.000000	0.187180
5.20000	0.000000	0.187180	5.25000	0.000000	0.187180
5.30000	0.000000	0.187180	5.35000	0.000000	0.187180
5.40000	0.000000	0.187180	5.45000	0.000000	0.187180
5.50000	0.000000	0.187180	6.00000	0.000000	0.187180
6.50000	0.000000	0.187180	7.00000	0.000000	0.187180
7.50000	0.000000	0.187180	8.00000	0.000000	0.187180
8.50000	0.000000	0.187180	9.00000	0.000000	0.187180
9.50000	0.000000	0.187180	10.00000	0.000000	0.187180
4.98500	0.000000	0.206290	5.00000	0.000000	0.206290
5.05000	0.000000	0.206290	5.10000	0.000000	0.206290
5.15000	0.000000	0.206290	5.20000	0.000000	0.206290
5.25000	0.000000	0.206290	5.30000	0.000000	0.206290
5.35000	0.000000	0.206290	5.40000	0.000000	0.206290
5.45000	0.000000	0.206290	5.50000	0.000000	0.206290
6.00000	0.000000	0.206290	6.50000	0.000000	0.206290
7.00000	0.000000	0.206290	7.50000	0.000000	0.206290
8.00000	0.000000	0.206290	8.50000	0.000000	0.206290
9.00000	0.000000	0.206290	9.50000	0.000000	0.206290
10.00000	0.000000	0.206290	4.98500	0.000000	0.225645
5.00000	0.000000	0.225645	5.05000	0.000000	0.225645
5.10000	0.000000	0.225645	5.15000	0.000000	0.225645
5.20000	0.000000	0.225645	5.25000	0.000000	0.225645
5.30000	0.000000	0.225645	5.35000	0.000000	0.225645
5.40000	0.000000	0.225645	5.45000	0.000000	0.225645
5.50000	0.000000	0.225645	6.00000	0.000000	0.225645
6.50000	0.000000	0.225645	7.00000	0.000000	0.225645
7.50000	0.000000	0.225645	8.00000	0.000000	0.225645
8.50000	0.000000	0.225645	9.00000	0.000000	0.225645
9.50000	0.000000	0.225645	10.00000	0.000000	0.225645
4.98500	0.000000	0.235445	5.00000	0.000000	0.235445
5.05000	0.000000	0.235445	5.10000	0.000000	0.235445
5.15000	0.000000	0.235445	5.20000	0.000000	0.235445
5.25000	0.000000	0.235445	5.30000	0.000000	0.235445
5.35000	0.000000	0.235445	5.40000	0.000000	0.235445
5.45000	0.000000	0.235445	5.50000	0.000000	0.235445
6.00000	0.000000	0.235445	6.50000	0.000000	0.235445
7.00000	0.000000	0.235445	7.50000	0.000000	0.235445
8.00000	0.000000	0.235445	8.50000	0.000000	0.235445
9.00000	0.000000	0.235445	9.50000	0.000000	0.235445

10.00000	0.000000	0.235445	4.98500	0.000000	0.245000
5.00000	0.000000	0.245000	5.05000	0.000000	0.245000
5.10000	0.000000	0.245000	5.15000	0.000000	0.245000
5.20000	0.000000	0.245000	5.25000	0.000000	0.245000
5.30000	0.000000	0.245000	5.35000	0.000000	0.245000
5.40000	0.000000	0.245000	5.45000	0.000000	0.245000
5.50000	0.000000	0.245000	6.00000	0.000000	0.245000
6.50000	0.000000	0.245000	7.00000	0.000000	0.245000
7.50000	0.000000	0.245000	8.00000	0.000000	0.245000
8.50000	0.000000	0.245000	9.00000	0.000000	0.245000
9.50000	0.000000	0.245000	10.00000	0.000000	0.245000

Appendix C

Slipstream Characteristics for DATA1

PROPELLER DESIGN (ADVANCED LIFTING MODEL)

REF = DATA1
ADVS = 1.0506
CT = 0.147
ITNO = 3

X = 0.37

AXIAL DISTANCE DOWNSTREAM (Y/R)			HYDRODYNAMIC PITCH (BETAI)			SLIPSTREAM RADIUS (X/X0)		
0.000	0.000	0.000	29.480	28.537	28.554	1.0000	1.0000	1.0000
0.053	0.053	0.052	41.335	40.830	41.179	0.9801	0.9738	0.9724
0.124	0.124	0.122	42.143	41.155	41.357	0.9606	0.9469	0.9437
0.259	0.251	0.242	45.221	44.011	44.220	0.9213	0.8941	0.8894
0.411	0.390	0.372	47.317	45.697	46.127	0.8812	0.8400	0.8341
0.568	0.530	0.499	49.199	47.370	47.965	0.8422	0.7862	0.7794
0.911	0.826	0.764	53.541	53.184	52.877	0.7698	0.6805	0.6677
1.289	1.159	1.068	57.535	60.178	61.019	0.7101	0.5850	0.5582
1.683	1.539	1.459	61.505	66.497	69.686	0.6671	0.5137	0.4613
2.095	1.946	1.926	63.401	70.872	76.712	0.6432	0.4858	0.4044
2.515	2.350	2.421	63.471	72.493	78.207	0.6346	0.4685	0.3901
2.940	2.756	2.918	63.974	72.827	78.554	0.6272	0.4661	0.3869
3.797	3.585	3.943	64.455	73.472	79.145	0.6246	0.4608	0.3821
4.662	4.423	4.983	64.764	73.756	79.363	0.6208	0.4577	0.3794
5.532	5.265	6.029	64.905	73.865	79.441	0.6192	0.4566	0.3787
6.405	6.110	7.080	65.007	73.965	79.507	0.6183	0.4559	0.3781
7.279	6.957	8.134	65.067	74.014	79.538	0.6178	0.4554	0.3778
8.154	7.805	9.190	65.106	74.050	79.560	0.6174	0.4551	0.3776
9.907	9.503	11.305	65.164	74.096	79.582	0.6169	0.4547	0.3773
11.662	11.204	13.424	65.194	74.125	79.598	0.6166	0.4545	0.3771
16.931	16.315	19.794	65.260	74.176	79.648	0.6162	0.4541	0.3770

AXIAL INDUCED VELOCITY (UA/VS)			TANGENTIAL INDUCED VELOCITY (UT/VS)			RADIAL INDUCED VELOCITY (UR/VS)		
0.126	0.110	0.112	-0.079	-0.067	-0.065	-0.005	-0.005	-0.005
0.244	0.235	0.242	-0.190	-0.182	-0.184	-0.005	-0.005	-0.004
0.214	0.201	0.206	-0.192	-0.178	-0.178	-0.005	-0.005	-0.005
0.197	0.180	0.185	-0.194	-0.175	-0.174	-0.005	-0.005	-0.005
0.183	0.160	0.169	-0.198	-0.171	-0.173	-0.005	-0.005	-0.005
0.172	0.142	0.147	-0.196	-0.166	-0.172	-0.005	-0.005	-0.005
0.149	0.120	0.108	-0.189	-0.167	-0.159	-0.004	-0.004	-0.005
0.139	0.110	0.099	-0.184	-0.164	-0.162	-0.002	-0.003	-0.004
0.133	0.107	0.098	-0.184	-0.177	-0.190	-0.001	-0.002	-0.002
0.124	0.099	0.085	-0.178	-0.184	-0.214	-0.001	-0.001	-0.001
0.118	0.099	0.085	-0.163	-0.186	-0.214	0.000	0.000	0.000
0.117	0.099	0.085	-0.164	-0.186	-0.215	0.000	0.000	0.000
0.116	0.100	0.085	-0.169	-0.190	-0.218	0.000	0.000	0.000
0.115	0.099	0.084	-0.168	-0.190	-0.218	0.000	0.000	0.000
0.115	0.099	0.084	-0.168	-0.190	-0.218	0.000	0.000	0.000
0.114	0.099	0.084	-0.168	-0.190	-0.218	0.000	0.000	0.000
0.114	0.099	0.084	-0.168	-0.191	-0.218	0.000	0.000	0.000
0.114	0.099	0.084	-0.168	-0.191	-0.219	0.000	0.000	0.000
0.114	0.099	0.083	-0.168	-0.191	-0.219	0.000	0.000	0.000
0.114	0.099	0.083	-0.168	-0.191	-0.219	0.000	0.000	0.000
0.114	0.099	0.083	-0.169	-0.191	-0.219	0.000	0.000	0.000

X = 0.41

AXIAL DISTANCE DOWNSTREAM (Y/R)			HYDRODYNAMIC PITCH (BETAI)			SLIPSTREAM RADIUS (X/X0)		
0.000	0.000	0.000	34.279	34.170	34.255	1.0000	1.0000	1.0000
0.062	0.061	0.061	40.643	40.434	40.492	0.9845	0.9798	0.9787
0.134	0.133	0.132	41.687	41.244	41.211	0.9692	0.9591	0.9568
0.279	0.275	0.270	44.275	43.639	43.693	0.9386	0.9168	0.9117

0.434	0.426	0.413	46.230	45.557	45.744	0.9083	0.8730	0.8648
0.595	0.581	0.557	48.041	46.964	47.050	0.8796	0.8291	0.8171
0.937	0.905	0.848	51.711	51.030	50.599	0.8257	0.7459	0.7271
1.298	1.258	1.163	54.389	54.867	55.598	0.7793	0.6762	0.6473
1.665	1.629	1.508	56.939	59.357	60.879	0.7456	0.6258	0.5856
2.043	2.014	1.883	57.938	61.999	64.604	0.7270	0.6019	0.5574
2.427	2.400	2.271	58.056	62.846	66.075	0.7237	0.5956	0.5416
2.813	2.789	2.661	58.356	63.247	66.381	0.7193	0.5919	0.5401
3.593	3.576	3.454	58.915	63.851	67.016	0.7144	0.5864	0.5342
4.379	4.373	4.257	59.260	64.181	67.434	0.7114	0.5837	0.5313
5.170	5.172	5.065	59.347	64.332	67.569	0.7100	0.5828	0.5303
5.962	5.973	5.876	59.441	64.435	67.660	0.7090	0.5819	0.5296
6.757	6.776	6.689	59.500	64.506	67.727	0.7085	0.5814	0.5292
7.552	7.579	7.503	59.537	64.545	67.764	0.7081	0.5811	0.5289
9.144	9.188	9.134	59.597	64.606	67.820	0.7076	0.5807	0.5284
10.738	10.799	10.767	59.631	64.639	67.857	0.7073	0.5804	0.5282
15.524	15.639	15.671	59.694	64.688	67.945	0.7068	0.5800	0.5279

AXIAL INDUCED VELOCITY (UA/VS)			TANGENTIAL INDUCED VELOCITY (UT/VS)			RADIAL INDUCED VELOCITY (UR/VS)		
0.125	0.123	0.125	-0.087	-0.086	-0.086	-0.005	-0.006	-0.005
0.204	0.198	0.199	-0.167	-0.162	-0.161	-0.005	-0.005	-0.005
0.198	0.187	0.187	-0.177	-0.166	-0.164	-0.005	-0.006	-0.005
0.190	0.170	0.170	-0.183	-0.166	-0.163	-0.006	-0.006	-0.006
0.182	0.155	0.157	-0.189	-0.165	-0.163	-0.006	-0.006	-0.006
0.176	0.143	0.140	-0.190	-0.163	-0.161	-0.005	-0.006	-0.006
0.167	0.123	0.113	-0.197	-0.158	-0.141	-0.004	-0.005	-0.005
0.165	0.119	0.111	-0.203	-0.158	-0.155	-0.003	-0.003	-0.004
0.161	0.118	0.108	-0.202	-0.167	-0.166	-0.001	-0.001	-0.002
0.152	0.113	0.102	-0.197	-0.175	-0.188	-0.001	-0.001	-0.001
0.149	0.114	0.102	-0.191	-0.178	-0.192	-0.001	0.000	-0.001
0.148	0.114	0.103	-0.191	-0.179	-0.193	0.000	0.000	0.000
0.148	0.114	0.103	-0.195	-0.182	-0.196	0.000	0.000	0.000
0.147	0.114	0.102	-0.195	-0.182	-0.197	0.000	0.000	0.000
0.146	0.114	0.102	-0.194	-0.182	-0.198	0.000	0.000	0.000
0.146	0.114	0.102	-0.195	-0.183	-0.198	0.000	0.000	0.000
0.146	0.113	0.102	-0.195	-0.183	-0.198	0.000	0.000	0.000
0.145	0.113	0.102	-0.195	-0.183	-0.198	0.000	0.000	0.000
0.145	0.113	0.102	-0.195	-0.183	-0.198	0.000	0.000	0.000
0.145	0.113	0.102	-0.195	-0.183	-0.199	0.000	0.000	0.000
0.145	0.113	0.102	-0.196	-0.183	-0.200	0.000	0.000	0.000

X = 0.45

AXIAL DISTANCE DOWNSTREAM (Y/R)			HYDRODYNAMIC PITCH (BETAI)			SLIPSTREAM RADIUS (X/X0)		
0.000	0.000	0.000	33.491	33.428	33.433	1.0000	1.0000	1.0000
0.062	0.062	0.062	37.511	37.469	37.472	0.9857	0.9816	0.9806
0.131	0.131	0.131	38.598	38.441	38.428	0.9727	0.9644	0.9623
0.271	0.271	0.268	40.612	40.382	40.342	0.9472	0.9303	0.9262
0.418	0.416	0.410	42.351	41.996	41.902	0.9228	0.8972	0.8909
0.569	0.567	0.554	43.995	43.512	43.345	0.8993	0.8654	0.8568
0.882	0.884	0.851	47.242	46.737	46.506	0.8544	0.8043	0.7894
1.207	1.221	1.160	49.540	49.512	49.648	0.8159	0.7475	0.7257
1.538	1.568	1.479	51.131	52.105	52.855	0.7924	0.7057	0.6761
1.877	1.924	1.813	52.171	54.268	55.694	0.7795	0.6806	0.6456
2.222	2.285	2.157	52.687	55.168	57.134	0.7727	0.6713	0.6294
2.569	2.648	2.504	52.870	55.522	57.461	0.7694	0.6684	0.6279
3.269	3.380	3.205	53.379	56.107	58.087	0.7642	0.6624	0.6216
3.974	4.121	3.914	53.781	56.501	58.547	0.7608	0.6592	0.6181
4.684	4.866	4.628	53.936	56.724	58.778	0.7591	0.6579	0.6166
5.397	5.612	5.345	54.023	56.820	58.875	0.7581	0.6570	0.6159

6.111	6.360	6.064	54.097	56.899	58.960	0.7576	0.6565	0.6153
6.825	7.109	6.784	54.139	56.951	59.015	0.7571	0.6561	0.6149
8.257	8.609	8.225	54.210	57.018	59.082	0.7565	0.6556	0.6144
9.690	10.111	9.669	54.236	57.056	59.119	0.7562	0.6553	0.6141
13.994	14.619	14.005	54.272	57.113	59.182	0.7557	0.6549	0.6137

AXIAL INDUCED VELOCITY (UA/VS)			TANGENTIAL INDUCED VELOCITY (UT/VS)			RADIAL INDUCED VELOCITY (UR/VS)		
0.102	0.100	0.101	-0.070	-0.070	-0.070	-0.006	-0.006	-0.006
0.160	0.156	0.156	-0.123	-0.121	-0.120	-0.006	-0.006	-0.006
0.165	0.158	0.157	-0.135	-0.130	-0.128	-0.006	-0.006	-0.006
0.165	0.151	0.149	-0.143	-0.135	-0.131	-0.006	-0.007	-0.007
0.165	0.145	0.141	-0.152	-0.138	-0.132	-0.007	-0.007	-0.007
0.166	0.138	0.132	-0.158	-0.138	-0.131	-0.006	-0.006	-0.007
0.169	0.126	0.117	-0.171	-0.138	-0.123	-0.004	-0.005	-0.006
0.169	0.124	0.114	-0.178	-0.137	-0.127	-0.003	-0.003	-0.004
0.168	0.123	0.114	-0.180	-0.141	-0.135	-0.002	-0.002	-0.002
0.165	0.121	0.112	-0.180	-0.149	-0.149	-0.001	-0.001	-0.001
0.162	0.120	0.111	-0.179	-0.150	-0.155	-0.001	-0.001	-0.001
0.161	0.121	0.112	-0.178	-0.151	-0.156	0.000	0.000	-0.001
0.161	0.121	0.112	-0.180	-0.154	-0.158	0.000	0.000	0.000
0.161	0.120	0.112	-0.182	-0.155	-0.160	0.000	0.000	0.000
0.160	0.120	0.112	-0.182	-0.155	-0.160	0.000	0.000	0.000
0.160	0.120	0.112	-0.182	-0.155	-0.161	0.000	0.000	0.000
0.159	0.120	0.112	-0.182	-0.156	-0.161	0.000	0.000	0.000
0.159	0.120	0.112	-0.182	-0.156	-0.161	0.000	0.000	0.000
0.159	0.120	0.111	-0.182	-0.156	-0.161	0.000	0.000	0.000
0.159	0.120	0.111	-0.182	-0.156	-0.161	0.000	0.000	0.000
0.158	0.120	0.111	-0.182	-0.156	-0.162	0.000	0.000	0.000

X = 0.53

AXIAL DISTANCE DOWNSTREAM (Y/R)			HYDRODYNAMIC PITCH (BETAI)			SLIPSTREAM RADIUS (X/X0)		
0.000	0.000	0.000	30.865	30.844	30.837	1.0000	1.0000	1.0000
0.064	0.064	0.064	32.840	32.881	32.881	0.9862	0.9825	0.9816
0.131	0.131	0.131	33.717	33.783	33.787	0.9742	0.9670	0.9652
0.268	0.267	0.267	35.139	35.331	35.357	0.9507	0.9368	0.9333
0.408	0.407	0.406	36.252	36.568	36.605	0.9287	0.9085	0.9034
0.550	0.549	0.546	37.321	37.829	37.883	0.9077	0.8814	0.8749
0.839	0.840	0.835	39.286	40.219	40.294	0.8691	0.8308	0.8207
1.133	1.139	1.130	40.747	42.058	42.284	0.8385	0.7892	0.7748
1.432	1.442	1.429	41.926	43.538	43.920	0.8200	0.7640	0.7464
1.736	1.752	1.735	42.837	44.661	45.230	0.8097	0.7511	0.7309
2.045	2.067	2.047	43.405	45.370	46.111	0.8041	0.7448	0.7216
2.356	2.384	2.362	43.710	45.777	46.519	0.8004	0.7406	0.7179
2.984	3.024	2.998	44.134	46.281	47.046	0.7954	0.7348	0.7119
3.616	3.669	3.640	44.512	46.704	47.484	0.7917	0.7307	0.7077
4.253	4.319	4.287	44.781	46.993	47.796	0.7896	0.7287	0.7057
4.892	4.971	4.937	44.861	47.081	47.883	0.7887	0.7279	0.7050
5.533	5.625	5.588	44.935	47.167	47.971	0.7880	0.7271	0.7042
6.175	6.280	6.240	45.005	47.239	48.042	0.7875	0.7266	0.7038
7.460	7.591	7.546	45.067	47.306	48.112	0.7869	0.7261	0.7032
8.748	8.904	8.854	45.114	47.357	48.164	0.7865	0.7257	0.7028
12.614	12.848	12.784	45.180	47.420	48.231	0.7860	0.7252	0.7023

AXIAL INDUCED VELOCITY (UA/VS)			TANGENTIAL INDUCED VELOCITY (UT/VS)			RADIAL INDUCED VELOCITY (UR/VS)		
0.075	0.074	0.074	-0.046	-0.046	-0.046	-0.007	-0.008	-0.008
0.108	0.106	0.106	-0.071	-0.070	-0.070	-0.007	-0.008	-0.008
0.118	0.115	0.115	-0.081	-0.080	-0.080	-0.008	-0.008	-0.008
0.122	0.118	0.117	-0.088	-0.087	-0.086	-0.008	-0.008	-0.008
0.126	0.120	0.118	-0.095	-0.094	-0.092	-0.008	-0.008	-0.008

0.129	0.121	0.118	-0.099	-0.098	-0.096	-0.007	-0.007	-0.008
0.133	0.121	0.116	-0.106	-0.104	-0.099	-0.004	-0.006	-0.007
0.134	0.120	0.114	-0.110	-0.106	-0.100	-0.004	-0.004	-0.005
0.134	0.120	0.114	-0.111	-0.107	-0.102	-0.002	-0.002	-0.003
0.135	0.120	0.114	-0.113	-0.110	-0.107	-0.001	-0.001	-0.001
0.134	0.119	0.113	-0.114	-0.113	-0.110	-0.001	-0.001	-0.001
0.134	0.120	0.113	-0.114	-0.113	-0.111	-0.001	-0.001	-0.001
0.134	0.120	0.114	-0.114	-0.115	-0.113	0.000	0.000	0.000
0.134	0.120	0.114	-0.115	-0.116	-0.114	0.000	0.000	0.000
0.134	0.120	0.114	-0.116	-0.117	-0.115	0.000	0.000	0.000
0.133	0.120	0.114	-0.116	-0.117	-0.115	0.000	0.000	0.000
0.133	0.120	0.113	-0.116	-0.117	-0.115	0.000	0.000	0.000
0.133	0.120	0.113	-0.116	-0.117	-0.115	0.000	0.000	0.000
0.133	0.119	0.113	-0.116	-0.117	-0.116	0.000	0.000	0.000
0.133	0.119	0.113	-0.116	-0.118	-0.116	0.000	0.000	0.000
0.133	0.119	0.113	-0.117	-0.118	-0.116	0.000	0.000	0.000

X = 0.61

AXIAL DISTANCE DOWNSTREAM (Y/R)			HYDRODYNAMIC PITCH (BETAI)			SLIPSTREAM RADIUS (X/X0)		
0.000	0.000	0.000	28.305	28.308	28.308	1.0000	1.0000	1.0000
0.065	0.065	0.065	29.237	29.312	29.326	0.9876	0.9843	0.9835
0.131	0.131	0.131	29.780	29.908	29.935	0.9757	0.9692	0.9676
0.265	0.265	0.265	30.601	30.885	30.949	0.9530	0.9406	0.9374
0.400	0.400	0.399	31.404	31.837	31.933	0.9318	0.9137	0.9093
0.536	0.535	0.535	32.136	32.733	32.864	0.9121	0.8889	0.8832
0.810	0.810	0.808	33.460	34.373	34.576	0.8789	0.8458	0.8370
1.088	1.089	1.086	34.515	35.720	36.032	0.8547	0.8126	0.8004
1.370	1.372	1.367	35.421	36.868	37.273	0.8388	0.7911	0.7768
1.655	1.659	1.653	36.180	37.810	38.305	0.8292	0.7787	0.7632
1.945	1.951	1.944	36.716	38.466	39.007	0.8235	0.7718	0.7559
2.237	2.245	2.237	37.052	38.877	39.443	0.8199	0.7676	0.7515
2.826	2.838	2.830	37.425	39.316	39.899	0.8150	0.7619	0.7457
3.419	3.436	3.427	37.761	39.703	40.299	0.8111	0.7574	0.7411
4.016	4.038	4.029	38.035	39.996	40.606	0.8088	0.7549	0.7387
4.616	4.643	4.633	38.161	40.136	40.746	0.8077	0.7538	0.7376
5.218	5.249	5.239	38.229	40.215	40.825	0.8070	0.7530	0.7368
5.820	5.856	5.846	38.296	40.286	40.897	0.8064	0.7524	0.7362
7.027	7.073	7.063	38.374	40.370	40.983	0.8057	0.7517	0.7355
8.236	8.292	8.281	38.425	40.425	41.038	0.8053	0.7513	0.7351
11.868	11.953	11.941	38.489	40.491	41.105	0.8047	0.7507	0.7345

AXIAL INDUCED VELOCITY (UA/VS)			TANGENTIAL INDUCED VELOCITY (UT/VS)			RADIAL INDUCED VELOCITY (UR/VS)		
0.055	0.055	0.055	-0.030	-0.031	-0.031	-0.009	-0.009	-0.009
0.074	0.073	0.073	-0.042	-0.042	-0.042	-0.009	-0.009	-0.009
0.083	0.082	0.082	-0.049	-0.049	-0.049	-0.009	-0.009	-0.009
0.087	0.086	0.085	-0.054	-0.055	-0.054	-0.009	-0.009	-0.010
0.092	0.089	0.089	-0.059	-0.060	-0.059	-0.009	-0.010	-0.010
0.094	0.091	0.090	-0.062	-0.063	-0.063	-0.008	-0.008	-0.009
0.098	0.093	0.091	-0.066	-0.067	-0.066	-0.004	-0.006	-0.007
0.099	0.093	0.091	-0.069	-0.069	-0.067	-0.004	-0.005	-0.005
0.101	0.095	0.093	-0.070	-0.070	-0.068	-0.002	-0.003	-0.003
0.102	0.096	0.094	-0.071	-0.072	-0.071	-0.001	-0.001	-0.002
0.102	0.096	0.094	-0.072	-0.075	-0.075	-0.001	-0.001	-0.001
0.102	0.096	0.094	-0.072	-0.075	-0.075	-0.001	-0.001	-0.001
0.103	0.097	0.095	-0.072	-0.076	-0.076	0.000	0.000	0.000
0.103	0.097	0.095	-0.073	-0.077	-0.077	0.000	0.000	0.000
0.103	0.097	0.095	-0.073	-0.077	-0.078	0.000	0.000	0.000
0.103	0.097	0.095	-0.073	-0.077	-0.078	0.000	0.000	0.000
0.103	0.097	0.095	-0.074	-0.077	-0.078	0.000	0.000	0.000

0.102	0.097	0.095	-0.074	-0.078	-0.078	0.000	0.000	0.000
0.102	0.097	0.095	-0.074	-0.078	-0.078	0.000	0.000	0.000
0.102	0.097	0.095	-0.074	-0.078	-0.078	0.000	0.000	0.000
0.102	0.097	0.094	-0.074	-0.078	-0.079	0.000	0.000	0.000

X = 0.69

AXIAL DISTANCE DOWNSTREAM (Y/R)			HYDRODYNAMIC PITCH (BETAI)			SLIPSTREAM RADIUS (X/X0)		
0.000	0.000	0.000	25.565	25.579	25.584	1.0000	1.0000	1.0000
0.065	0.065	0.065	26.376	26.457	26.478	0.9888	0.9859	0.9852
0.132	0.132	0.132	26.868	27.012	27.049	0.9781	0.9724	0.9709
0.266	0.266	0.266	27.514	27.790	27.860	0.9582	0.9470	0.9441
0.401	0.401	0.400	28.135	28.539	28.641	0.9400	0.9236	0.9193
0.537	0.537	0.536	28.667	29.206	29.347	0.9235	0.9021	0.8964
0.810	0.810	0.809	29.672	30.478	30.691	0.8966	0.8664	0.8578
1.087	1.087	1.085	30.455	31.461	31.744	0.8773	0.8406	0.8297
1.367	1.367	1.364	31.155	32.336	32.684	0.8641	0.8230	0.8105
1.651	1.651	1.647	31.752	33.072	33.475	0.8557	0.8122	0.7989
1.937	1.939	1.934	32.190	33.597	34.035	0.8505	0.8059	0.7922
2.226	2.229	2.224	32.483	33.945	34.399	0.8471	0.8018	0.7879
2.808	2.813	2.808	32.813	34.330	34.798	0.8423	0.7962	0.7823
3.395	3.401	3.396	33.108	34.673	35.151	0.8386	0.7918	0.7778
3.984	3.994	3.988	33.352	34.939	35.428	0.8363	0.7893	0.7752
4.577	4.589	4.583	33.475	35.076	35.564	0.8352	0.7881	0.7741
5.171	5.185	5.180	33.539	35.147	35.637	0.8345	0.7874	0.7733
5.766	5.783	5.777	33.600	35.214	35.703	0.8339	0.7867	0.7727
6.958	6.980	6.975	33.676	35.295	35.786	0.8332	0.7860	0.7719
8.152	8.179	8.174	33.722	35.346	35.838	0.8328	0.7855	0.7715
11.739	11.781	11.776	33.784	35.411	35.904	0.8322	0.7850	0.7709

AXIAL INDUCED VELOCITY (UA/VS)			TANGENTIAL INDUCED VELOCITY (UT/VS)			RADIAL INDUCED VELOCITY (UR/VS)		
0.054	0.055	0.055	-0.027	-0.027	-0.027	-0.010	-0.010	-0.010
0.073	0.073	0.074	-0.036	-0.037	-0.037	-0.010	-0.010	-0.011
0.081	0.081	0.081	-0.042	-0.042	-0.042	-0.010	-0.010	-0.011
0.085	0.085	0.085	-0.046	-0.047	-0.047	-0.010	-0.011	-0.011
0.089	0.088	0.088	-0.050	-0.051	-0.051	-0.010	-0.011	-0.011
0.092	0.090	0.089	-0.052	-0.053	-0.053	-0.008	-0.009	-0.009
0.096	0.093	0.092	-0.055	-0.057	-0.057	-0.005	-0.006	-0.007
0.097	0.094	0.093	-0.057	-0.059	-0.057	-0.004	-0.004	-0.005
0.099	0.095	0.094	-0.058	-0.060	-0.059	-0.002	-0.003	-0.003
0.100	0.097	0.096	-0.059	-0.061	-0.061	-0.001	-0.001	-0.001
0.100	0.097	0.095	-0.060	-0.063	-0.064	-0.001	-0.001	-0.001
0.100	0.097	0.096	-0.060	-0.064	-0.064	-0.001	-0.001	-0.001
0.101	0.098	0.096	-0.060	-0.064	-0.065	0.000	0.000	0.000
0.101	0.098	0.097	-0.061	-0.065	-0.066	0.000	0.000	0.000
0.101	0.098	0.097	-0.061	-0.066	-0.066	0.000	0.000	0.000
0.101	0.098	0.096	-0.062	-0.066	-0.066	0.000	0.000	0.000
0.101	0.098	0.096	-0.062	-0.066	-0.067	0.000	0.000	0.000
0.101	0.098	0.096	-0.062	-0.066	-0.067	0.000	0.000	0.000
0.101	0.098	0.096	-0.062	-0.066	-0.067	0.000	0.000	0.000
0.101	0.098	0.096	-0.062	-0.066	-0.067	0.000	0.000	0.000
0.101	0.098	0.096	-0.062	-0.066	-0.067	0.000	0.000	0.000

X = 0.76

AXIAL DISTANCE DOWNSTREAM (Y/R)			HYDRODYNAMIC PITCH (BETAI)			SLIPSTREAM RADIUS (X/X0)		
0.000	0.000	0.000	23.296	23.312	23.318	1.0000	1.0000	1.0000
0.066	0.066	0.066	24.045	24.114	24.133	0.9909	0.9885	0.9879
0.133	0.133	0.132	24.417	24.536	24.567	0.9822	0.9775	0.9763

0.267	0.267	0.267		24.910	25.131	25.188	0.9658	0.9565	0.9541
0.402	0.402	0.402		25.383	25.702	25.785	0.9508	0.9373	0.9337
0.538	0.538	0.538		25.786	26.205	26.317	0.9373	0.9197	0.9150
0.812	0.812	0.811		26.545	27.154	27.320	0.9154	0.8910	0.8842
1.088	1.088	1.086		27.144	27.892	28.101	0.8995	0.8701	0.8616
1.367	1.367	1.365		27.688	28.557	28.807	0.8882	0.8554	0.8457
1.649	1.649	1.646		28.158	29.125	29.410	0.8808	0.8460	0.8357
1.934	1.934	1.931		28.513	29.544	29.849	0.8761	0.8401	0.8295
2.221	2.222	2.218		28.760	29.832	30.149	0.8728	0.8362	0.8255
2.799	2.800	2.796		29.050	30.168	30.496	0.8682	0.8308	0.8199
3.380	3.383	3.379		29.307	30.464	30.801	0.8646	0.8265	0.8155
3.965	3.969	3.965		29.522	30.698	31.045	0.8624	0.8240	0.8130
4.552	4.557	4.553		29.637	30.823	31.171	0.8613	0.8228	0.8118
5.141	5.148	5.144		29.695	30.889	31.237	0.8606	0.8220	0.8110
5.731	5.739	5.735		29.750	30.949	31.298	0.8601	0.8214	0.8103
6.913	6.923	6.919		29.822	31.026	31.375	0.8593	0.8206	0.8096
8.096	8.109	8.105		29.865	31.073	31.423	0.8589	0.8201	0.8091
11.652	11.673	11.669		29.923	31.135	31.486	0.8584	0.8195	0.8085

AXIAL INDUCED VELOCITY (UA/VS)			TANGENTIAL INDUCED VELOCITY (UT/VS)			RADIAL INDUCED VELOCITY (UR/VS)		
0.053	0.054	0.054	-0.023	-0.024	-0.024	-0.011	-0.011	-0.011
0.075	0.075	0.075	-0.033	-0.033	-0.033	-0.011	-0.011	-0.011
0.081	0.082	0.082	-0.037	-0.038	-0.038	-0.011	-0.011	-0.011
0.085	0.085	0.085	-0.040	-0.041	-0.041	-0.011	-0.011	-0.012
0.089	0.089	0.089	-0.043	-0.045	-0.045	-0.011	-0.011	-0.012
0.091	0.090	0.090	-0.045	-0.046	-0.046	-0.009	-0.009	-0.010
0.095	0.094	0.093	-0.047	-0.049	-0.049	-0.005	-0.005	-0.006
0.096	0.094	0.094	-0.049	-0.050	-0.050	-0.004	-0.004	-0.004
0.097	0.096	0.095	-0.050	-0.051	-0.051	-0.002	-0.003	-0.003
0.099	0.097	0.097	-0.050	-0.053	-0.053	-0.001	-0.001	-0.001
0.099	0.097	0.096	-0.051	-0.054	-0.055	-0.001	-0.001	-0.001
0.099	0.097	0.097	-0.052	-0.055	-0.055	-0.001	-0.001	-0.001
0.099	0.098	0.097	-0.052	-0.055	-0.056	0.000	0.000	0.000
0.100	0.098	0.098	-0.053	-0.056	-0.057	0.000	0.000	0.000
0.100	0.098	0.098	-0.053	-0.056	-0.057	0.000	0.000	0.000
0.100	0.098	0.098	-0.053	-0.057	-0.057	0.000	0.000	0.000
0.100	0.098	0.098	-0.053	-0.057	-0.057	0.000	0.000	0.000
0.100	0.098	0.098	-0.053	-0.057	-0.058	0.000	0.000	0.000
0.100	0.098	0.097	-0.053	-0.057	-0.058	0.000	0.000	0.000
0.100	0.098	0.097	-0.053	-0.057	-0.058	0.000	0.000	0.000
0.100	0.098	0.097	-0.053	-0.057	-0.058	0.000	0.000	0.000

X = 0.84

AXIAL DISTANCE DOWNSTREAM (Y/R)			HYDRODYNAMIC PITCH (BETAI)			SLIPSTREAM RADIUS (X/X0)		
0.000	0.000	0.000	21.411	21.426	21.430	1.0000	1.0000	1.0000
0.066	0.066	0.066	22.155	22.206	22.219	0.9924	0.9904	0.9899
0.133	0.133	0.133	22.426	22.517	22.539	0.9851	0.9812	0.9802
0.268	0.268	0.268	22.805	22.974	23.016	0.9714	0.9638	0.9618
0.404	0.404	0.404	23.170	23.413	23.475	0.9589	0.9478	0.9449
0.540	0.540	0.540	23.481	23.799	23.883	0.9476	0.9332	0.9294
0.814	0.814	0.813	24.068	24.524	24.648	0.9293	0.9094	0.9039
1.091	1.090	1.088	24.538	25.096	25.248	0.9158	0.8919	0.8852
1.369	1.368	1.366	24.971	25.616	25.795	0.9061	0.8794	0.8718
1.650	1.650	1.647	25.348	26.064	26.267	0.8996	0.8711	0.8630
1.934	1.933	1.930	25.638	26.403	26.620	0.8952	0.8657	0.8573
2.220	2.219	2.216	25.847	26.644	26.869	0.8921	0.8619	0.8534
2.794	2.794	2.790	26.103	26.938	27.172	0.8877	0.8567	0.8480
3.372	3.372	3.368	26.328	27.196	27.438	0.8843	0.8525	0.8438

3.953	3.954	3.950	26.518	27.403	27.653	0.8821	0.8501	0.8413
4.537	4.539	4.534	26.623	27.517	27.768	0.8810	0.8489	0.8401
5.122	5.125	5.120	26.676	27.577	27.828	0.8803	0.8481	0.8393
5.708	5.711	5.706	26.727	27.632	27.884	0.8798	0.8475	0.8386
6.883	6.887	6.882	26.793	27.703	27.956	0.8790	0.8467	0.8378
8.059	8.065	8.059	26.833	27.746	28.000	0.8786	0.8462	0.8373
11.593	11.603	11.596	26.887	27.804	28.058	0.8780	0.8456	0.8367

AXIAL INDUCED VELOCITY (UA/VS)			TANGENTIAL INDUCED VELOCITY (UT/VS)			RADIAL INDUCED VELOCITY (UR/VS)		
0.052	0.052	0.053	-0.021	-0.021	-0.021	-0.011	-0.012	-0.012
0.078	0.078	0.078	-0.030	-0.031	-0.031	-0.012	-0.012	-0.012
0.083	0.083	0.083	-0.034	-0.034	-0.034	-0.012	-0.012	-0.012
0.086	0.086	0.086	-0.036	-0.037	-0.037	-0.012	-0.012	-0.012
0.089	0.089	0.089	-0.039	-0.039	-0.039	-0.012	-0.012	-0.012
0.091	0.090	0.090	-0.040	-0.041	-0.041	-0.009	-0.009	-0.010
0.094	0.093	0.093	-0.041	-0.043	-0.043	-0.005	-0.005	-0.006
0.095	0.094	0.094	-0.043	-0.044	-0.043	-0.004	-0.004	-0.004
0.096	0.095	0.095	-0.044	-0.045	-0.044	-0.002	-0.002	-0.003
0.098	0.097	0.096	-0.044	-0.046	-0.046	-0.001	-0.001	-0.001
0.098	0.097	0.096	-0.045	-0.047	-0.048	-0.001	-0.001	-0.001
0.098	0.097	0.097	-0.046	-0.048	-0.048	-0.001	0.000	-0.001
0.099	0.098	0.097	-0.046	-0.048	-0.049	0.000	0.000	0.000
0.099	0.098	0.098	-0.046	-0.049	-0.049	0.000	0.000	0.000
0.099	0.098	0.098	-0.046	-0.049	-0.050	0.000	0.000	0.000
0.099	0.098	0.098	-0.047	-0.049	-0.050	0.000	0.000	0.000
0.099	0.098	0.098	-0.047	-0.050	-0.050	0.000	0.000	0.000
0.099	0.098	0.098	-0.047	-0.050	-0.050	0.000	0.000	0.000
0.099	0.098	0.098	-0.047	-0.050	-0.050	0.000	0.000	0.000
0.099	0.098	0.098	-0.047	-0.050	-0.050	0.000	0.000	0.000

X = 0.92

AXIAL DISTANCE DOWNSTREAM (Y/R)			HYDRODYNAMIC PITCH (BETAI)			SLIPSTREAM RADIUS (X/X0)		
0.000	0.000	0.000	19.794	19.805	19.801	1.0000	1.0000	1.0000
0.066	0.066	0.066	20.487	20.497	20.484	0.9936	0.9919	0.9915
0.134	0.134	0.133	20.667	20.709	20.703	0.9874	0.9842	0.9833
0.269	0.269	0.268	20.959	21.062	21.074	0.9759	0.9695	0.9678
0.405	0.404	0.403	21.241	21.399	21.427	0.9653	0.9559	0.9535
0.541	0.540	0.539	21.484	21.694	21.742	0.9557	0.9436	0.9405
0.815	0.813	0.811	21.942	22.250	22.329	0.9400	0.9235	0.9191
1.090	1.088	1.085	22.318	22.696	22.797	0.9285	0.9086	0.9032
1.367	1.365	1.361	22.665	23.106	23.226	0.9200	0.8977	0.8916
1.647	1.644	1.639	22.971	23.464	23.601	0.9141	0.8902	0.8837
1.929	1.925	1.919	23.212	23.741	23.887	0.9100	0.8852	0.8784
2.212	2.209	2.202	23.391	23.945	24.099	0.9071	0.8817	0.8747
2.783	2.778	2.770	23.616	24.201	24.362	0.9029	0.8766	0.8694
3.356	3.351	3.341	23.814	24.426	24.592	0.8995	0.8726	0.8653
3.933	3.928	3.916	23.982	24.608	24.782	0.8975	0.8702	0.8628
4.512	4.507	4.493	24.079	24.713	24.888	0.8964	0.8689	0.8615
5.092	5.087	5.071	24.127	24.767	24.942	0.8957	0.8681	0.8607
5.674	5.668	5.651	24.174	24.818	24.993	0.8951	0.8675	0.8601
6.839	6.832	6.812	24.236	24.886	25.061	0.8944	0.8667	0.8592
8.005	7.999	7.975	24.272	24.925	25.101	0.8940	0.8662	0.8587
11.511	11.502	11.469	24.323	24.979	25.156	0.8934	0.8655	0.8581

AXIAL INDUCED VELOCITY (UA/VS)			TANGENTIAL INDUCED VELOCITY (UT/VS)			RADIAL INDUCED VELOCITY (UR/VS)		
0.051	0.052	0.051	-0.019	-0.019	-0.019	-0.012	-0.012	-0.012
0.078	0.077	0.077	-0.028	-0.028	-0.027	-0.012	-0.012	-0.012
0.081	0.080	0.079	-0.030	-0.030	-0.029	-0.012	-0.012	-0.012

0.084	0.083	0.082	-0.032	-0.032	-0.031	-0.012	-0.012	-0.012
0.086	0.085	0.084	-0.034	-0.034	-0.033	-0.012	-0.012	-0.012
0.088	0.086	0.085	-0.034	-0.035	-0.034	-0.009	-0.009	-0.010
0.090	0.088	0.088	-0.035	-0.036	-0.036	-0.004	-0.005	-0.005
0.092	0.089	0.088	-0.037	-0.037	-0.036	-0.004	-0.004	-0.004
0.093	0.090	0.089	-0.037	-0.038	-0.037	-0.002	-0.002	-0.002
0.094	0.091	0.091	-0.038	-0.039	-0.038	-0.001	-0.001	-0.001
0.094	0.091	0.090	-0.039	-0.040	-0.040	-0.001	-0.001	-0.001
0.094	0.091	0.091	-0.039	-0.040	-0.040	-0.001	0.000	0.000
0.095	0.092	0.091	-0.039	-0.041	-0.041	0.000	0.000	0.000
0.095	0.092	0.092	-0.040	-0.041	-0.041	0.000	0.000	0.000
0.095	0.092	0.092	-0.040	-0.041	-0.042	0.000	0.000	0.000
0.095	0.092	0.092	-0.040	-0.042	-0.042	0.000	0.000	0.000
0.095	0.093	0.092	-0.040	-0.042	-0.042	0.000	0.000	0.000
0.095	0.093	0.092	-0.040	-0.042	-0.042	0.000	0.000	0.000
0.095	0.093	0.092	-0.040	-0.042	-0.042	0.000	0.000	0.000
0.095	0.093	0.092	-0.041	-0.042	-0.042	0.000	0.000	0.000
0.095	0.093	0.092	-0.041	-0.042	-0.042	0.000	0.000	0.000

X = 0.96

AXIAL DISTANCE DOWNSTREAM (Y/R)			HYDRODYNAMIC PITCH (BETAI)			SLIPSTREAM RADIUS (X/X0)		
0.000	0.000	0.000	19.090	19.093	19.069	1.0000	1.0000	1.0000
0.066	0.066	0.066	19.803	19.747	19.686	0.9941	0.9926	0.9922
0.134	0.134	0.133	19.951	19.921	19.865	0.9884	0.9854	0.9847
0.270	0.269	0.268	20.242	20.267	20.222	0.9778	0.9719	0.9704
0.406	0.405	0.403	20.517	20.594	20.559	0.9680	0.9594	0.9572
0.543	0.542	0.539	20.757	20.879	20.857	0.9592	0.9481	0.9452
0.817	0.816	0.812	21.194	21.393	21.408	0.9448	0.9296	0.9255
1.092	1.093	1.087	21.547	21.833	21.871	0.9341	0.9159	0.9108
1.370	1.371	1.365	21.871	22.234	22.281	0.9262	0.9058	0.9000
1.649	1.652	1.644	22.148	22.563	22.640	0.9206	0.8988	0.8926
1.931	1.935	1.927	22.366	22.827	22.906	0.9168	0.8940	0.8876
2.214	2.220	2.210	22.528	23.023	23.120	0.9139	0.8906	0.8840
2.784	2.792	2.782	22.744	23.276	23.379	0.9098	0.8856	0.8788
3.357	3.368	3.357	22.931	23.500	23.606	0.9066	0.8818	0.8748
3.933	3.947	3.936	23.090	23.676	23.791	0.9046	0.8795	0.8724
4.511	4.528	4.517	23.173	23.769	23.895	0.9035	0.8783	0.8712
5.091	5.111	5.099	23.214	23.820	23.948	0.9028	0.8775	0.8704
5.671	5.694	5.683	23.259	23.870	23.998	0.9022	0.8768	0.8698
6.834	6.863	6.851	23.316	23.934	24.064	0.9015	0.8760	0.8690
7.999	8.033	8.022	23.349	23.972	24.104	0.9011	0.8756	0.8685
11.500	11.548	11.540	23.390	24.025	24.154	0.9005	0.8749	0.8678

AXIAL INDUCED VELOCITY (UA/VS)			TANGENTIAL INDUCED VELOCITY (UT/VS)			RADIAL INDUCED VELOCITY (UR/VS)		
0.052	0.052	0.051	-0.018	-0.018	-0.017	-0.012	-0.012	-0.012
0.083	0.078	0.075	-0.027	-0.026	-0.024	-0.012	-0.012	-0.012
0.085	0.080	0.077	-0.028	-0.027	-0.025	-0.012	-0.012	-0.012
0.089	0.084	0.081	-0.031	-0.030	-0.028	-0.012	-0.012	-0.012
0.092	0.088	0.084	-0.033	-0.032	-0.030	-0.012	-0.012	-0.012
0.094	0.090	0.086	-0.034	-0.033	-0.031	-0.009	-0.009	-0.009
0.098	0.093	0.090	-0.035	-0.035	-0.033	-0.004	-0.004	-0.005
0.100	0.095	0.093	-0.037	-0.036	-0.035	-0.003	-0.003	-0.003
0.102	0.098	0.095	-0.038	-0.038	-0.036	-0.002	-0.002	-0.002
0.103	0.099	0.097	-0.038	-0.039	-0.037	-0.001	-0.001	-0.001
0.103	0.100	0.097	-0.039	-0.040	-0.039	-0.001	-0.001	-0.001
0.103	0.101	0.098	-0.039	-0.041	-0.040	-0.001	0.000	0.000
0.104	0.102	0.099	-0.040	-0.041	-0.040	0.000	0.000	0.000
0.104	0.103	0.100	-0.040	-0.042	-0.041	0.000	0.000	0.000
0.104	0.103	0.100	-0.040	-0.042	-0.042	0.000	0.000	0.000

0.104	0.103	0.101	-0.040	-0.042	-0.042	0.000	0.000	0.000
0.104	0.103	0.101	-0.040	-0.042	-0.042	0.000	0.000	0.000
0.104	0.103	0.101	-0.040	-0.043	-0.042	0.000	0.000	0.000
0.104	0.103	0.101	-0.041	-0.043	-0.042	0.000	0.000	0.000
0.104	0.103	0.101	-0.041	-0.043	-0.042	0.000	0.000	0.000
0.103	0.103	0.101	-0.040	-0.043	-0.042	0.000	0.000	0.000

X = 1.00

AXIAL DISTANCE DOWNSTREAM (Y/R)			HYDRODYNAMIC PITCH (BETAI)			SLIPSTREAM RADIUS (X/X0)		
0.000	0.000	0.000	17.984	18.016	17.973	1.0000	1.0000	1.0000
0.063	0.063	0.063	18.117	17.960	17.837	0.9945	0.9932	0.9928
0.127	0.127	0.126	18.175	18.035	17.914	0.9892	0.9865	0.9859
0.255	0.253	0.251	18.434	18.327	18.215	0.9791	0.9740	0.9727
0.383	0.380	0.377	18.692	18.641	18.510	0.9699	0.9625	0.9606
0.512	0.508	0.504	18.908	18.925	18.707	0.9615	0.9520	0.9496
0.770	0.765	0.759	19.293	19.331	19.172	0.9478	0.9346	0.9310
1.029	1.023	1.015	19.588	19.716	19.661	0.9374	0.9211	0.9164
1.290	1.283	1.274	19.843	20.075	20.029	0.9294	0.9108	0.9054
1.552	1.545	1.534	20.128	20.321	20.365	0.9236	0.9033	0.8974
1.817	1.808	1.796	20.329	20.634	20.626	0.9195	0.8981	0.8919
2.082	2.074	2.060	20.489	20.842	20.840	0.9164	0.8943	0.8879
2.617	2.608	2.593	20.701	21.088	21.096	0.9122	0.8891	0.8824
3.155	3.145	3.129	20.877	21.300	21.309	0.9087	0.8849	0.8780
3.696	3.686	3.668	21.028	21.477	21.490	0.9064	0.8821	0.8750
4.239	4.229	4.210	21.139	21.602	21.633	0.9051	0.8806	0.8734
4.784	4.773	4.754	21.178	21.649	21.681	0.9044	0.8798	0.8726
5.330	5.318	5.298	21.217	21.695	21.728	0.9038	0.8790	0.8718
6.424	6.411	6.390	21.282	21.770	21.806	0.9029	0.8780	0.8709
7.520	7.505	7.483	21.312	21.804	21.844	0.9025	0.8775	0.8703
10.813	10.794	10.769	21.367	21.869	21.914	0.9018	0.8767	0.8694

AXIAL INDUCED VELOCITY (UA/VS)			TANGENTIAL INDUCED VELOCITY (UT/VS)			RADIAL INDUCED VELOCITY (UR/VS)		
0.029	0.031	0.028	-0.009	-0.009	-0.009	-0.012	-0.011	-0.011
0.032	0.022	0.016	-0.007	-0.004	-0.002	-0.012	-0.012	-0.012
0.030	0.020	0.014	-0.007	-0.003	-0.001	-0.012	-0.012	-0.012
0.034	0.024	0.017	-0.008	-0.005	-0.002	-0.012	-0.012	-0.012
0.037	0.028	0.020	-0.010	-0.007	-0.004	-0.012	-0.012	-0.012
0.040	0.032	0.021	-0.011	-0.008	-0.004	-0.010	-0.010	-0.010
0.043	0.035	0.025	-0.012	-0.009	-0.005	-0.005	-0.005	-0.005
0.046	0.038	0.032	-0.014	-0.011	-0.007	-0.004	-0.004	-0.004
0.046	0.041	0.034	-0.014	-0.011	-0.008	-0.003	-0.002	-0.002
0.049	0.040	0.037	-0.015	-0.011	-0.010	-0.001	-0.001	-0.001
0.049	0.044	0.038	-0.015	-0.013	-0.011	-0.001	-0.001	-0.001
0.049	0.045	0.039	-0.016	-0.014	-0.011	-0.001	0.000	-0.001
0.050	0.046	0.040	-0.016	-0.014	-0.012	0.000	0.000	0.000
0.051	0.047	0.041	-0.016	-0.015	-0.012	0.000	0.000	0.000
0.051	0.048	0.041	-0.016	-0.015	-0.013	0.000	0.000	0.000
0.051	0.048	0.042	-0.016	-0.015	-0.013	0.000	0.000	0.000
0.051	0.048	0.042	-0.016	-0.015	-0.013	0.000	0.000	0.000
0.051	0.048	0.042	-0.016	-0.015	-0.013	0.000	0.000	0.000
0.051	0.048	0.042	-0.016	-0.015	-0.013	0.000	0.000	0.000
0.051	0.048	0.043	-0.016	-0.015	-0.013	0.000	0.000	0.000

Propeller Design Output for DATA1

PROPELLER DESIGN WITH IRREGULAR HELICAL SLIPSTREAM
(PROGRAM FPST.FOR)

INPUT DATA

DHP	RPM	VS	1-WT	DIAMETER	BLADES
348.6	3000.0	50.00	0.885	490.00	3

RADIUS	1-WN	THICKNESS	CHORD	DRAG COEFF
0.37	0.4550			
0.41	0.6490	0.000	172.500	0.00950
0.45	0.7400	0.000	180.000	0.00930
0.53	0.8410	0.000	195.000	0.00920
0.61	0.9042	0.000	208.000	0.00910
0.69	0.9130	0.000	212.200	0.00900
0.76	0.9206	0.000	204.500	0.00890
0.84	0.9273	0.000	184.000	0.00880
0.92	0.9334	0.000	142.000	0.00870
0.96	0.9362	0.000	105.000	0.00860
1.00	0.9388			

DERIVED DESIGN CONDITIONS

KQ	JVS
0.01143	1.0506

RESULTS

CIRCULATION COEFFICIENTS

0.0109891 0.0024569 0.0012071 0.0005494 0.0000597 0.0000659 -0.0000341 0.0000734 0.0000270

RADIUS	BETA	BETAI	CIRCULATION	UT/VS	UA/VS	UR/VS	CCL/D	CL	DKQ	DKT
0.41	27.95	34.26	0.009046	-0.08644	0.12506	-0.00548	0.04133	0.11740	0.00833	0.05053
0.45	28.86	33.43	0.010761	-0.06951	0.10056	-0.00618	0.04432	0.12064	0.01179	0.06763
0.53	28.04	30.84	0.011148	-0.04617	0.07405	-0.00767	0.03924	0.09860	0.01620	0.08392
0.61	26.52	28.31	0.010483	-0.03071	0.05532	-0.00919	0.03255	0.07669	0.01934	0.09092
0.69	24.02	25.58	0.009903	-0.02708	0.05482	-0.01044	0.02776	0.06411	0.02208	0.09711
0.76	21.95	23.32	0.009030	-0.02391	0.05386	-0.01127	0.02305	0.05522	0.02402	0.09880
0.84	20.22	21.43	0.007729	-0.02116	0.05269	-0.01169	0.01811	0.04822	0.02430	0.09318
0.92	18.72	19.80	0.005809	-0.01876	0.05147	-0.01168	0.01255	0.04332	0.02134	0.07666
0.96	18.04	19.07	0.003999	-0.01740	0.05118	-0.01156	0.00831	0.03880	0.01619	0.05485

XTEPSI	KQ	KT	EFFY
0.3512	0.01144	0.04998	0.646

Propeller Design Output for DATA2

PROPELLER DESIGN WITH IRREGULAR HELICAL SLIPSTREAM
(PROGRAM FPST.FOR)

INPUT DATA

DHP	RPM	VS	1-WT	DIAMETER	BLADES
348.6	2000.0	15.00	0.873	490.00	3

RADIUS	1-WN	THICKNESS	CHORD	DRAG COEFF
0.37	0.4050			
0.41	0.6030	0.000	172.500	0.00950
0.45	0.6970	0.000	180.000	0.00930
0.53	0.8050	0.000	195.000	0.00920
0.61	0.8750	0.000	208.000	0.00910
0.69	0.9134	0.000	212.200	0.00900
0.76	0.9210	0.000	204.500	0.00890
0.84	0.9276	0.000	184.000	0.00880
0.92	0.9337	0.000	142.000	0.00870
0.96	0.9365	0.000	105.000	0.00860
1.00	0.9391			

DERIVED DESIGN CONDITIONS

KQ	JVS
0.03858	0.4728

RESULTS

CIRCULATION COEFFICIENTS

0.1277742 0.0014378 0.0026742 0.0007187 0.0001994 0.0001398 -0.0001501 0.0000495 -0.0001035

RADIUS	BETA	BETAI	CIRCULATION	UT/VS	UA/VS	UR/VS	CCL/D	CL	DKQ	DKT
0.41	12.51	28.61	0.066369	-0.42202	0.64927	-0.03213	0.15945	0.45294	0.01859	0.15865
0.45	13.15	27.54	0.088308	-0.43533	0.63182	-0.03968	0.19306	0.52554	0.02869	0.23483
0.53	12.92	25.25	0.111118	-0.40791	0.65762	-0.05522	0.20364	0.51171	0.04691	0.35981
0.61	12.26	23.10	0.122033	-0.37611	0.68262	-0.07057	0.19317	0.45506	0.06350	0.46523
0.69	11.35	21.09	0.125346	-0.34671	0.70822	-0.08445	0.17474	0.40349	0.07756	0.55039
0.76	10.28	19.23	0.121667	-0.32157	0.73739	-0.09528	0.15179	0.36370	0.08687	0.60416
0.84	9.41	17.67	0.109795	-0.29670	0.76046	-0.10235	0.12405	0.33036	0.08905	0.60751
0.92	8.67	16.33	0.085412	-0.27016	0.78023	-0.10536	0.08803	0.30378	0.07794	0.52184
0.96	8.34	15.74	0.062682	-0.24755	0.79331	-0.10658	0.06175	0.28818	0.06068	0.40184

XTEPSI	KQ	KT	EFFY
0.4100	0.03865	0.27459	0.467

Propeller Design Output for DATA3

PROPELLER DESIGN WITH IRREGULAR HELICAL SLIPSTREAM
(PROGRAM FPST.FOR)

INPUT DATA

DHP	RPM	VS	1-WT	DIAMETER	BLADES
45414.6	98.7	26.50	0.833	7560.00	6

RADIUS	1-WN	THICKNESS	CHORD	DRAG COEFF
0.22	0.4642			
0.25	0.4840	0.000	1892.000	0.00830
0.30	0.5330	0.000	1981.000	0.00810
0.40	0.6440	0.000	2160.000	0.00770
0.50	0.7950	0.000	2305.000	0.00740
0.60	0.8580	0.000	2410.000	0.00720
0.70	0.8910	0.000	2453.000	0.00700
0.80	0.9050	0.000	2387.000	0.00690
0.90	0.9080	0.000	2081.000	0.00700
0.95	0.9090	0.000	1689.000	0.00730
1.00	0.9100			

DERIVED DESIGN CONDITIONS

KQ	JVS
0.04784	1.0969

RESULTS

CIRCULATION COEFFICIENTS

0.0215733 0.0004887 0.0014633 -0.0000992 -0.0001972 -0.0001537 0.0000469 0.0000268 0.0000776

RADIUS	BETA	BETAI	CIRCULATION	UT/VS	UA/VS	UR/VS	CCL/D	CL	DKQ	DKT
0.25	34.06	46.97	0.009598	-0.16873	0.10234	0.03546	0.07519	0.30043	0.00818	0.05780
0.30	31.81	43.72	0.014896	-0.16970	0.12641	0.02738	0.09810	0.37438	0.01709	0.11407
0.40	29.34	38.75	0.019213	-0.15492	0.15117	0.00536	0.09503	0.33259	0.03565	0.21184
0.50	29.04	35.53	0.019849	-0.12016	0.14185	-0.01562	0.07737	0.25375	0.05487	0.28914
0.60	26.53	31.74	0.019947	-0.10122	0.14251	-0.03300	0.06591	0.20675	0.07172	0.35794
0.70	23.96	28.40	0.019634	-0.08819	0.14516	-0.04668	0.05662	0.17450	0.08674	0.41750
0.80	21.55	25.50	0.018458	-0.07926	0.15020	-0.05598	0.04732	0.14988	0.09688	0.45284
0.90	19.41	23.03	0.015089	-0.07297	0.15692	-0.05969	0.03483	0.12655	0.09267	0.41849
0.95	18.47	21.96	0.011526	-0.07110	0.15966	-0.05932	0.02535	0.11348	0.07695	0.33741

XTEPSI	KQ	KT	EFFY
0.4520	0.04775	0.23579	0.718

Propeller Design Output for DATA4

PROPELLER DESIGN WITH IRREGULAR HELICAL SLIPSTREAM
(PROGRAM FPST.FOR)

INPUT DATA

DHP	RPM	VS	1-WT	DIAMETER	BLADES
26789.5	85.0	15.00	0.721	8340.00	4

RADIUS	1-WN	THICKNESS	CHORD	DRAG COEFF
0.20	0.3080			
0.25	0.3320	0.000	2002.000	0.00880
0.30	0.3630	0.000	2103.000	0.00850
0.40	0.4350	0.000	2285.000	0.00800
0.50	0.5610	0.000	2439.000	0.00760
0.60	0.7150	0.000	2550.000	0.00740
0.70	0.7920	0.000	2596.000	0.00720
0.80	0.8470	0.000	2526.000	0.00700
0.90	0.8690	0.000	2202.000	0.00710
0.95	0.8740	0.000	1787.000	0.00730
1.00	0.8780			

DERIVED DESIGN CONDITIONS

KQ	JVS
0.02704	0.6535

RESULTS

CIRCULATION COEFFICIENTS

0.0491752 0.0040149 0.0019995 -0.0004596 -0.0002282 0.0001568 0.0000396 0.0000353 -0.0001489

RADIUS	BETA	BETAI	CIRCULATION	UT/VS	UA/VS	UR/VS	CCL/D	CL	DKQ	DKT
0.25	15.44	32.88	0.028781	-0.27697	0.26592	0.04910	0.16421	0.68406	0.00589	0.07083
0.30	14.13	29.92	0.037920	-0.27542	0.30849	0.03267	0.17700	0.70192	0.01047	0.11790
0.40	12.75	25.50	0.046724	-0.24662	0.36451	-0.00890	0.15808	0.57699	0.02063	0.20879
0.50	13.14	22.84	0.048655	-0.20343	0.36585	-0.04921	0.12805	0.43787	0.03150	0.28517
0.60	13.92	21.03	0.046759	-0.15862	0.33298	-0.08245	0.10061	0.32906	0.04176	0.33907
0.70	13.24	18.95	0.043739	-0.13058	0.31853	-0.10697	0.08036	0.25818	0.04933	0.37601
0.80	12.42	17.16	0.038913	-0.10943	0.30646	-0.12167	0.06253	0.20645	0.05347	0.38609
0.90	11.36	15.51	0.030507	-0.09517	0.30528	-0.12548	0.04365	0.16533	0.04996	0.34227
0.95	10.83	14.78	0.022826	-0.08789	0.30753	-0.12344	0.03096	0.14451	0.04096	0.27070

XTEPSI	KQ	KT	EFFY
0.3220	0.02695	0.21426	0.596

Propeller Design Output for DATA5

PROPELLER DESIGN WITH IRREGULAR HELICAL SLIPSTREAM
(PROGRAM FPST.FOR)

INPUT DATA

DHP	RPM	VS	1-WT	DIAMETER	BLADES
38272.8	105.0	19.60	0.610	7560.00	5

RADIUS	1-WN	THICKNESS	CHORD	DRAG COEFF
0.22	0.6274			
0.25	0.5950	0.000	2342.000	0.00790
0.30	0.5470	0.000	2460.000	0.00770
0.40	0.4620	0.000	2674.000	0.00730
0.50	0.4000	0.000	2853.000	0.00710
0.60	0.3860	0.000	2984.000	0.00690
0.70	0.5010	0.000	3037.000	0.00670
0.80	0.6570	0.000	2955.000	0.00670
0.90	0.8220	0.000	2576.000	0.00670
0.95	0.8910	0.000	2090.000	0.00690
1.00	0.9470			

DERIVED DESIGN CONDITIONS

KQ	JVS
0.03348	0.7626

RESULTS

CIRCULATION COEFFICIENTS

0.0408459 0.0005600 -0.0021657 0.0001210 0.0003671 0.0000050 -0.0000053 -0.0000493 0.0001696

RADIUS	BETA	BETAI	CIRCULATION	UT/VS	UA/VS	UR/VS	CCL/D	CL	DKQ	DKT
0.25	30.02	41.37	0.014495	-0.20616	0.13031	0.07113	0.08298	0.26786	0.00620	0.05312
0.30	23.88	35.91	0.023312	-0.21073	0.19523	0.06014	0.11574	0.35568	0.01221	0.10745
0.40	15.66	27.71	0.034206	-0.21824	0.28882	0.01836	0.13310	0.37631	0.02433	0.22109
0.50	10.99	22.35	0.040746	-0.20944	0.36061	-0.03301	0.12797	0.33911	0.03719	0.34141
0.60	8.88	19.01	0.043553	-0.19075	0.39999	-0.08181	0.11343	0.28738	0.05018	0.45002
0.70	9.86	17.78	0.041255	-0.15609	0.37346	-0.12042	0.09050	0.22528	0.06303	0.50909
0.80	11.27	17.09	0.035107	-0.12026	0.31937	-0.14372	0.06640	0.16988	0.07066	0.50302
0.90	12.50	16.57	0.024832	-0.08758	0.25490	-0.14903	0.04131	0.12124	0.06518	0.40386
0.95	12.83	16.25	0.017254	-0.07587	0.22725	-0.14529	0.02712	0.09810	0.05197	0.29625

XTEPSI	KQ	KT	EFFY
0.3390	0.03373	0.26152	0.574

Stator Design Output for DATA1

STATOR DESIGN

STATOR D. (In Meter)= 0.45636 NO. OF BLADES= 6
Axial Distance (AXD/R(pr)= 0.6000

RADIUS	1-WN	THICKNESS	CHORD	DRAG COEFF
0.30				
0.32	0.6502	0.000	0.040	0.01575
0.37	0.7554	0.000	0.040	0.01582
0.44	0.8573	0.000	0.039	0.01600
0.54	0.8972	0.000	0.037	0.01637
0.65	0.9120	0.001	0.033	0.01711
0.76	0.9216	0.001	0.028	0.01824
0.86	0.9290	0.001	0.022	0.02029
0.93	0.9342	0.001	0.016	0.02311
0.98	0.9373	0.001	0.012	0.02698
1.00				

CIR. COEFF.(H) -0.00774855 -0.00211062 -0.00141739 -0.00053735 -0.00042435 -0.00005820 -0.00034659 0.00009578 -0.00006360

, RADIUS	BETAI	CIRCULATION	UTS/VS	UTP/VS	UAP/VS	CCL/D	CL	TKQ	TKT
0.317	81.14	-0.006016	0.04490	-0.16695	0.13246	0.04772	0.54858	0.46	0.80
0.367	83.99	-0.007916	0.05477	-0.14842	0.13391	0.05562	0.63774	0.79	0.76
0.444	87.28	-0.008007	0.06757	-0.11412	0.12360	0.05123	0.59644	1.06	0.22
0.542	88.78	-0.007521	0.05258	-0.07387	0.09866	0.04744	0.57886	1.24	-0.07
0.650	89.23	-0.006473	0.04106	-0.05447	0.09009	0.04058	0.55448	1.28	-0.15
0.758	89.31	-0.005838	0.03400	-0.04620	0.09078	0.03623	0.58425	1.36	-0.15
0.856	89.25	-0.004875	0.02647	-0.03974	0.08976	0.03006	0.63513	1.29	-0.13
0.933	88.64	-0.003155	0.00993	-0.03414	0.08610	0.01943	0.55407	0.92	-0.08
0.983	88.33	-0.002515	0.00391	-0.03384	0.08622	0.01543	0.60708	0.77	-0.05

STATOR TORQUE(KNM)= 0.78 THRUST(KN)= 0.04
PROPELLER TORQUE(KNM)= 0.83 THRUST(KN)= 7.39
PROPULSORS EFFICIENCY =0.650 GAIN(%) = 0.553

STATOR DESIGN AFTER BALANCING THE TORQUE

0.317	81.34	-0.006398	0.04775	-0.16695	0.13246	0.05078	0.58370	0.49	0.84
0.367	84.21	-0.008418	0.05825	-0.14842	0.13391	0.05917	0.67848	0.84	0.78
0.444	87.53	-0.008515	0.07185	-0.11412	0.12360	0.05449	0.63441	1.13	0.20
0.542	88.97	-0.007998	0.05592	-0.07387	0.09866	0.05045	0.61563	1.31	-0.09
0.650	89.38	-0.006883	0.04366	-0.05447	0.09009	0.04316	0.58968	1.37	-0.17
0.758	89.43	-0.006209	0.03616	-0.04620	0.09078	0.03853	0.62134	1.45	-0.16
0.856	89.35	-0.005184	0.02815	-0.03974	0.08976	0.03197	0.67544	1.38	-0.13
0.933	88.68	-0.003356	0.01057	-0.03414	0.08610	0.02066	0.58923	0.97	-0.07
0.983	88.34	-0.002674	0.00416	-0.03384	0.08622	0.01641	0.64561	0.82	-0.05

STATOR TORQUE(KNM)= 0.83 THRUST(KN)= 0.04
PROPELLER TORQUE(KNM)= 0.83 THRUST(KN)= 7.39
PROPULSORS EFFICIENCY =0.650 GAIN(%) = 0.500

Stator Design Output for DATA2

STATOR DESIGN

STATOR D. (In Meter)= 0.46286 NO. OF BLADES= 9
Axial Distance (AXD/R(pr)= 0.5000

RADIUS	1-WN	THICKNESS	CHORD	DRAG COEFF
0.36				
0.38	0.7453	0.000	0.111	0.01229
0.42	0.8029	0.000	0.117	0.01216
0.49	0.8562	0.000	0.123	0.01205
0.58	0.9025	0.000	0.126	0.01201
0.68	0.9135	0.001	0.124	0.01211
0.78	0.9223	0.001	0.115	0.01236
0.87	0.9291	0.001	0.103	0.01277
0.94	0.9339	0.001	0.089	0.01328
0.98	0.9369	0.001	0.080	0.01369
1.00				

CIR. COEFF.(H) -0.06187876 -0.00170077 -0.01304239 0.00236780 -0.00427068 0.00317130 -0.00036964 0.00200809 0.00028287

RADIUS	BETAI	CIRCULATION	UTS/VS	UTP/VS	UAP/VS	CCL/D	CL	TKQ	TKT
0.376	80.16	-0.028707	0.34908	-0.62013	0.81720	0.11374	0.47600	0.73	1.23
0.422	80.91	-0.052590	0.41277	-0.69653	0.97100	0.18393	0.72890	1.69	2.48
0.493	86.72	-0.052669	0.54499	-0.65265	1.02486	0.17564	0.66203	2.09	0.72
0.582	80.42	-0.053086	0.49777	-0.83814	1.11420	0.16309	0.59910	2.68	2.95
0.680	81.50	-0.052455	0.42750	-0.73998	1.17676	0.15594	0.58303	3.21	2.61
0.779	82.26	-0.050255	0.38198	-0.67743	1.25119	0.14395	0.57739	3.66	2.32
0.868	83.29	-0.046742	0.37576	-0.63909	1.30764	0.13040	0.58828	3.90	1.86
0.939	83.84	-0.044591	0.18460	-0.43225	1.36024	0.12142	0.63074	4.13	1.65
0.984	83.56	-0.039604	0.13482	-0.39609	1.37630	0.10690	0.61770	3.88	1.54

STATOR TORQUE(KNM)= 1.92 THRUST(KN)= 1.31
PROPELLER TORQUE(KNM)= 1.24 THRUST(KN)= 18.04
PROPULSORS EFFICIENCY =0.501 GAIN(%) = 6.784

STATOR DESIGN AFTER BALANCING THE TORQUE

0.376	75.85	-0.018607	0.22627	-0.62013	0.81720	0.07256	0.30365	0.47	1.14
0.422	76.41	-0.034088	0.26755	-0.69653	0.97100	0.11736	0.46507	1.10	2.42
0.493	80.96	-0.034140	0.35326	-0.65265	1.02486	0.11262	0.42448	1.36	1.56
0.582	75.66	-0.034410	0.32265	-0.83814	1.11420	0.10387	0.38155	1.74	2.88
0.680	77.51	-0.034000	0.27710	-0.73998	1.17676	0.09979	0.37308	2.09	2.49
0.779	78.81	-0.032574	0.24759	-0.67743	1.25119	0.09238	0.37052	2.38	2.16
0.868	79.97	-0.030298	0.24357	-0.63909	1.30764	0.08381	0.37808	2.54	1.80
0.939	82.24	-0.028903	0.11966	-0.43225	1.36024	0.07843	0.40745	2.68	1.27
0.984	82.40	-0.025671	0.08739	-0.39609	1.37630	0.06912	0.39939	2.52	1.09

STATOR TORQUE(KNM)= 1.25 THRUST(KN)= 1.30
PROPELLER TORQUE(KNM)= 1.24 THRUST(KN)= 18.04
PROPULSORS EFFICIENCY =0.501 GAIN(%) = 6.706

Stator Design Output for DATA3

STATOR DESIGN

STATOR D. (In Meter)= 7.30863 NO. OF BLADES= 9
Axial Distance (AXD/R(pr)= 0.6000

RADIUS	1-WN	THICKNESS	CHORD	DRAG COEFF
0.24				
0.26	0.4880	0.001	0.976	0.00780
0.32	0.5396	0.002	1.034	0.00774
0.40	0.6293	0.005	1.086	0.00770
0.51	0.7778	0.008	1.107	0.00771
0.62	0.8585	0.011	1.073	0.00781
0.74	0.8930	0.014	0.971	0.00803
0.84	0.9055	0.017	0.835	0.00836
0.93	0.9079	0.020	0.673	0.00887
0.98	0.9090	0.021	0.567	0.00932
1.00				

CIR. COEFF.(H) -0.01623082 -0.00010303 -0.00221844 0.00041324 -0.00065649 0.00025794 -0.00060102 -0.00010238 -0.00030706

RADIUS	BETAI	CIRCULATION	UTS/VS	UTP/VS	UAP/VS	CCL/D	CL	TKQ	TKT
0.263	71.65	-0.007530	0.10920	-0.31521	0.13327	0.07229	0.54124	650.91	213.93
0.317	74.89	-0.010807	0.13981	-0.34079	0.20466	0.08808	0.62245	1345.70	298.71
0.400	80.74	-0.014184	0.16831	-0.31050	0.24274	0.10086	0.67910	2611.97	270.55
0.505	85.62	-0.014342	0.15237	-0.22976	0.23171	0.08900	0.58739	3858.85	132.62
0.622	86.85	-0.014375	0.12552	-0.18578	0.23749	0.08229	0.56048	5167.84	93.23
0.739	87.50	-0.014046	0.11009	-0.15993	0.25029	0.07712	0.58033	6254.91	68.90
0.844	87.75	-0.013004	0.09885	-0.14479	0.26498	0.06976	0.61041	6773.45	56.06
0.928	86.28	-0.010989	0.05734	-0.13413	0.27308	0.05834	0.63365	6349.15	95.47
0.982	85.17	-0.008566	0.03353	-0.13330	0.27286	0.04538	0.58542	5241.41	99.98

STATOR TORQUE(KNM)= 3432.28 THRUST(KN)= 105.56
PROPELLER TORQUE(KNM)= 3279.41 THRUST(KN)= 2138.23
PROPULSORS EFFICIENCY =0.752 GAIN(%) = 4.705

STATOR DESIGN AFTER BALANCING THE TORQUE

0.263	71.25	-0.007195	0.10434	-0.31521	0.13327	0.06890	0.51592	622.13	208.99
0.317	74.44	-0.010326	0.13359	-0.34079	0.20466	0.08398	0.59346	1286.11	294.00
0.400	80.26	-0.013552	0.16081	-0.31050	0.24274	0.09624	0.64795	2496.11	272.22
0.505	85.23	-0.013703	0.14558	-0.22976	0.23171	0.08499	0.56093	3687.48	138.88
0.622	86.56	-0.013735	0.11993	-0.18578	0.23749	0.07860	0.53536	4938.20	98.73
0.739	87.26	-0.013420	0.10518	-0.15993	0.25029	0.07367	0.55437	5976.84	73.88
0.844	87.54	-0.012425	0.09445	-0.14479	0.26498	0.06664	0.58313	6472.26	60.10
0.928	86.16	-0.010499	0.05478	-0.13413	0.27308	0.05573	0.60534	6066.80	93.91
0.982	85.10	-0.008184	0.03203	-0.13330	0.27286	0.04335	0.55929	5008.37	96.25

STATOR TORQUE(KNM)= 3279.77 THRUST(KN)= 107.23
PROPELLER TORQUE(KNM)= 3279.41 THRUST(KN)= 2138.23
PROPULSORS EFFICIENCY =0.752 GAIN(%) = 4.775

Stator Design Output for DATA4

STATOR DESIGN

STATOR D. (In Meter)= 7.87960 NO. OF BLADES= 10
Axial Distance (AXD/R(pr)= 0.6000

RADIUS	1-WN	THICKNESS	CHORD	DRAG COEFF
0.23				
0.25	0.3244	0.001	1.726	0.00701
0.30	0.3543	0.002	1.730	0.00702
0.39	0.4109	0.005	1.708	0.00706
0.50	0.5207	0.008	1.629	0.00715
0.61	0.6851	0.012	1.494	0.00730
0.73	0.7867	0.015	1.282	0.00758
0.84	0.8441	0.019	1.028	0.00799
0.93	0.8636	0.021	0.779	0.00858
0.98	0.8717	0.023	0.624	0.00913
1.00				

CIR. COEFF.(H) -0.02446066 -0.00314498 -0.00379712 0.00011798 -0.00131048 -0.00015413 -0.00109232 -0.00021951 -0.00033132

RADIUS	BETAI	CIRCULATION	UTS/VS	UTP/VS	UAP/VS	CCL/D	CL	TKQ	TKT
0.248	71.58	-0.014939	0.23536	-0.47653	0.39983	0.12297	0.56148	632.83	206.88
0.303	69.87	-0.019378	0.29439	-0.61066	0.50855	0.13249	0.60353	1194.10	354.00
0.388	77.47	-0.023436	0.33033	-0.55353	0.59344	0.14313	0.66047	2150.78	297.05
0.495	82.06	-0.023337	0.27493	-0.43328	0.61457	0.12792	0.61876	3089.35	202.18
0.614	85.31	-0.021213	0.20979	-0.31198	0.55944	0.10674	0.56300	3816.68	108.88
0.734	86.47	-0.019380	0.16584	-0.24767	0.54034	0.09159	0.56296	4437.94	73.95
0.841	87.02	-0.017079	0.13844	-0.21010	0.53376	0.07778	0.59594	4654.88	54.18
0.926	85.52	-0.014133	0.07981	-0.18999	0.54399	0.06290	0.63628	4335.60	76.88
0.981	84.28	-0.010915	0.04690	-0.18894	0.54654	0.04812	0.60770	3574.99	78.62

STATOR TORQUE(KNM)= 2563.78 THRUST(KN)= 121.98
PROPELLER TORQUE(KNM)= 2246.28 THRUST(KN)= 2134.24
PROPULSORS EFFICIENCY =0.628 GAIN(%) = 5.406

STATOR DESIGN AFTER BALANCING THE TORQUE

0.248	69.53	-0.013089	0.20621	-0.47653	0.39983	0.10639	0.48577	555.14	202.92
0.303	67.76	-0.016978	0.25793	-0.61066	0.50855	0.11444	0.52131	1047.51	345.48
0.388	75.27	-0.020534	0.28942	-0.55353	0.59344	0.12424	0.57330	1886.04	308.38
0.495	80.38	-0.020447	0.24088	-0.43328	0.61457	0.11157	0.53969	2708.46	216.33
0.614	84.12	-0.018586	0.18381	-0.31198	0.55944	0.09334	0.49233	3345.55	121.63
0.734	85.59	-0.016980	0.14530	-0.24767	0.54034	0.08016	0.49272	3889.71	83.02
0.841	86.31	-0.014964	0.12129	-0.21010	0.53376	0.06810	0.52176	4079.58	60.43
0.926	85.12	-0.012383	0.06993	-0.18999	0.54399	0.05508	0.55716	3799.65	72.67
0.981	84.05	-0.009563	0.04109	-0.18894	0.54654	0.04214	0.53222	3133.13	70.47

STATOR TORQUE(KNM)= 2247.32 THRUST(KN)= 126.49
PROPELLER TORQUE(KNM)= 2246.28 THRUST(KN)= 2134.24
PROPULSORS EFFICIENCY =0.629 GAIN(%) = 5.595

Stator Design Output for DATA5

STATOR DESIGN

STATOR D. (In Meter)= 7.09022 NO. OF BLADES= 10
Axial Distance (AXD/R(pr)= 0.6000

RADIUS	1-WN	THICKNESS	CHORD	DRAG COEFF
0.25				
0.27	0.5930	0.001	0.870	0.00797
0.32	0.5453	0.002	1.045	0.00772
0.40	0.4792	0.004	1.260	0.00747
0.51	0.4138	0.007	1.424	0.00733
0.63	0.3879	0.011	1.429	0.00736
0.74	0.4952	0.014	1.275	0.00757
0.85	0.6460	0.017	0.969	0.00807
0.93	0.7737	0.019	0.650	0.00893
0.98	0.8505	0.021	0.411	0.01018
1.00				

CIR. COEFF.(H) -0.02454865 -0.00182562 -0.00038189 0.00063836 -0.00136373 0.00007112 -0.00079019 -0.00026125 -0.00053521

, RADIUS	BETAI	CIRCULATION	UTS/VS	UTP/VS	UAP/VS	CCL/D	CL	TKQ	TKT
0.269	73.26	-0.010615	0.17374	-0.40436	0.17378	0.08329	0.67890	641.83	194.01
0.322	78.36	-0.014881	0.23163	-0.41527	0.34604	0.10274	0.69707	1251.48	213.25
0.405	80.70	-0.021693	0.28528	-0.44290	0.48290	0.13981	0.78691	2474.57	265.63
0.509	81.38	-0.024537	0.28073	-0.43851	0.62699	0.14646	0.72942	3808.99	298.10
0.625	82.35	-0.025276	0.23808	-0.38242	0.68719	0.14640	0.72646	4973.60	278.16
0.741	84.98	-0.021619	0.18579	-0.28316	0.61384	0.12201	0.67860	5199.50	151.55
0.846	86.60	-0.016890	0.13423	-0.20264	0.50592	0.09196	0.67311	4812.76	76.03
0.928	86.21	-0.012572	0.06893	-0.14730	0.40935	0.06662	0.72618	4040.33	66.17
0.982	85.21	-0.009511	0.03920	-0.14415	0.40286	0.04751	0.82009	3424.85	70.12

STATOR TORQUE(KNM)= 2817.55 THRUST(KN)= 145.64
PROPELLER TORQUE(KNM)= 2597.87 THRUST(KN)= 2683.98
PROPULSORS EFFICIENCY =0.609 GAIN(%) = 5.147

STATOR DESIGN AFTER BALANCING THE TORQUE

0.269	72.34	-0.009788	0.16019	-0.40436	0.17378	0.07642	0.62285	592.11	189.16
0.322	77.25	-0.013721	0.21357	-0.41527	0.34604	0.09433	0.64003	1154.42	216.06
0.405	79.41	-0.020002	0.26304	-0.44290	0.48290	0.12840	0.72271	2282.49	280.27
0.509	80.21	-0.022624	0.25884	-0.43851	0.62699	0.13459	0.67032	3513.29	313.98
0.625	81.38	-0.023305	0.21951	-0.38242	0.68719	0.13466	0.66820	4587.23	290.33
0.741	84.24	-0.019934	0.17130	-0.28316	0.61384	0.11236	0.62492	4795.27	161.80
0.846	86.08	-0.015573	0.12377	-0.20264	0.50592	0.08474	0.62027	4438.32	82.03
0.928	85.95	-0.011592	0.06356	-0.14730	0.40935	0.06141	0.66935	3725.79	64.97
0.982	85.07	-0.008770	0.03614	-0.14415	0.40286	0.04380	0.75599	3158.21	65.91

STATOR TORQUE(KNM)= 2598.56 THRUST(KN)= 151.69
PROPELLER TORQUE(KNM)= 2597.87 THRUST(KN)= 2683.98
PROPULSORS EFFICIENCY =0.611 GAIN(%) = 5.349